Answers to reviewer #1

Poulain and coauthors describe a measurement campaign at a forest site in central Germany in 2010 involving the investigation of sources of carbonaceous aerosols using aerosol mass spectrometer (organic and inorganic aerosol) and multi angle absorption photometer (equivalent black carbon) measurements. Particle number-size distributions and light scattering were also measured using a dual mobility particle sizer and a nephelometer, respectively. Although originally chosen as an upwind site for a cloud processing study the dataset is also well suited to source apportionment of local and transported carbonaceous aerosols, which is the focus of this work. Good mass closure was obtained for AMS+MAAP data relative to expected mass concentrations derived using size distribution data and composition-dependent density values. AMS mass concentrations were observed to agree well with supporting on-line measurements (Monitor for AeRosol and Gases in Ambient Air, MARGA) and off-line size-resolved filter analysis (ion chromatography/UV-Vis and OC/EC analysis). Organic aerosol as measured by the AMS was apportioned using PMF/ME-2 constrained with reference mass spectra for hydrocarbon-like organic aerosol (HOA) and biomass burning organic aerosol (BBOA). Five factors were derived: HOA, BBOA and three oxidized organic aerosol factors: semivolatile (SV-OOA), less oxidized (LO-OOA) and more oxidized (MO-OOA). eBC was found to be predominantly associated with longrange transport through multiple linear regression analysis, which is somewhat unexpected, and this observation is supported by the size-dependence of eBC during different air mass periods. Under marine air masses, locally emitted carbonaceous aerosol sources become more important in terms of fractional composition, however continental air masses from the East result in the worst local air quality at the site. Overall, I find the manuscript to be well written and the quantification and apportionment procedures are rigorous and comprehensive. The dependence of aerosol composition on air mass origin is established well and the findings reported here are a useful reference point for central European background sites.
I only have a few minor comments.

We would like to thank the referee for his/her constructive comments and suggestions made to improve and clarify our manuscript. Our responses are given below. For clarity, comments from the referee are in black, our responses in blue, and change on the text of the manuscript in **bold blue**.

R1: How do the size distribution shapes for the impactor off-line analysis (Figure 2) agree with the AMS size distributions for nitrate/sulfate/ammonium/OC(or OA)?
A1: Comparison between AMS and Berner impactor size distribution was added to the supplementary information for each FCE and NCE as followed:
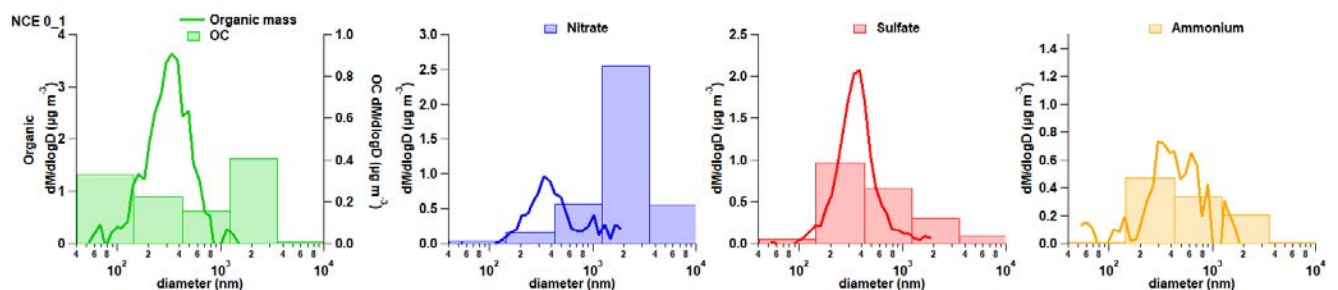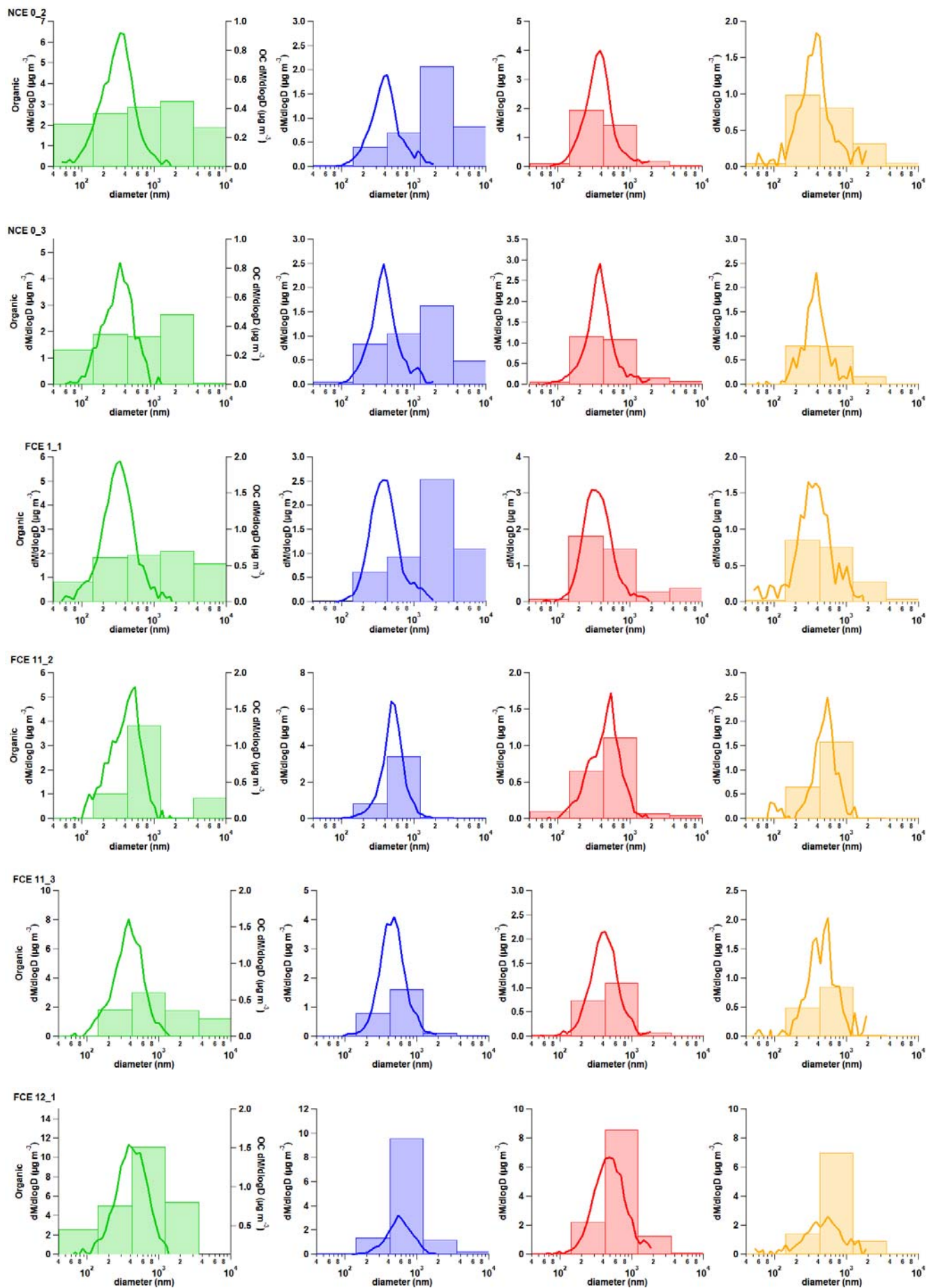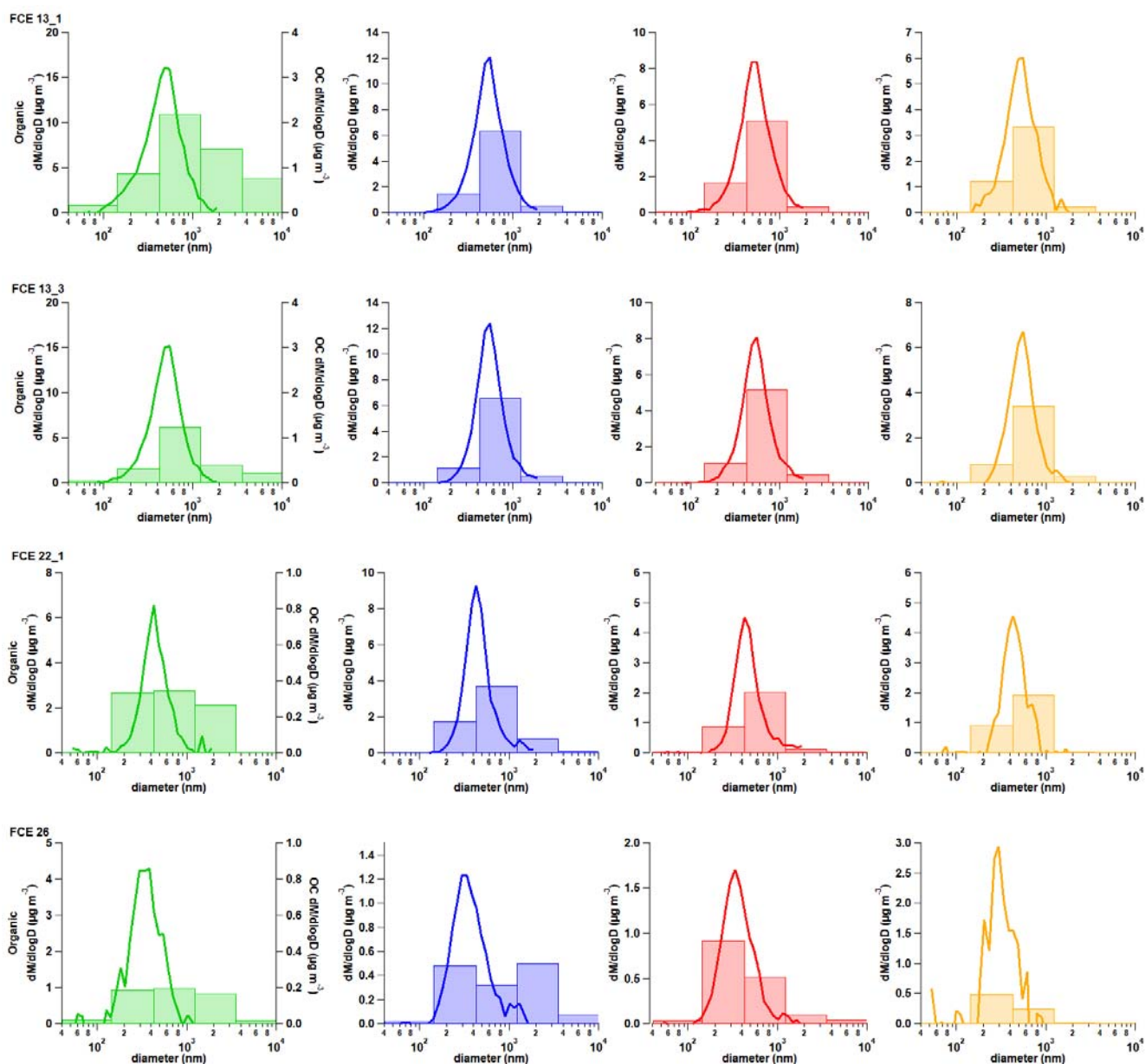
Figure SI-5: Comparison between the AMS and Berner impactor size distribution for organic (organic mass for the AMS and OC for the Berner impactor), nitrate, sulfate, and ammonium for the different FCE and NCE events.

The following text discussing the comparison was included in the supplementary information section SI-3:

The MARGA (PM$_{10}$, Fig. SI-2 & SI-3) and Berner impactor PM$_{1.2}$ (sum of the three first stages, Fig. SI-4) mass concentration of ammonium, nitrate, and sulfate also present an excellent correlation with the AMS measurements regarding individual instrumental limitations. This includes the limited number of samples and the reduced sampling time of the Berner impactor, as well as the specific upper size cut-off (near-PM$_1$ for the AMS, PM$_{1.2}$ for the Berner impactor, and PM$_{10}$ for MARGA). **The size distribution measured by the Berner-impactor and the AMS was compared to each other for organic (Organic mass for the AMS, OC for the Berner impactor), nitrate, sulfate, and ammonium (Fig. SI-5). Similar size distributions were obtained for the inorganic species, except for FCE 12.1 which shows higher nitrate and ammonium mass concentrations on stage 3 compared to the AMS size distribution. A**

comparison between the two organics measurement methods is more difficult since the AMS directly measures the organic mass concentration, while the OC from the Berner impactor was obtained according to the two-step thermographic method (VDI standard). Moreover, the presence of different nitrate salts can also explain the discrepancy between AMS and MARGA (see discussion on main text).

R2:Figure 2 caption define NCE and FCE here also Figure 2: different colour for sodium needed here

A2: The definition of NCE and FCE was added to the figure caption and the color code of the different chemical species (including sodium) was changed.
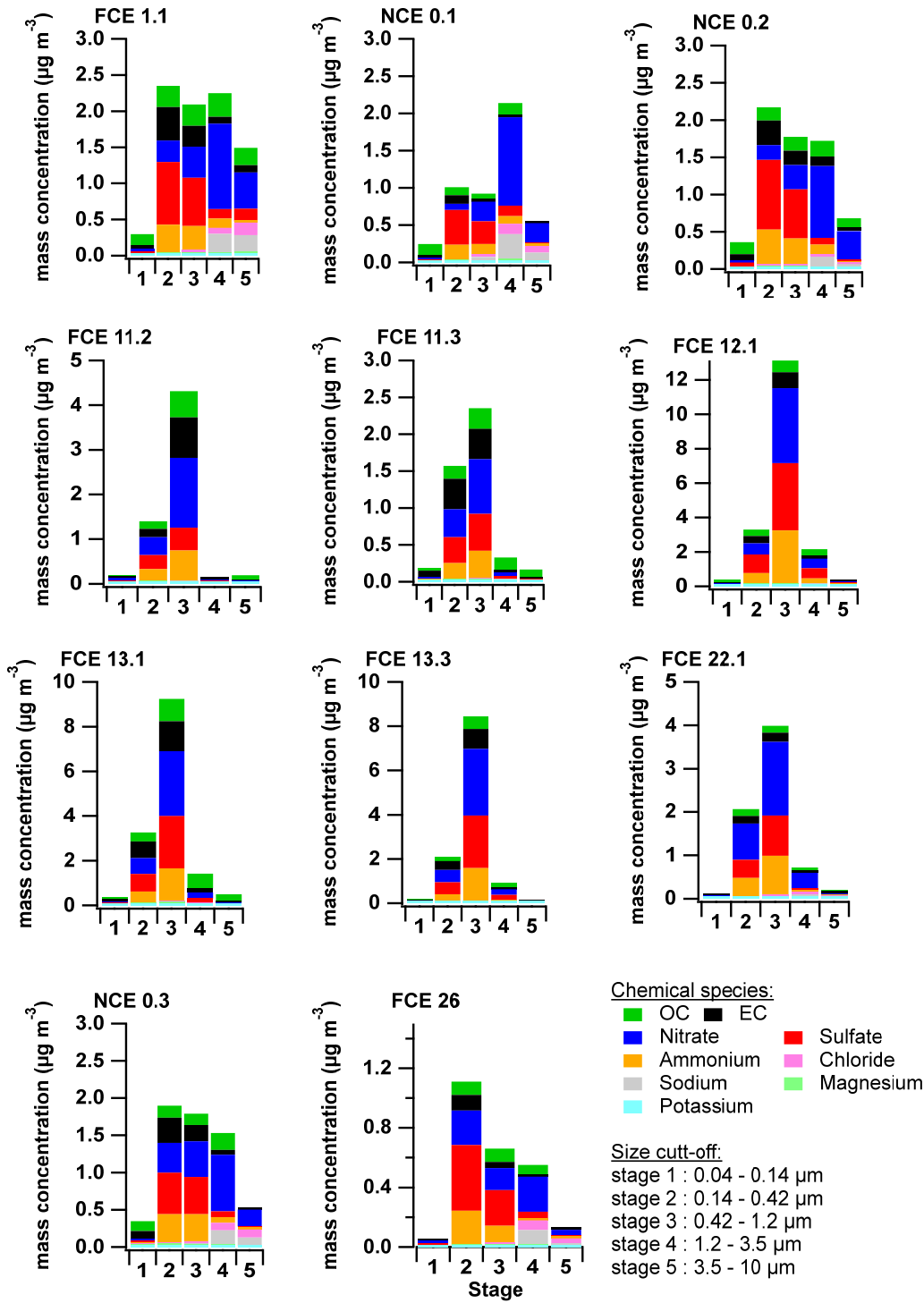
Figure 2: Size distribution of OC, EC, and major water-soluble ions from Berner impactor measurements for the different full cloud events (FCE) and non cloud event (NCE)

R3: Replace size cutting with size cut-off throughout the text

A3: We replaced it in the main text, figures, and supplementary information.

R4 Line 230: The temperature dependence could also be related to less evaporation or oxidation of locally produced vehicle exhaust HOA. Is there more local wind stagnation at lower temperatures? This could also boost the contribution of local vehicle emissions.

A4: Thanks for pointing out this aspect. This is true that during low temperature periods, slower evaporation of the vehicle exhaust, as well as their oxidation, might be expected. Moreover, during the cold period, the wind speed was most of the time below 1 m s^{-1}, which could also contribute to lead higher local emission mass concentration by reducing the dilution effect. Moreover, during the entire campaign, relatively low wind speed was reported ranging up to 5 m s^{-1}.

The text was modified as follows:

This temperature dependency indicates that HOA should be mostly associated with local residential house heating rather than **a significant increase in car emissions. Moreover, the low temperature period can also lead to an artificial increase of the HOA concentration by slowing down the evaporation process of the emitted particles as well as their oxidation processes. Finally, the cold period was also associated with low wind speed and stable stratification (Fig. 1) (Tilgner et al., 2014), which might also contribute to higher concentrations of locally emitted aerosol by reducing both mixing and transport processes.**

R5: Figure 8: add the regression statistics

A5: regression slope and statistics are now included in the figure. The figure caption was modified accordingly.
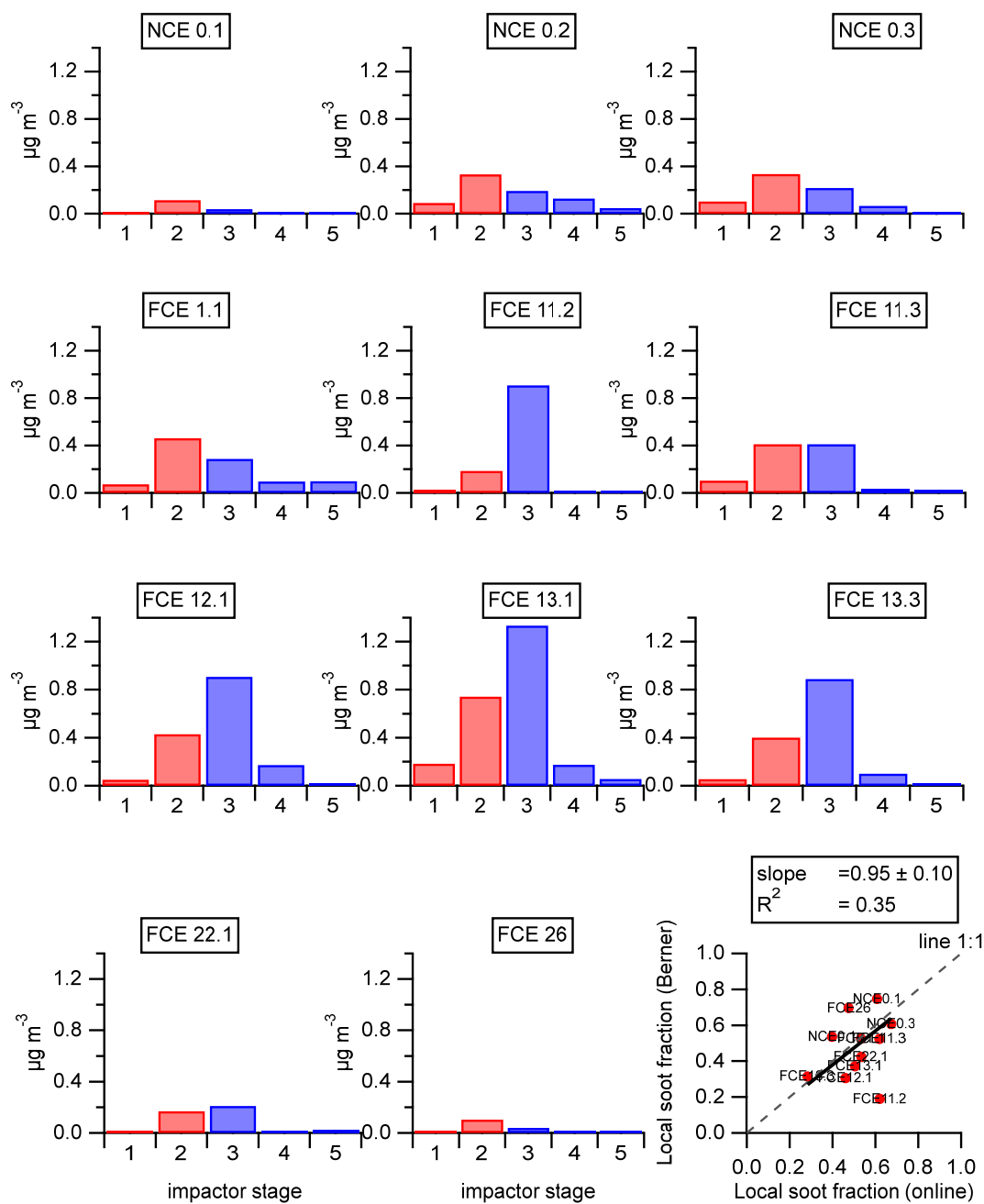
Figure 8: Overview of the EC size distribution measured by the 5-stages Berner impactor. Color corresponds to the following EC classification: red = local and blue = regional/transport. The scatter plot on the bottom right shows the comparison between the local soot fractions estimated using the two different approaches: Berner impactor (y-axis) and on-line multilinear regression (x-axis). **Regression (black line) was made using the least orthogonal distance fit method.**

<u>Reference</u>

Tilgner, A., Schone, L., Brauer, P., van Pinxteren, D., Hoffmann, E., Spindler, G., Styler, S. A., Mertes, S., Birmili, W., Otto, R., Merkel, M., Weinhold, K., Wiedensohler, A., Deneke, H., Schrodner, R., Wolke, R., Schneider, J., Haunold, W., Engel, A., Weber, A., and Herrmann, H.: Comprehensive assessment of meteorological conditions and airflow connectivity during HCCT-2010, Atmos. Chem. Phys., 14, 9105-9128, 10.5194/acp-14-9105-2014, 2014.

Answers to reviewer #2

This manuscript presents a thorough analysis of the aerosol composition and their source apportionment at a mountain forest site in Central Germany using detailed aerosol and gas measurements for 40+ days in late-2010. The topic is important, the methodology is clear, and the findings are very well presented. By using detailed particle composition, organic aerosol source apportionment (ME2), and back trajectory analysis, Poulain et al. provide insights into sources of aerosol at this site. Among other things, their findings on more than half of Equivalent black carbon (eBC) coming from long-range transport is especially interesting and potentially relevant for ongoing and future studies as well. I think the importance and quality of this manuscript warrants its publication in Atmospheric Chemistry and Physics.

We would like to thank the referee for his/her constructive comments and suggestions made to improve and clarify our manuscript. Our responses are given below. For clarity, comments from the referee are in black, our responses in blue, and change on the text of the manuscript in **bold blue**.

I only have some minor comments:
R1: Fig 1: Consider including Boundary Layer Height (BLH) timeseries either in Fig1 or in Fig S5. Reanalysis BLH (can easily be obtained from ECMWF's ERA5) seems to suggest potential role of changes in BLH height on the total aerosol mass loadings for the observed period.
A1: As suggested, the boundary layer height (BLH) time series was included in Fig. 1. Here the BLH time series was retrieved from the HYSPLIT GDAS (1 degree resolution) input, which was used for the trajectory analysis.

The text was modified as follow:
Section: 2.3 Back-trajectories and cluster calculations
The 96 h back trajectories were used to determine the influence of the air mass origin on aerosol. The trajectories were calculated for every hour from 13 September until 24 October 2010 for the altitude of 500 m above model ground with the NOAA Hybrid Single Particle Lagrangian Integrated Trajectory (HYSPLIT-4) Model (http://www.ready.noaa.gov/ready/hysplit4.html; Draxler and Hess, 2004) using the 1 degree resolution GDAS input data. The different back-trajectory clusters were calculated using the program R (http://www.r-project.org/; R Core Team, 2013) with the package openair (http://www.openair-project.org; Carslaw and Ropkins, 2012;Ropkins and Carslaw, 2012). **The same GDAS input data was used to retrieve the boundary layer height (BLH) at the sampling site from the HYSPLIT model output.**

Section: 3.1.1 Overall AMS-MAAP time series
Aerosol particle chemical composition (mass concentration and mass fraction) as measured by AMS and MAAP as well as the particle number size distribution over the entire time-period are shown in Figure 1. On average, the near-PM_1 particulate chemical composition was principally made-up of organic aerosol, OA (41 % of the total mass, Fig. 1). Sulfate and nitrate have quite similar contributions (19 % and 18 %, respectively). The rest of the aerosol particle mass concentration was made of ammonium (11 %), eBC (10.0 %), and chloride (1 %). Despite their similar contribution to the particle mass fraction, sulfate and nitrate showed a clear time dependency (Fig. 1). Although sulfate dominates the inorganic fraction at the beginning of the measurement period, nitrate becomes more important over time. This can be directly linked to a decrease of temperature during the sampling period (Fig. SI-5), inducing a change in nitrate partitioning between gas and particle phase. A last factor that must be considered is the decrease of solar radiation from summer to winter, influencing the photochemical formation of sulfate. **Variation of the BLH over the sampling period can also influence the local PM mass concentration (Fig.1). At the beginning of the campaign, the BLH reached above 1000 m during daytime, while the maximum altitude of the BLH decreased to below 800 m later on. This decrease**

in the maximum altitude of the BLH certainly contributes to the observed increase of the overall PM mass concentration during the day by reducing the ventilation effect. However, it is important to note that high uncertainties on the absolute value of the BLH for such a mountain area have to be expected due to the 1 degree resolution of the GDAS input data. Variations of the organics and eBC mass concentration over the sampling period will be discussed in sections 3.2 and 3.3, respectively.
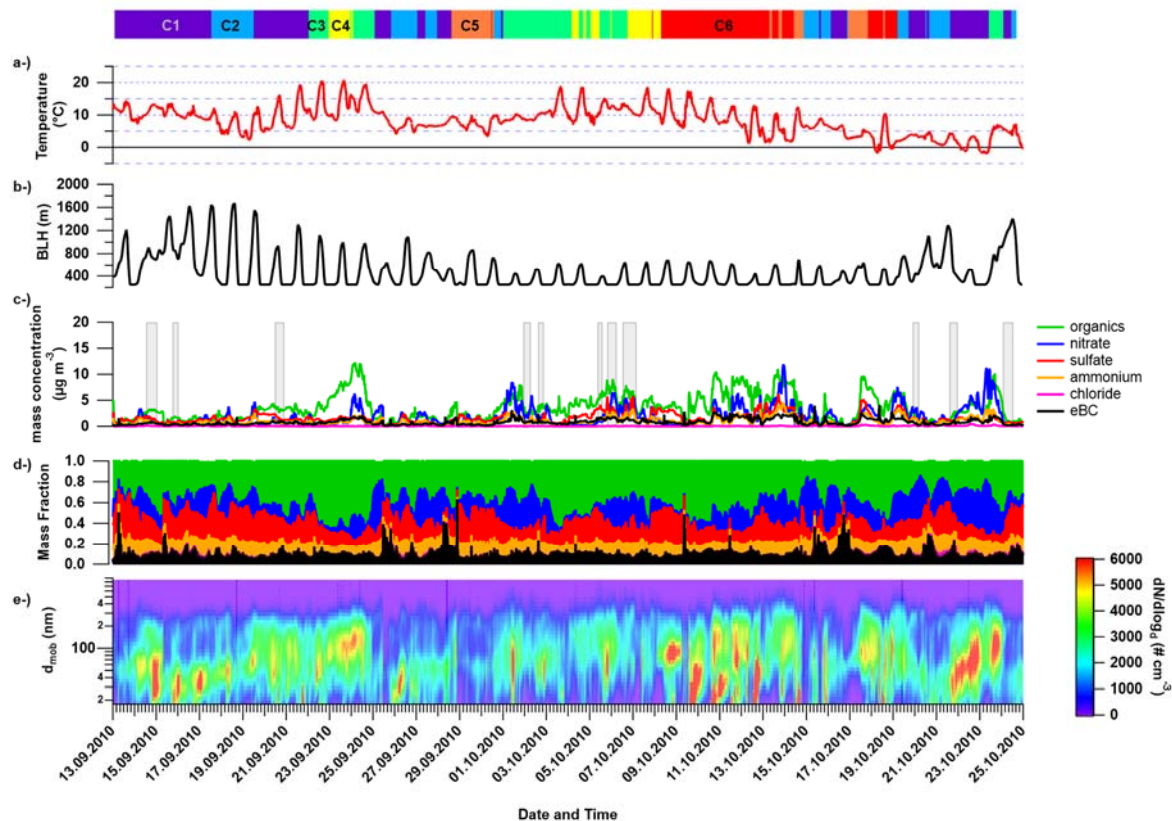

Figure 1: Time series of the ambient temperature (a), **estimated boundary layer height (BLH) obtained from HYSPLIT GDAS input (b),** the particulate near-PM$_1$ chemical composition as measured by the AMS and completed by MAAP for equivalent black carbon (c), the corresponding mass fraction (d), and particle number size distribution (e) during HCCT-2010 at the site of Goldlauter. The colored bars and numbers at the top refer to the six different air mass clusters (see section 3.4), and the grey bars refer to the different cloud and non-cloud events as defined in Table SI-2.

R2: Mention measurement period in Introduction or Site and instrumentations.
A2: The following sentence was modified in the introduction section to include reviewer's suggestion:
The measurements **took place on September-October 2010 as part** of the "Hill Cap Cloud Thuringia 2010" (HCCT-2010) experiment, which aimed to investigate the impact of cloud processing to aerosol physico-chemical properties.

R3: FigS5: Subplot-4 check colors.
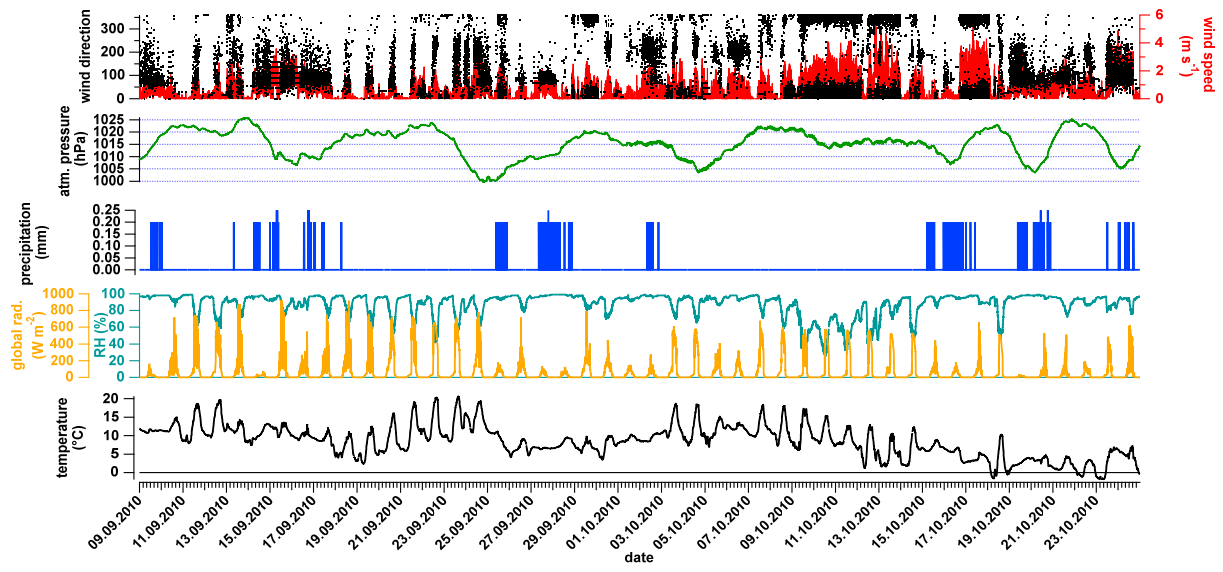A3: Colors for global radiation and relative humidity were corrected in Fig. S4.

Figure SI-5: Overview of the meteorological conditions during the sampling period.

Source apportionment and impact of long-range transport on carbonaceous aerosol particles in Central Germany during HCCT-2010

5 Laurent Poulain[1], Benjamin Fahlbusch[1, *], Gerald Spindler[1], Konrad Müller[1], Dominik van Pinxteren[1], Zhijun Wu[1,**], Yoshiteru Iinuma[1,***], Wolfram Birmili[1,****], Alfred Wiedensohler[1], Hartmut Herrmann[1]

[1] Leibniz Institut für Troposphärenforschung, (TROPOS), Leipzig, 04318, Germany
[*] Now at Eurofins, Friedrichsdorf, 61381, Germany
[**] Now at College of Environment Sciences and Engineering, Peking University, Beijing, 100871, China
10 [***] Now at: Okinawa Institute of Science and Technology Graduate University (OIST), Okinawa, 904-0495, Japan
[****] Now at: Umweltbundesamt (UBA), Berlin, 14195, Germany

Correspondence to: Hartmut Herrmann (herrmann@tropos.de) and Laurent Poulain (poulain@tropos.de)

Abstract. The identification of different sources of the carbonaceous aerosol (organics and black carbon) was investigated at
15 a mountain forest site located in central Germany from September to October 2010 to characterize incoming air masses during
the "Hill Cap Cloud Thuringia 2010" (HCCT-2010) experiment. The near-PM_1 chemical composition, as measured by an
Aerosol Mass Spectrometer (HR-ToF-AMS), was dominated by organics (OA, 41 %), followed by sulfate (19 %) and nitrate
(18 %). Source apportionment of the OA fraction was performed using the Multilinear Engine approach (ME-2), resulting in
the identification of five factors: Hydrocarbon-like OA (HOA, 3 % of OA mass), biomass burning OA (BBOA, 13 %), semi-
20 volatile-like OA (SVOOA, 19 %), and two oxygenated OA (OOA) factors. The more-oxidized OOA (MO-OOA, 28 %) was
interpreted as being influenced by aged polluted continental air masses, whereas the less-oxidized OOA (LO-OOA, 37 %) was
found to be more linked to aged biogenic sources. Equivalent black carbon (eBC) measured by a multi-angle absorption
photometer, MAAP, represented 10 % of the total PM. The eBC was clearly associated with the three factors HOA, BBOA,
and MO-OOA (all together $R^2 = 0.83$). Therefore, eBC's contribution to each factor was achieved using a multi-linear
25 regression model. More than half of the eBC (52 %) was associated with long-range transport (i.e. MO-OOA), whereas liquid
fuel eBC (35 %) and biomass burning eBC (13 %) were associated with local emissions leading to a complete apportionment
of the carbonaceous aerosol. The separation between local and transported eBC was well supported by the mass size
distribution of elemental carbon (EC) from Berner-impactor samples.

Air masses with the strongest marine influence based on back trajectory analysis corresponded with a low particle mass
30 concentration (6.4-7.5 µg m^{-3}) and organic fraction ($\approx$ 30 %). However, they also had the largest contribution of primary OA
(HOA $\approx$ 4 % and BBOA 15-20 %), which was associated with local emissions. Continental air masses had the highest mass
concentration (11.4-12.6 µg m^{-3}) and a larger fraction of oxygenated OA ($\approx$ 45 %) indicated highly processed OA. The present

results emphasize the key role played by long-range transport processes not only on the OA fraction but also on the eBC mass concentration and the importance of improving our knowledge on the identification of eBC sources.

1 Introduction

Atmospheric aerosol particles affect global climate through direct and indirect radiative forcing (IPCC, 2013), human health (Lelieveld et al., 2015;Burnett et al., 2014;Pope et al., 2011), as well as the ecosystems (Bohlmann et al., 2005;Jickells et al., 2005). Chemical composition of atmospheric particles at a specific sampling place (e.g. rural, urban, or marine environment) is not only depending on the local environment and sources but is also influenced by the history of the particles reaching the sampling site. During transport, so-called aging processes not only modify the chemical composition of the particles but also affect their physical properties (e.g. size distribution, volatility, hygroscopicity, CCN activity, optical properties, Donahue et al., 2014;Farmer et al., 2015;Moise et al., 2015). As a consequence, aerosol particles at a specific location result from a complex mixture of different sources combined with complex processing.

Carbonaceous aerosol particles are a dominant fraction of total particle mass and are made of a large number of chemical species, which can be divided into organic aerosol (OA) and black carbon (BC) (e.g. Cabada et al., 2002). One of the most significant aerosol particle components influenced by atmospheric aging processes is the OA fraction, which can represent up to 90 % of the fine aerosol particle mass (e.g. Zhang et al., 2007). To better understand the origins of OA, source apportionment analysis is commonly applied to distinguish primary organic sources (e.g. related to fossil fuel, biomass, or coal combustion) from secondary organic aerosol (SOA) sources based on either on-line measurements (e.g. Zhang et al., 2011;Canonaco et al., 2013), off-line chemical analysis (e.g. van Pinxteren et al., 2016;Srivastava et al., 2018) or a combination of both (Srivastava et al., 2019). Black carbon is associated with primary emissions from combustion processes of either anthropogenic (car, house heating, industry) or biogenic (e.g. wildfires) origins. In contrast to OA, source identification of BC remains sparse and only the recent development of an aethalometer model approach allows now to distinguish equivalent BC (eBC) related to traffic emissions from wood combustion eBC (e.g. Sandradewi et al., 2008;Laborde et al., 2013;Zhu et al., 2018;Martinsson et al., 2017;Liakakou et al., 2020). Not only local sources drive the aerosol particle chemical composition; long-range transport, influenced by air mass origin, also plays an important role in local number size distribution and aerosol particle chemical composition (e.g. van Pinxteren et al., 2016;van Pinxteren et al., 2019;Waked et al., 2018). Therefore, not all the eBC mass concentration has to be linked to local sources, and a significant fraction can be attributed to long-range transport (e.g. Healy et al., 2012;van Pinxteren et al., 2019).

The present work investigates the aerosol particle chemical composition and the different sources of carbonaceous particles reaching a site close to the village of Goldlauter in the Thuringian forest in Central Germany. The measurements took place on September-October 2010 as were part of the "Hill Cap Cloud Thuringia 2010" (HCCT-2010) experiment, which aimed to

investigate the impact of cloud processing to aerosol physico-chemical properties. The Goldlauter site served as upwind site to study air masses before entering hill cap clouds at the Schmücke mountain. The present study focusses on an in-depth characterization at this site, while companion papers have related upwind site data to the other experiment sites (see https://www.atmos-chem-phys.net/special_issue287.html and e.g. Harris et al., 2013). The presented results stand for themselves, but can also be used to further interpret HCCT-2010 results and guide associated modeling and future experimental studies in the Schmücke area.

2 Site and instrumentations

2.1 Site

For the "Hill Cap Cloud Thuringia 2010" (HCCT-2010) experiment, the same places were used as for the FEBUKO/MODMEP experiments in 2001/02 (Herrmann et al., 2005). This work is focused on measurements performed at the upwind site (10◦45'20'' E, 50◦38'25'' N, 605 m a.s.l.) and approximately 6 km from the nearest city of Suhl. The sampling place is located on the outskirts of the forest in front of the mountain site "Schmücke" under the prevailing SW wind direction and about 350 m below the mountain site "Schmücke" (see Tilgner et al. (2014) for more details). In the following, the upwind-site will be referred to as Goldlauter (GL). All times in the manuscript are given in Central European Summer Time (CEST).

2.2 Instrumentation

A large setup of on-line and off-line instruments was deployed during HCCT-2010, covering both gas and particle phases. On-line instruments were sitting in two nearby laboratory containers and were operated continuously during the entire campaign. On the other hand, off-line sampling systems were applied only during specific intensive observation periods (IOPs) associated with two different conditions: 1- SW wind direction and presence of cloud at the Mt. Schmücke site for the full cloud events (FCE) and 2- SW or NE wind direction and no clouds or fog at any site for the non-cloud events (NCE). A detailed overview of these events is given by Tilgner et al. (2014).

2.2.1 Gas-phase measurements

The trace gases O_3, SO_2, and NO_x (NO and NO_2) were quantified continuously using standard gas monitor systems for the whole duration of the experiment (Table SI-1). Non-methane hydrocarbon sampling (NMHC) was carried out with stainless steel containers every 2 hours during IOP events only. Ambient air was sucked into the container for three minutes before closing the valves. Analysis of the NMHC was carried out by the German Federal Environmental Protection Agency (UBA) at their laboratory at Schmücke (UBA and GAW site) within 72 hours after sampling, using a GC-FID gas chromatographic analysis (Rappenglück et al., 2006). The cleaning of the stainless-steel container was carried out overnight through heating and evacuating.

Additionally, a Monitor for AeRosol and Gases in Ambient Air (MARGA 1S ADI 208, Metrohm AG, Switzerland, Rumsey
et al., 2014;Twigg et al., 2015;Stieger et al., 2017) connected to a Teflon-coated PM_{10} inlet was deployed for the detection of
the major water-soluble inorganic compounds in both gas phase and particle phase. A good correlation for the MARGA SO_2
and the UV-fluorescence monitor was reported in agreement with previous works from Makkonen et al. (2012);Stieger et al.
(2017).

2.2.2 Aerosol particle measurements

2.2.2.1 Online aerosol particle measurements

The online physico-chemical characterization of the ambient aerosol particles was performed using a large set of instruments.
A High-Resolution Time-of-Flight Aerosol Mass Spectrometer (HR-ToF-AMS, Aerodyne Research Inc, DeCarlo et al. (2006),
later referred to as AMS), a dual mobility particle size spectrometer (TROPOS-Type T-MPSS, Birmili et al., 1999), a Multi-
Angle Absorption Photometer (MAAP, Model 5012, Thermo Scientific, Petzold and Schönlinner, 2004), a three-wavelength
nephelometer (TSI Model 3563, Heintzenberg et al., 2006). All these instruments were located in the same laboratory container
and connected to the same sampling inlet consisting of a PM_{10} inlet located approximately 6 m above ground level directly
followed by an automatic aerosol diffusion dryer system maintaining the relative humidity in the sampling line below 30 %
(Tuch et al., 2009). Moreover, water-soluble PM_{10} inorganic ions were also measured by MARGA.

2.2.2.2 AMS data analysis and positive matrix factorization

The AMS data was processed under the Squirrel version 1.52L and the PIKA version 1.13B (downloaded from
http://cires.colorado.edu/jimenez-group/ToFAMSResources/ToFSoftware) using the IGOR Pro software package
(Wavemetrics Inc, Portland, USA). A Chemical Dependent Collection Efficiency (CDCE) correction was applied on the AMS
mass concentration according to Middlebrook et al. (2012). Quality assurance on the AMS data was achieved by comparing it
to the MARGA and ~~Berner~~ Berner-impactors (sum of the first three stages) for individual species, while mass closure of the
PM_1 aerosol particle chemical mass concentration as measured by the AMS and MAAP was achieved by comparing it to the
estimated mass concentration from the T-MPSS and ~~Berner~~ Berner-impactors. Description and results can be found in sections
3.1.2 and 3.1.3 as well as in supplementary information SI-3 (AMS data validation, Fig. SI-1 to SI-~~4~~5).
Source apportionment was performed on the high-resolution organic mass spectra dataset using the multi-linear engine (ME-
2) model developed by Paatero (1999) and using the Source Finder tool (Sofi4.9, Canonaco et al., 2013) developed at the Paul
Scherrer Institute (PSI, Switzerland). Prior to analysis, the high-resolution organic mass spectra matrix was prepared according
to the recommendations of Ulbrich et al. (2009). Isotope ions, which are calculated as a constant fraction of the parent ion,
were removed. A minimum counting error was applied and ions with a signal-to-noise (SNR) ratio between 0.2 < SNR < 2
were down-weighted by a factor of 2, and ions with SNR < 0.2 were down-weighted by a factor of 10. Finally, ions related to
CO_2^+ were also down-weighted since they are calculated as a fraction of the ion CO_2^+ (Allan et al., 2004). The source
apportionment was made following the recommendation of Crippa et al. (2014): in a first step, a non-constrained model

approach was investigated. Since primary factors were not properly resolved during this first approach, a partially constrained approach was then investigated. Elemental analysis of the identified mass spectra was performed using the Analytic Procedure for Elemental Separation (APES 1.06) based on Aiken et al. (2008) and including the improved approach from Canagaratna et al. (2015). A detailed description of the source apportionment analysis can be found in the supplementary information SI-5.

2.2.2.3 Off-line aerosol collection by 5-stage Berner-impactors and laboratory analysis

In parallel to the on-line measurements, a five-stage low-pressure Berner-impactor (LPI 80/0.05/2.9; Hauke GmbH und Co. KG, Austria, Berner and Lurzer, 1980) was used to collect PM size segregated during the IOPs using a humidity-controlled inlet (RH < 80 %). Water-soluble ions, organic carbon (OC), elemental carbon (EC), as well as sugar and anhydrosaccharide analyses were performed. Details on the sampling conditions, sample preparation, as well as analytical methods can be found in the supplementary information (section SI-2). In the following, only results of IOPs longer than 2 h are considered in order to collect enough material on each stage of the impactor. Details on the sampling period for each considered IOP is provided in a dedicated section on the supplementary Information and in Table SI-2.

2.3 Back-trajectories and cluster calculations

The 96 h back trajectories were used to determine the influence of the air mass origin on aerosol. The trajectories were calculated for every hour from 13 September until 24 October 2010 for the altitude of 500 m above model ground with the NOAA Hybrid Single Particle Lagrangian Integrated Trajectory (HYSPLIT-4) Model (http://www.ready.noaa.gov/ready/hysplit4.html; Draxler and Hess, 2004) using the 1 degree resolution GDAS input data. The different back-trajectory clusters were calculated using the program R (http://www.r-project.org/; R Core Team, 2013) with the package openair (http://www.openair-project.org; Carslaw and Ropkins, 2012;Ropkins and Carslaw, 2012). The same GDAS input data was used to retrieve the boundary layer height (BLH) at the sampling site from the HYSPLIT model output.

3 Results

Data analysis will first focus on the overall aerosol particle chemical composition and mass closure. The second part will discuss the source apportionment of both organic aerosol and eBC. Finally, the third section will investigate the influence of the air mass origins on aerosol particle chemical composition and size distribution.

3.1 Aerosol particle chemical composition

3.1.1 Overall AMS-MAAP time series

Aerosol particle chemical composition (mass concentration and mass fraction) as measured by AMS and MAAP as well as the particle number size distribution over the entire time-period are shown in Figure 1. On average, the near-PM$_1$ particulate chemical composition was principally made-up of organic aerosol, OA (41 % of the total mass, Fig. 1). Sulfate and nitrate

5

have quite similar contributions (19 % and 18 %, respectively). The rest of the aerosol particle mass concentration was made of ammonium (11 %), eBC (10.0 %), and chloride (1 %). Despite their similar contribution to the particle mass fraction, sulfate and nitrate showed a clear time dependency (Fig. 1). Although sulfate dominates the inorganic fraction at the beginning of the measurement period, nitrate becomes more important over time. This can be directly linked to a decrease of temperature during the sampling period (Fig. SI-56), inducing a change in nitrate partitioning between gas and particle phase. A last factor that must be considered is the decrease of solar radiation from summer to winter, influencing the photochemical formation of sulfate. Variation of the BLH over the sampling period can also influence the local PM mass concentration (Fig.1). At the beginning of the campaign, the BLH reached above 1000 m during daytime, while the maximum altitude of the BLH decreased to below 800 m later on. This decrease in the maximum altitude of the BLH certainly contributes to the observed increase of the overall PM mass concentration during the day by reducing the ventilation effect. However, it is important to note that high uncertainties on the absolute value of the BLH for such a mountain area have to be expected due to the 1 degree resolution of the GDAS input data. Variations of the organics and eBC mass concentration over the sampling period will be discussed in sections 3.2 and 3.3, respectively.

3.1.2 ~~Berner~~ Berner-impactor data

Parallel to online measurements, Berner-impactor provides size-resolved chemical composition up to 10 µm (Fig. 2). Over the samples, $PM_{1.2}$ mass concentration (sum of the first three stages) represents more than 75 % of the PM_{10}. The only exceptions are for FCE 1.1, NCE 0.1, NCE 0.2, and NCE 0.3, which are all associated with back trajectory cluster C1-West and maritime air masses (see section 3.4). However, it is important to note that such aged maritime air masses do not systematically include an important super-µm fraction (for example, FCE 22.1). A simple reason for that is a washout of the air mass during rain events before it reaches the sampling site. A systematic look at the $PM_{1.2}$ to PM_{10} ratio for the main aerosol component shows that EC and sulfate are principally present on the $PM_{1.2}$ (> 80 % each), while $OC-PM_{1.2}$ represents more than 60 % of the PM_{10} mass concentration. Nitrate is the only species that has a strong variability on the $PM_{1.2}$ to PM_{10} ratio ranging from 20 to > 90 %).

3.1.3 AMS comparison with MARGA

According to the large contribution of the $PM_{1.2}$ mass concentration to PM_{10} discussed above and despite their respective size ~~cutting~~cutt-off, AMS and MARGA were successfully compared for ammonium, nitrate, and sulfate (Fig. 3, SI-2 and SI-3), indicating that these compounds were principally present in the PM_1 size range. In spite of the observed agreement, certain limitations must be considered. For example, the presence of organo-nitrates (ONs) and organo-sulfates (OSs) can interfere with the quantification of inorganic nitrate and sulfate by the AMS (Farmer et al., 2010;Bruns et al., 2010). The presence of such compounds might explain the slight overestimation of the AMS nitrate (Fig. 3) and sulfate (Fig. SI-2) happening from time to time when they are compared to MARGA.

6

Additionally, some specific periods were also found in which the nitrate mass concentration measured by the MARGA appears to be higher and not related to the AMS's one (Fig. 3). This clearly indicates a larger contribution of super-µm particles that are not detected by the AMS as previously reported for the Berner-impactor samples. During these periods, MARGA's nitrate contains a larger fraction of sodium nitrate, which originates during the aging of marine aerosol when it crosses polluted areas (e.g. Dasgupta et al., 2007), as confirmed by both the concomitant increase of sodium mass concentration, and the attribution of these periods to marine influence clusters (C1-West and C2-Northwest) with RTI_{water} above 0.5 (Fig. 3 and further discussion in section 3.4). Stieger et al. (2018) drew similar conclusions by comparing the MARGA PM_{10} measurements with an ACSM at the research site Melpitz in rural Germany. The very good results for the sulfate are also supported by that its size distribution inside the Berne-impactor samples.

3.1.4 Overall result of PM analysis

AMS, MARGA, and MAAP measurements provide complementary information on the aerosol particle chemical composition. Therefore, eBC from MAAP, organics from AMS, and inorganic ions from MARGA were combined to provide a comprehensive picture of the ambient PM_{10} particle composition (Fig. 4) in a similar way as Schlag et al. (2016). The main advantage of combining these three instruments is to provide a more detailed description of the ambient particles than if they were used individually. However, some limitations must be considered: i) crustal material is detected neither by MARGA nor AMS and therefore will not be considered at all in the following discussion; ii) the use of different upper-size ~~cutting~~ cut-off for the OA might lead to an underestimation of the total OA mass as expected from the OC distribution. However, the resulting PM_{10} estimation correlates very well with the PM_{10} mass concentration measured by the Berner-impactor (slope of 0.98, R^2 = 0.96, Fig. 4), indicating a minor contribution of non-considered species (i.e. dust, calcium, magnesium, and trace metals) to the total PM_{10} mass, as well as a lower organic contribution to the super-µm size range. Although the estimated PM_{10} mass was validated only during the IOPs, it appears to be reasonable to consider it as accurate over the entire experiment within the previously mentioned limitations.

3.2 Organic aerosol source apportionment

An investigation of the organic aerosol source apportionment highlights the presence of five different factors, which were identified based on their individual time series, mass spectra, diurnal variability, and comparison with external measurements (Fig. 5). A detailed description of the different steps of the analysis as well as the identification of the different factors is given in the supplementary information (Section SI-5). Briefly, in a first step, a non-constrained model was run, and, in a second step, a series of partly constrained runs were investigated in order to better distinguish the different primary organic factors. The selected final solution results in a partially constrained model with two primary organic factors: Hydrocarbon-like organic aerosol (HOA) and biomass burning organic aerosol (BBOA). HOA was constrained using the mass spectra reported by Mohr et al. (2012) in Barcelona (Spain) and is available on the AMS mass spectra database (http://cires.colorado.edu/jimenez-group/HRAMSsd/, Ulbrich et al., 2009). For BBOA, the mass spectra identified during the source analysis process itself was

7

used (see details in section SI-5). In addition to these two primary OA factors, three distinct oxygenated organic aerosols (OOA) were identified as semi-volatile OOA (SV-OOA), low-oxidized OOA (LO-OOA) and more-oxidized OOA (MO-OOA) (Fig. 5). It is important to note that the three OOA factors were already identified in the first step of the source apportionment analysis during the non-constrained approach.

3.2.1 HOA

HOA is commonly considered a surrogate for fossil fuel combustion emissions, especially related to traffic emissions. The HOA mass spectrum is characterized by a larger contribution of hydrocarbon-like ions ($C_xH_y^+$ fragments, Fig. 5), resulting in a low O:C (0.04) and high H:C (2.00), which is in agreement with previously reported values from Canagaratna et al. (2015). HOA correlates reasonably with *trans*-2-pentene ($R^2 = 0.43$), *cis*-2-pentene ($R^2 = 0.56$), eBC ($R^2 = 0.45$), benzene ($R^2 = 0.62$), toluene ($R^2 = 0.35$), NO_2 ($R^2 = 0.31$), and CO ($R^2 = 0.25$) (Fig. SI-~~16~~17). Moreover, eBC, CO, and NO_x have similar diurnal patterns as HOA, with two maxima (early in the morning (09:00) and early in the evening (18:00), Fig. SI-~~17~~18), which is typical for car emissions and/or house heating using fossil fuel. Correlation between HOA and eBC must be carefully interpreted, since periods with similar trends alternate with periods of very different covariance (Fig. 5). This clearly indicates the presence of other eBC related sources, as will be discussed later on. On average, over the whole period, HOA contributed 3 ± 3 % (mean ± standard deviation) of the total organic mass concentration, designating HOA as a minor source of OA at the sampling place. A clear dependency of HOA contribution on OA and temperature was observed (Fig. 6), ranging from around 1 % during the warmest period up to 5 % for the coldest period. This temperature dependency indicates that HOA should be mostly associated with local residential house heating rather than a significant increase in car emissions. Moreover, the low temperature period can also lead to an artificial increase of the HOA concentration by slowing down the evaporation process of the emitted particles as well as their oxidation processes. Finally, the cold period was also associated with low wind speed and stable stratification (Fig. 1) (Tilgner et al., 2014), which might also contribute to higher concentrations of locally emitted aerosol by reducing both mixing and transport processes.~~than car exhaust~~.

3.2.2 BBOA

The BBOA factor (13.3 ± 10.0 % of the total OA) is related to biomass burning emissions and its mass spectrum is characterized by the presence of two specific fragments: $C_2H_4O_2^+$ at m/z 60 and $C_3H_5O_2^+$ at m/z 73 (Fig. 5); they are known to be related to anhydrous sugars like levoglucosan (e.g. Schneider et al., 2006). This is confirmed by the correlation observed in off-line levoglucosan ($R^2 = 0.84$, Fig. SI-~~16~~17). The elemental ratios of the BBOA factor correspond with the lower range of all the reported values in Canagaratna et al. (2015). Although BBOA mass spectrum is influenced by the type of wood used, the combustion conditions, as well as the wetness of the wood (Ortega et al., 2013), the low O:C value of the BBOA factor indicates that it is mostly freshly emitted. BBOA also correlates with specific NMHC compounds like ethane ($R^2 = 0.34$), ethylene ($R^2 = 0.55$), *m,p*-xylene ($R^2 = 0.32$), and more generally with the total alkenes ($R^2 = 0.40$), as previously reported by Gaeggeler et al. (2008) and Schauer and Cass (2000). Similarly to HOA, the BBOA fraction to total OA increases with the

8

decrease of the temperature, representing almost 20 % of the OA during the coldest period (Fig. 6). The correlation between BBOA and HOA ($R^2 = 0.86$) clearly indicates that these two factors are emitted from a similar origin. This supports our conclusions on the HOA as being mostly associated with residential house heating.

255 Wood combustion used for residential house heating dominates the local anthropogenic emissions in the surrounding area of the sampling place. This is in agreement with the reported BBOA contribution of 20 % for a similar place in Germany in winter (Poulain et al., 2011). The predominance of biomass burning emissions compared to liquid fuel is also supported by the benzene to toluene ratio value during the IOPs (mean: 1.1, min.: 0.47, max.:2.65), which is comparable to the ratio reported by Gaeggeler et al. (2008) for a similar location in Switzerland.

260

Overall, the sum of the primary OA (POA = HOA + BBOA) were principally associated with back-trajectory clusters C1-West and C2-Northwest (20-25 % of OA) (see section 3.4), while they only contribute < 11 % to the other clusters. Consequently, taking all of them together, the C1-West and C2-Northwest clusters might be impacted by the village of Goldlauter, as discussed later in section 3.4.

265 **3.2.3 SV-OOA**

The SV-OOA was identified according to the relative similarity of its time series with nitrate ($R^2 = 0.40$) and its diurnal profile, which shows the highest concentrations during nighttime, a decrease in the early morning hours, and a minimum during daytime (Fig. SI-~~17~~18). The SV-OOA mass spectrum is characterized by a higher contribution of the ions $C_2H_3O^+$ (m/z 43) compared to CO_2^+ (m/z 44). The elemental analysis of the SV-OOA mass spectra shows an O:C of 0.40 and a H:C of 1.70

270 (Fig. 5), which is in the lowest range of the reported SV-OOA values from Canagaratna et al. (2015). Its MS is also similar to the median SV-OOA mass spectra based on 25 AMS measurements over Europe ($R^2 = 0.69$) described by Crippa et al. (2014). The difference was mainly attributed to a smaller contribution of the CO_2^+ ion (m/z 44) on our factor. On average, throughout the entire sampling period, SV-OOA represented 19 ± 11 % of the total OA, ranging from 12 to 22 %, with a clear temperature dependency similar to the POAs (Fig. 6). Nevertheless, this is in agreement with the fact that SV-OOA is generally associated

275 with gas-to-particle partitioning of semi-volatile organic compounds (*e.g.* Ulbrich et al., 2009;Zhang et al., 2011). Consequently, it has to be related to a more local and /or regional influence. Interestingly, SV-OOA also correlates with anthropogenic NMHC gases like toluene ($R^2 = 0.55$), *i*-pentane ($R^2 = 0.52$), benzene ($R^2 = 0.46$), as well as the sum of aromatics NMHC ($R^2 = 0.60$) (Fig. SI-~~18~~19). This correlation may be a consequence of the presence of semi-volatile organic compounds and intermediate volatility organic compounds (VOCs and IVOCs, respectively) either directly emitted from anthropogenic

280 sources or resulting from the dilution of the POA (e.g. Lipsky and Robinson, 2006;May et al., 2013). Ambient relative humidity and, subsequently, aerosol liquid water content seem to be two of the essential parameters driving the partitioning of the anthropogenic VOCs and IVOCs in the particle phase (Murphy et al., 2017). Therefore, correlations between SV-OOA and NMHC might be results from the condensation of semi-volatile compounds emitted by anthropogenic sources.

9

3.2.4 OOAs

285 Finally, the two OOAs referred to as low-oxidized oxygenated organic aerosol (LO-OOA) and more-oxidized oxygenated organic aerosol (MO-OOA) were identified during an early stage of the source apportionment analysis, as discussed in the supplementary information (section SI-5). They present two distinct time series and mass spectra, indicating two different sources rather than an artificial splitting by the model (Fig. 5). Both are characterized by a high contribution of mass m/z 44 (mostly CO_2^+), while only LO-OOA has a strong contribution of m/z 43 (mostly $C_2H_3O^+$). Their elemental ratios reflect this

290 difference. MO-OOA is more oxygenated (O:C = 0.89) than LO-OOA (O:C = 0.58). The difference between the two OOAs might be related to either different precursors or aging processes.

The two OOAs are the two most important contributors to the total OA fraction (28 ± 12 % and 37 ± 18 % of the OA for MO-OOA and LO-OOA, respectively). However, their individual relative contributions strongly vary over time. LO-OOA dominated at the beginning of the measurement period and contributed up to ca. 60 % of OA (Fig. 5). The fragment $C_7H_7^+$

295 (m/z 91) was frequently associated with biogenic SOA, even though it cannot be considered as a specific tracer (Lee et al., 2016). $C_7H_7^+$ arises from the fragmentation of aromatic compounds and can, therefore, have several sources. Here, the contribution of $C_7H_7^+$ to total OA (f_{91}) is higher in LO-OOA than MO-OOA, which might indicate a larger contribution of biogenic SOA to LO-OOA. Opposite to the anthropogenic related factors, the mass fraction of LO-OOA decreases with the decrease of temperature (Fig. 6).

300

This can be associated with the decrease of the biogenic VOC emissions from late summer to early winter (Helmig et al., 2013). The impact of biogenic sources is also supported by the air mass cluster analysis, which associated the highest fraction of LO-OOA with a cluster with the highest RIT over natural vegetation (Table 1 and discussion in section 3.4).

In contrast, MO-OOA does not show a pronounced temperature dependency, but it strongly correlates with eBC (R^2 = 0.79,

305 Fig. 5 and SI-~~16~~17), which is higher than the coefficient correlation for the POA factors. MO-OOA also correlates better with oxalic acid (R^2 = 0.81) than LO-OOA (R^2 = 0.65) (not shown). Moreover, MO-OOA correlates moderately with SO_2 (R^2 = 0.35), suggesting an anthropogenic influence. It is known that the aging of primary OA leads to mass spectra with a similar pattern to OOA (Jimenez et al., 2009). Consequently, MO-OOA can be identified as being related to processed polluted/anthropogenic air masses from long-range transport.

310 **3.3 Equivalent black carbon (eBC) source apportionment**

As mentioned before, eBC correlated with three different organic factors (HOA, BBOA, and MO-OOA) identified during source apportionment analysis. Taken together, the sum of these factors correlates strongly with eBC (R^2 = 0.83) as shown in Figure 7-a. Therefore, using a multilinear regression model, the different sources of eBC were assessed for each factor following Laborde et al. (2013) and Zhu et al. (2018). The assumption made here is that the eBC mass is attributed to individual

315 contribution of each OA factor (i.e. eBC$_{HOA}$, eBC$_{BBOA}$, and eBC$_{MO-OOA}$) at any time as following:

$$eBC(t) = eBC_{HOA}(t) + eBC_{BBOA}(t) + eBC_{MO-OOA}(t) \qquad (1)$$

The eBC emission related to each source is assumed to be proportional to the individual source mass concentration released
320 (m_{HOA}, m_{BBOA}, and m_{MO-OOA}, respectively). Therefore, the multilinear regression model could be explained as follows:

$$eBC(t) = a\, m_{HOA}(t) + b\, m_{BBOA}(t) + c\, m_{MO-OOA}(t) \qquad (2)$$

Where a, b, and c respectively represent the linear regression coefficient for m_{HOA}, m_{BBOA}, and m_{MO-OOA}, which will be used
325 to estimate the respective eBC contribution towards each OA factor.

A very good correlation between measured and modeled eBC was obtained (Figure 7-b), and modeled eBC explained 96 % of the measured one. Based on this approach, long-range transport particles associated with MO-OOA are the largest source of eBC during the measurement period, contributing to half of it (52 %), while eBC associated with local emissions of HOA and BBOA represents 35 % and 13 %, respectively. Considering only local eBC sources, fossil fuel combustion dominates the
330 eBC fraction (73 % for eBC_{HOA} and 27 % for eBC_{BBOA}), which in agreement with previous works (e.g. Healy et al., 2012;Herich et al., 2011).

Using single-particle mass spectrometer measurements, Healy et al. (2012) reported that size distribution of EC can also directly be used to apportion soot sources: a local EC source was related to particles with a vacuum aerodynamic diameter
335 (d_{va}) of < 400 nm, while continental transported soot was related to particles with d_{va} > of 400 nm. A similar cut-off diameter was applied to the Berner-impactor measurements to split the EC into freshly emitted and transported one, assuming that the first two stages (i.e. aerodynamic diameter ranging from 50 to 420 nm) were associated with the local EC, and the three larger ones (i.e. diameter ranging from 420 nm to 10 µm) with continental transport (Fig. 8). The resulting EC classification provides quite similar results than the one discussed before and using the multilinear regression approach (Fig. 8) with an uncertainty
340 of approximately 20 % (mean ratio between the two approaches excluding FCE 11.2) supporting our conclusions. Only FCE 11.2 provides completely different results between the two approaches without any clear explanation. In summary, comparisons between the two approaches (multilinear regression and impactor size ~~cutting~~cutt-off) support each other and both confirm the importance of a minimum near 400 nm (in aerodynamic diameter) in EC size distribution for distinguishing freshly emitted from long-range transported soot. The importance of long-range continental transport of soot is also in
345 agreement with the measurements made by Roth et al. (2016) at the summit station by the ALABAMA. The authors reported that soot was mainly found in particles with diameters larger than 450 nm, which correspond with aged/processed soot.

11

3.4 Influence of air mass origin to chemical composition and particle number size distribution

A total of 6 clusters was obtained based on 96 h backward air mass trajectories (Fig. 9) and they are characterized in Table 1 by their residence time index (RTI) over different types of ground before reaching the sampling place, based on the approach described in van Pinxteren et al. (2010), and their meteorological conditions. Cluster C1-West and C2-Northwest correspond to two different types of marine-influenced air masses with RTI_{water} of 0.34 and 0.47, respectively. C1-West starts near Iceland, while C2-Northwest comes from the Norwegian Sea. These trajectories occurred during 31 % and 17 %, respectively, of the measurement period. Although the cluster C3-Southwest (18 % of the time) also contains a maritime component at the starting point of the air masses (RTI_{water} = 0.12), it is dominated by an RTI associated with continental areas (France and South-Germany). Cluster C4-South is characteristic of southern Europe, coming from an industrial and polluted area of northern Italia via Austria and the south of Germany. It also presents the highest RTI (0.51) related to natural vegetation (i.e. forest). Furthermore, it corresponds to the warm period. However, this cluster only occurs for a short period (8 % of the total sampling period). Cluster C5-Northeast is an issue of the boreal area (north of Sweden), spending some time over the Baltic Sea (near Finnish, Latvian, and Polish coasts) before entering the north of Germany. Although it might also contain a small maritime component (RTI_{water} = 0.18), this cluster mostly follows coastal areas. Therefore, it should present an important continental and polluted aspect. Similar to C4-South, it is not very common (9 % of the sampling period). Finally, C6-East clearly represents continental air masses coming from the east side of Europe (crossing Russia, Ukraine, Poland, and the Czech Republic). The sampling site was under its influence 17 % of the time, mostly during the second part of the experiment. Not surprisingly, the air mass clusters with the highest continental background (C3-Southwest, C4-South, and C6-East) also correspond with the ones with the highest aerosol particle mass concentrations (Table 1).

The aerosol particle chemical composition, number size distribution (PNSD), and trace gases were averaged according to the different air mass clusters and are presented in Figure 10, and summarized in the supplementary information (Table SI-4). The highest particle mass concentrations were observed for clusters with the strongest continental influence (i.e. C3-Southwest, 11.5 µg m^{-3}; C4-South, 11.4 µg m^{-3}, and C6-East 12.6 µg m^{-3}). The largest mass concentrations of chloride, sodium, and potassium salts were associated with C1-West and C2-Northwest, which have the largest marine influence (Fig. 10 and Table 1). These two clusters also correspond to the periods with the lowest particle mass (7.5 µg m^{-3} and 6.4 µg m^{-3}, respectively) and trace gas concentrations (Table SI-4). Although the lowest absolute and relative mass concentrations of organics ($\approx$ 30 %) and eBC (7-8 %) were also observed for these two clusters, they show the largest fraction of anthropogenic sources (HOA $\approx$ 4 % and BBOA 15-20 % of OA). The average particle number size distributions for these two clusters present the highest concentration of Aitken mode particles (centering on 40-50 nm), supporting the influence of local anthropogenic emissions. Increasing the RTI value of the air masses over continental areas leads to an increase of the carbonaceous fraction in both absolute and relative mass concentrations. The highest mass concentrations of OA and eBC are associated with C4-South (5.4 µg m^{-3} and 1.0 µg m^{-3}, respectively) and C6-East (5.8 µg m^{-3} and 1.3 µg m^{-3}, respectively). The averaged particle size

12

380 distribution for C3-Southwest and C4-South are almost unimodal, centering on 100 nm, indicating well-processed particles not impacted by local anthropogenic sources. The highest mass concentrations of eBC and OA are both linked to air masses coming from eastern Europe (C6-East). This is also true in regard to gas composition since the cluster C6-East also shows the highest concentrations of SO_2, HNO_3, and O_3 (Table SI-4). Interestingly, the different nucleation events observed during the sampling period (Wu et al., 2015) were mainly connected to clusters C5-Northeast and C6-East, as reflected by the large

385 contribution of the smallest particle diameters (nucleation mode) to their respective PNSD profiles, which did not appear on the other clusters. Nucleation processes strongly depend on the sulfuric acid formation (Kulmala et al., 2004;Birmili et al., 2003), which is certainly promoted by the SO_2 concentration. Finally, the two continental eastern clusters also show a large particle mode (approx. 200 nm), indicating long-range processed particles in agreement with the large fraction of MO-OOA and its associated eBC. Taken together, the aerosol particle and trace gas compositions of C6-East confirm the strong

390 anthropogenic influence on air masses originating from this sector, which is in agreement with long-term measurements performed at the German station of Melpitz located approximately 250 km to the north-east of the Goldlauter site (Spindler et al., 2013).

4 Summary and Conclusion

In the frame of the HCCT-2010 campaign, a detailed description of the aerosol particle chemical composition reaching the site

395 of Goldlauter was made by combining continuous online measurements (AMS, MARGA, MAAP, and MPSS) with offline impactor samples performed during specific IOPs. Merging online results from the AMS, MAAP, and MARGA together provides an hourly time-resolved chemical picture of the ambient PM_{10} composition. The consistency with the merged total PM_{10} mass and the one measured by the Berner-impactor highlight the fact that OA on the super-µm size range should be low, and non-considered species (i.e. dust, Calcium, Magnesium, and trace metals) should play a minor role in the total PM_{10} mass

400 during our study. A total of five factors were identified from the source apportionment of the OA, including two primary organic aerosols related to fossil fuel combustion, HOA (3 % of total OA), biomass burning combustion BBOA (13 %), and three oxygenated organic aerosols including a semi-volatile SV-OOA (19 %), a MO-OOA (28 %) associated with long-range transport of polluted continental air masses, and a LO-OOA (37 %) related to aged biogenic aerosol. Using the correlation between HOA, BBOA, and MO-OOA with eBC, a multilinear regression approach was applied to performed source

405 apportionment of eBC. This analysis highlights eBC contributions related to the source of HOA (35 %), BBOA (13 %), and MO-OOA (52 %). It was therefore possible to distinguish local eBC emissions (48 % of the total eBC) dominated by fossil fuel combustion (73 % of the local eBC) from long-range transported eBC. Size resolved EC from the Berner-impactor supports our founding and confirms the applicability of the size ~~cutting~~ cut-off at 400 nm for distinguishing local EC (< 400 nm) from transported EC (> 400 nm) as mentioned by Healy et al. (2012). Local sources of organic aerosol, appear to

410 play a smaller role compared to long-range transport, which is responsible for 65 % of OA. These results confirm the importance of long-range transport to the total mass concentration of OA and eBC not only during high pollution events (e.g.

13

van Pinxteren et al., 2019;Petit et al., 2017;Waked et al., 2018). HOA and BBOA are properly depicted by the primary anthropogenic sources of liquid fuel and biomass burning emissions, respectively. However, during their transport, aging processes will lead to signatures closer to OOA (Jimenez et al., 2009). A direct consequence is that the MO-OOA associated
415 with long-range transport of polluted air masses, might result from such aging processes of anthropogenic sources and it highlights the complexity of the internal chemical composition of the OOAs. Consequently, further efforts should be made in the future on the improvement of the OOAs' identification in order to properly distinguish between biogenic-SOA and anthropogenic-SOA, as well as between locally formed and transported SOA, which could be critical for rural and remote stations.
420

Data availability: All data is available upon request to the corresponding author.

Authors contributions: LP, FB, GS, KM, DvP, ZW, YI, collected the data, LP performed data analysis on the AMS, FB, GS, KM, DvP, ZW, YI contributed to the evaluation of the off-line chemical analysis dataset and WB evaluated the MPSS dataset.
425 All co-authors participated in the interpretation of the results. LP lead the writing of the manuscript to which all authors contributed.

Competing of interest: the authors declare that they have no conflict of interest.

References

Aiken, A. C., Decarlo, P. F., Kroll, J. H., Worsnop, D. R., Huffman, J. A., Docherty, K. S., Ulbrich, I. M., Mohr, C., Kimmel,
435 J. R., Sueper, D., Sun, Y., Zhang, Q., Trimborn, A., Northway, M., Ziemann, P. J., Canagaratna, M. R., Onasch, T. B., Alfarra, M. R., Prevot, A. S. H., Dommen, J., Duplissy, J., Metzger, A., Baltensperger, U., and Jimenez, J. L.: O/C and OM/OC ratios of primary, secondary, and ambient organic aerosols with high-resolution time-of-flight aerosol mass spectrometry, Environ. Sci. Technol., 42, 4478-4485, doi:10.1021/es703009q, 2008.
Allan, J., Delia, A. E., Coe, H., Bower, K. N., Alfarra, R. M., Jimenez, J. L., Middlebrook, A. M., Drewnick, F., Onasch, T.
440 B., Canagaratna, M. R., Jayne, J. T., and Worsnop, D. R.: A generalised method for the extraction of chemically resolved mass spectra from Aerodyne aerosol mass spectrometer data, J. Aerosol Sci., 35, 909 - 922, doi:10.1016/j.jaerosci.2004.02.007, 2004.

Berner, A., and Lurzer, C.: Mass Size Distributions of Traffic Aerosols at Vienna, J. Phys. Chem., 84, 2079-2083, doi 10.1021/j100453a016, 1980.

445   Birmili, W., Stratmann, F., and Wiedensohler, A.: Design of a DMA-based size spectrometer for a large particle size range and stable operation, J. Aerosol Sci., 30, 549-553, doi 10.1016/S0021-8502(98)00047-0, 1999.

Birmili, W., Berresheim, H., Plass-Dulmer, C., Elste, T., Gilge, S., Wiedensohler, A., and Uhrner, U.: The Hohenpeissenberg aerosol formation experiment (HAFEX): a long-term study including size-resolved aerosol, H_2SO_4, OH, and monoterpenes measurements, Atmos. Chem. Phys., 3, 361-376, doi: 10.5194/acp-3-361-2003, 2003.

450   Bohlmann, N., Meissner, R., Bernsdorf, S., Bohme, F., Russow, R., and Wegener, U.: Studies of atmospheric nitrogen deposition in a mire of the German National Park Hochharz Mountains using two different methods, Water Air Soil Poll., 168, 17-32, doi 10.1007/s11270-005-0587-0, 2005.

Bruns, E. A., Perraud, V., Zelenyuk, A., Ezell, M. J., Johnson, S. N., Yu, Y., Imre, D., Finlayson-Pitts, B. J., and Alexander, M. L.: Comparison of FTIR and Particle Mass Spectrometry for the Measurement of Particulate Organic Nitrates, Environ.

455   Sci. Technol., 44, 1056-1061, Doi 10.1021/Es9029864, 2010.

Burnett, R. T., Pope, C. A., Ezzati, M., Olives, C., Lim, S. S., Mehta, S., Shin, H. H., Singh, G., Hubbell, B., Brauer, M., Anderson, H. R., Smith, K. R., Balmes, J. R., Bruce, N. G., Kan, H. D., Laden, F., Pruss-Ustun, A., Michelle, C. T., Gapstur, S. M., Diver, W. R., and Cohen, A.: An Integrated Risk Function for Estimating the Global Burden of Disease Attributable to Ambient Fine Particulate Matter Exposure, Environ. Health Perspect., 122, 397-403, 2014.

460   Cabada, J. C., Pandis, S. N., and Robinson, A. L.: Sources of atmospheric carbonaceous particulate matter in Pittsburgh, Pennsylvania, J. Air Waste Manage. Assoc., 52, 732-741, doi 10.1080/10473289.2002.10470811, 2002.

Canagaratna, M. R., Jimenez, J. L., Kroll, J. H., Chen, Q., Kessler, S. H., Massoli, P., Ruiz, L. H., Fortner, E., Williams, L. R., Wilson, K. R., Surratt, J. D., Donahue, N. M., Jayne, J. T., and Worsnop, D. R.: Elemental ratio measurements of organic compounds using aerosol mass spectrometry: characterization, improved calibration, and implications, Atmos. Chem. Phys.,

465   15, 253-272, doi 10.5194/acp-15-253-2015, 2015.

Canonaco, F., Crippa, M., Slowik, J. G., Prévôt, A. S. H., and Baltensperger, U.: SoFi, an IGOR-based interface for the efficient use of the generalized multilinear engine (ME-2) for the source apportionment: ME-2 application to aerosol mass spectrometer data, Atmos. Meas. Tech., 6, 3649-3661, doi:10.5194/amt-6-3649-2013, 2013.

Carslaw, D. C., and Ropkins, K.: openair - An R package for air quality data analysis, Environ. Modell. Softw., 27-28, 52-61,

470   2012.

Crippa, M., Canonaco, F., Lanz, V. A., Äijälä, M., Allan, J. D., Carbone, S., Capes, G., Ceburnis, D., Dall'Osto, M., Day, D. A., DeCarlo, P. F., Ehn, M., Eriksson, A., Freney, E., Hildebrandt Ruiz, L., Hillamo, R., Jimenez, J. L., Junninen, H., Kiendler-Scharr, A., Kortelainen, A. M., Kulmala, M., Laaksonen, A., Mensah, A. A., Mohr, C., Nemitz, E., O'Dowd, C., Ovadnevaite, J., Pandis, S. N., Petäjä, T., Poulain, L., Saarikoski, S., Sellegri, K., Swietlicki, E., Tiitta, P., Worsnop, D. R., Baltensperger,

475   U., and Prévôt, A. S. H.: Organic aerosol components derived from 25 AMS data sets across Europe using a consistent ME-2 based source apportionment approach, Atmos. Chem. Phys., 14, 6159-6176, doi:10.5194/acp-14-6159-2014, 2014.

15

Dasgupta, P. K., Campbell, S. W., Al-Horr, R. S., Ullah, S. M. R., Li, J. Z., Amalfitano, C., and Poor, N. D.: Conversion of sea salt aerosol to $NaNO_3$ and the production of HCl: Analysis of temporal behavior of aerosol chloride/nitrate and gaseous HCl/HNO_3 concentrations with AIM, Atmos. Environ., 41, 4242-4257, doi 10.1016/j.atmosenv.2006.09.054, 2007.

480 DeCarlo, P. F., Kimmel, J. R., Trimborn, A., Northway, M. J., Jayne, J. T., Aiken, A. C., Gonin, M., Fuhrer, K., Horvath, T., Docherty, K. S., Worsnop, D. R., and Jimenez, J. L.: Field-deployable, high-resolution, time-of-flight aerosol mass spectrometer, Anal. Chem., 78, 8281-8289, doi 10.1021/ac061249n, 2006.

Donahue, N. M., Robinson, A. L., Trump, E. R., Riipinen, I., and Kroll, J. H.: Volatility and Aging of Atmospheric Organic Aerosol, in: Atmospheric and Aerosol Chemistry, edited by: McNeill, V. F., and Ariya, P. A., Springer Berlin Heidelberg,

485 Berlin, Heidelberg, 97-143, 2014.

Draxler, R., and Hess, G.: Description of the HYSPLIT4 modeling system, NOAA Technical Memorandum, ERL, ARL-224, 2004.

Farmer, D. K., Matsunaga, A., Docherty, K. S., Surratt, J. D., Seinfeld, J. H., Ziemann, P. J., and Jimenez, J. L.: Response of an aerosol mass spectrometer to organonitrates and organosulfates and implications for atmospheric chemistry, Proc. Nat.

490 Acad. Sci., 107, 6670-6675, doi 10.1073/pnas.0912340107, 2010.

Farmer, D. K., Cappa, C. D., and Kreidenweis, S. M.: Atmospheric Processes and Their Controlling Influence on Cloud Condensation Nuclei Activity, Chem. Rev., 115, 4199-4217, doi 10.1021/cr5006292, 2015.

Gaeggeler, K., Prevot, A. S. H., Dommen, J., Legreid, G., Reimann, S., and Baltensperger, U.: Residential wood burning in an Alpine valley as a source for oxygenated volatile organic compounds, hydrocarbons and organic acids, Atmos. Environ.,

495 42, 8278-8287, doi 10.1016/j.atmosenv.2008.07.038, 2008.

Harris, E., Sinha, B., van Pinxteren, D., Tilgner, A., Fomba, K. W., Schneider, J., Roth, A., Gnauk, T., Fahlbusch, B., Mertes, S., Lee, T., Collett, J., Foley, S., Borrmann, S., Hoppe, P., and Herrmann, H.: Enhanced Role of Transition Metal Ion Catalysis During In-Cloud Oxidation of SO_2, Science, 340, 727-730, doi 10.1126/science.1230911 2013.

Healy, R. M., Sciare, J., Poulain, L., Kamili, K., Merkel, M., Muller, T., Wiedensohler, A., Eckhardt, S., Stohl, A., Sarda-

500 Esteve, R., McGillicuddy, E., O'Connor, I. P., Sodeau, J. R., and Wenger, J. C.: Sources and mixing state of size-resolved elemental carbon particles in a European megacity: Paris, Atmos. Chem. Phys., 12, 1681-1700, doi 10.5194/acp-12-1681-2012, 2012.

Heintzenberg, J., Wiedensohler, A., Tuch, T. M., Covert, D. S., Sheridan, P., Ogren, J. A., Gras, J., Nessler, R., Kleefeld, C., Kalivitis, N., Aaltonen, V., Wilhelm, R. T., and Havlicek, M.: Intercomparisons and aerosol calibrations of 12 commercial

505 integrating nephelometers of three manufacturers, J. Atmos. Ocean. Tech., 23, 902-914, 2006.

Helmig, D., Daly, R. W., Milford, J., and Guenther, A.: Seasonal trends of biogenic terpene emissions, Chemosphere, 93, 35-46, 10.1016/j.chemosphere.2013.04.058, 2013.

Herich, H., Hueglin, C., and Buchmann, B.: A 2.5 year's source apportionment study of black carbon from wood burning and fossil fuel combustion at urban and rural sites in Switzerland, Atmos. Meas. Tech., 4, 1409-1420, 2011.

16

510   Herrmann, H., Wolke, R., Muller, K., Bruggemann, E., Gnauk, T., Barzaghi, P., Mertes, S., Lehmann, K., Massling, A., Birmili, W., Wiedensohler, A., Wierprecht, W., Acker, K., Jaeschke, W., Kramberger, H., Svrcina, B., Bachmann, K., Collett, J. L., Galgon, D., Schwirn, K., Nowak, A., van Pinxteren, D., Plewka, A., Chemnitzer, R., Rud, C., Hofmann, D., Tilgner, A., Diehl, K., Heinold, B., Hinneburg, D., Knoth, O., Sehili, A. M., Simmel, M., Wurzler, S., Majdik, Z., Mauersberger, G., and Muller, F.: FEBUKO and MODMEP: Field measurements and modelling of aerosol and cloud multiphase processes, Atmos.

515   Environ., 39, 4169-4183, 2005.

IPCC: Climate Change 2013: The Physical Science Basis. Contribution of Working Group I to the Fifth Assessment Report of the Intergovernmental Panel on Climate Change, Cambridge University Press, Cambridge, United Kingdom and New York, NY, USA, 1535 pp., 2013.

Jickells, T. D., An, Z. S., Andersen, K. K., Baker, A. R., Bergametti, G., Brooks, N., Cao, J. J., Boyd, P. W., Duce, R. A.,

520   Hunter, K. A., Kawahata, H., Kubilay, N., laRoche, J., Liss, P. S., Mahowald, N., Prospero, J. M., Ridgwell, A. J., Tegen, I., and Torres, R.: Global iron connections between desert dust, ocean biogeochemistry, and climate, Science, 308, 67-71, doi:10.1126/science.1105959, 2005.

Jimenez, J. L., Canagaratna, M. R., Donahue, N. M., Prevot, A. S. H., Zhang, Q., Kroll, J. H., DeCarlo, P. F., Allan, J. D., Coe, H., Ng, N. L., Aiken, A. C., Docherty, K. S., Ulbrich, I. M., Grieshop, A. P., Robinson, A. L., Duplissy, J., Smith, J. D., Wilson,

525   K. R., Lanz, V. A., Hueglin, C., Sun, Y. L., Tian, J., Laaksonen, A., Raatikainen, T., Rautiainen, J., Vaattovaara, P., Ehn, M., Kulmala, M., Tomlinson, J. M., Collins, D. R., Cubison, M. J., E, Dunlea, J., Huffman, J. A., Onasch, T. B., Alfarra, M. R., Williams, P. I., Bower, K., Kondo, Y., Schneider, J., Drewnick, F., Borrmann, S., Weimer, S., Demerjian, K., Salcedo, D., Cottrell, L., Griffin, R., Takami, A., Miyoshi, T., Hatakeyama, S., Shimono, A., Sun, J. Y., Zhang, Y. M., Dzepina, K., Kimmel, J. R., Sueper, D., Jayne, J. T., Herndon, S. C., Trimborn, A. M., Williams, L. R., Wood, E. C., Middlebrook, A. M., Kolb, C.

530   E., Baltensperger, U., and Worsnop, D. R.: Evolution of organic aerosols in the atmosphere, Science, 326, 1525-1529, doi:10.1126/science.1180353, 2009.

Kulmala, M., Vehkamaki, H., Petaja, T., Dal Maso, M., Lauri, A., Kerminen, V. M., Birmili, W., and McMurry, P. H.: Formation and growth rates of ultrafine atmospheric particles: a review of observations, J. Aerosol Sci., 35, 143-176, DOI 10.1016/j.jaerosci.2003.10.003, 2004.

535   Laborde, M., Crippa, M., Tritscher, T., Juranyi, Z., Decarlo, P. F., Temime-Roussel, B., Marchand, N., Eckhardt, S., Stohl, A., Baltensperger, U., Prevot, A. S. H., Weingartner, E., and Gysel, M.: Black carbon physical properties and mixing state in the European megacity Paris, Atmos. Chem. Phys., 13, 5831-5856, 2013.

Lee, A. K. Y., Abbatt, J. P. D., Leaitch, W. R., Li, S. M., Sjostedt, S. J., Wentzell, J. J. B., Liggio, J., and Macdonald, A. M.: Substantial secondary organic aerosol formation in a coniferous forest: observations of both day- and nighttime chemistry,

540   Atmos. Chem. Phys., 16, 6721-6733, 10.5194/acp-16-6721-2016, 2016.

Lelieveld, J., Evans, J. S., Fnais, M., Giannadaki, D., and Pozzer, A.: The contribution of outdoor air pollution sources to premature mortality on a global scale, Nature, 525, 367-+, 2015.

Liakakou, E., Kaskaoutis, D. G., Grivas, G., Stavroulas, I., Tsagkaraki, M., Paraskevopoulou, D., Bougiatioti, A., Dumka, U. C., Gerasopoulos, E., and Mihalopoulos, N.: Long-term brown carbon spectral characteristics in a Mediterranean city (Athens), Sci. Total Environ., 708, 2020.

Lipsky, E. M., and Robinson, A. L.: Effects of dilution on fine particle mass and partitioning of semivolatile organics in diesel exhaust and wood smoke, Environ. Sci. Technol., 40, 155-162, 10.1021/es050319p, 2006.

Makkonen, U., Virkkula, A., Mantykentta, J., Hakola, H., Keronen, P., Vakkari, V., and Aalto, P. P.: Semi-continuous gas and inorganic aerosol measurements at a Finnish urban site: comparisons with filters, nitrogen in aerosol and gas phases, and aerosol acidity, Atmos. Chem. Phys., 12, 5617-5631, 2012.

Martinsson, J., Azeem, H. A., Sporre, M. K., Bergstrom, R., Ahlberg, E., Ostrom, E., Kristensson, A., Swietlicki, E., and Stenstrom, K. E.: Carbonaceous aerosol source apportionment using the Aethalometer model - evaluation by radiocarbon and levoglucosan analysis at a rural background site in southern Sweden, Atmos. Chem. Phys., 17, 4265-4281, 10.5194/acp-17-4265-2017, 2017.

May, A. A., Levin, E. J. T., Hennigan, C. J., Riipinen, I., Lee, T., Collett, J. L., Jimenez, J. L., Kreidenweis, S. M., and Robinson, A. L.: Gas-particle partitioning of primary organic aerosol emissions: 3. Biomass burning, Journal of Geophysical Research-Atmospheres, 118, 11327-11338, 10.1002/jgrd.50828, 2013.

Middlebrook, A. M., Bahreini, R., Jimenez, J. L., and Canagaratna, M. R.: Evaluation of Composition-Dependent Collection Efficiencies for the Aerodyne Aerosol Mass Spectrometer using Field Data, Aerosol Sci. Technol., 46, 258-271, doi:10.1080/02786826.2011.620041, 2012.

Mohr, C., DeCarlo, P. F., Heringa, M. F., Chirico, R., Slowik, J. G., Richter, R., Reche, C., Alastuey, A., Querol, X., Seco, R., Penuelas, J., Jimenez, J. L., Crippa, M., Zimmermann, R., Baltensperger, U., and Prevot, A. S. H.: Identification and quantification of organic aerosol from cooking and other sources in Barcelona using aerosol mass spectrometer data, Atmos. Chem. Phys., 12, 1649-1665, 2012.

Moise, T., Flores, J. M., and Rudich, Y.: Optical Properties of Secondary Organic Aerosols and Their Changes by Chemical Processes, Chem. Rev., 115, 4400-4439, 2015.

Murphy, B. N., Woody, M. C., Jimenez, J. L., Carlton, A. M. G., Hayes, P. L., Liu, S., Ng, N. L., Russell, L. M., Setyan, A., Xu, L., Young, J., Zaveri, R. A., Zhang, Q., and Pye, H. O. T.: Semivolatile POA and parameterized total combustion SOA in CMAQv5.2: impacts on source strength and partitioning, Atmos. Chem. Phys., 17, 11107-11133, 10.5194/acp-17-11107-2017, 2017.

Paatero, P.: The multilinear engine - A table-driven, least squares program for solving multilinear problems, including the n-way parallel factor analysis model, J. Comput. Graph. Stat., 8, 854-888, doi:10.2307/1390831, 1999.

Petit, J. E., Amodeo, T., Meleux, F., Bessagnet, B., Menut, L., Grenier, D., Pellan, Y., Ockler, A., Rocq, B., Gros, V., Sciare, J., and Favez, O.: Characterising an intense PM pollution episode in March 2015 in France from multi-site approach and near real time data: Climatology, variabilities, geographical origins and model evaluation, Atmos. Environ., 155, 68-84, doi:10.1016/j.atmosenv.2017.02.012, 2017.

18

Petzold, A., and Schönlinner, M.: Multi-angle absorption photometry - a new method for the measurement of aerosol light absorption and atmospheric black carbon, J. Aerosol Sci., 35, 421-441, doi: 10.1016/j.jaerosci.2003.09.005, 2004.

Pope, C. A., Brook, R. D., Burnett, R. T., and Dockery, D. W.: How is cardiovascular disease mortality risk affected by duration and intensity of fine particulate matter exposure? An integration of the epidemiologic evidence, Air Quality Atmosphere and Health, 4, 5-14, 2011.

Poulain, L., Iinuma, Y., Müller, K., Birmili, W., Weinhold, K., Bruggemann, E., Gnauk, T., Hausmann, A., Löschau, G., Wiedensohler, A., and Herrmann, H.: Diurnal variations of ambient particulate wood burning emissions and their contribution to the concentration of Polycyclic Aromatic Hydrocarbons (PAHs) in Seiffen, Germany, Atmos. Chem. Phys., 11, 12697-12713, doi: 10.5194/acp-11-12697-2011, 2011.

Rappenglück, B., Apel, E., Bauerfeind, M., Bottenheim, J., Brickell, P., Cavolka, P., Cech, J., Gatti, L., Hakola, H., Honzak, J., Junek, R., Martin, D., Noone, C., Plass-Dülmer, C., Travers, D., and Wang, D.: The first VOC intercomparison exercise within the Global Atmosphere Watch (GAW), Atmos. Environ., 40, 7508-7527, 2006.

Ropkins, K., and Carslaw, D. C.: openair - Data Analysis Tools for the Air Quality Community, R Journal, 4, 20-29, 2012.

Roth, A., Schneider, J., Klimach, T., Mertes, S., van Pinxteren, D., Herrmann, H., and Borrmann, S.: Aerosol properties, source identification, and cloud processing in orographic clouds measured by single particle mass spectrometry on a central European mountain site during HCCT-2010, Atmos. Chem. Phys., 16, 505-524, 2016.

Rumsey, I. C., Cowen, K. A., Walker, J. T., Kelly, T. J., Hanft, E. A., Mishoe, K., Rogers, C., Proost, R., Beachley, G. M., Lear, G., Frelink, T., and Otjes, R. P.: An assessment of the performance of the Monitor for AeRosols and GAses in ambient air (MARGA): a semi-continuous method for soluble compounds, Atmos. Chem. Phys., 14, 5639-5658, 2014.

Sandradewi, J., Prevot, A. S. H., Szidat, S., Perron, N., Alfarra, M. R., Lanz, V. A., Weingartner, E., and Baltensperger, U.: Using aerosol light absorption measurements for the quantitative determination of wood burning and traffic emission contributions to particulate matter, Environ. Sci. Technol., 42, 3316-3323, doi:10.1021/Es702253m, 2008.

Schauer, J. J., and Cass, G. R.: Source apportionment of wintertime gas-phase and particle-phase air pollutants using organic compounds as tracers, Environ. Sci. Technol., 34, 1821-1832, 2000.

Schlag, P., Kiendler-Scharr, A., Blom, M. J., Canonaco, F., Henzing, J. S., Moerman, M., Prevot, A. S. H., and Holzinger, R.: Aerosol source apportionment from 1-year measurements at the CESAR tower in Cabauw, the Netherlands, Atmos. Chem. Phys., 16, 8831-8847, 10.5194/acp-16-8831-2016, 2016.

Schneider, J., Weimer, S., Drewnick, F., Borrmann, S., Helas, G., Gwaze, P., Schmid, O., Andreae, M. O., and kirchner, U.: Mass spectrometric analysis and aerodynamic properties of various types of combustion-related aerosol particles, Int. J. Mass. Spectrom., 258, 37-49, doi:10.1016/j.ijms.2006.07.008, 2006.

Spindler, G., Grüner, A., Müller, K., Schlimper, S., and Herrmann, H.: Long-term size-segregated particle (PM$_{10}$, PM$_{2.5}$, PM$_1$) characterization study at Melpitz - influence of air mass inflow, weather conditions and season, J. Atmos. Chem., 70, 165-195, doi:10.1007/s10874-013-9263-8, 2013.

610 Srivastava, D., Tomaz, S., Favez, O., Lanzafame, G. M., Golly, B., Besombes, J. L., Alleman, L. Y., Jaffrezo, J. L., Jacob, V., Perraudin, E., Villenave, E., and Albinet, A.: Speciation of organic fraction does matter for source apportionment. Part 1: A one-year campaign in Grenoble (France), Sci. Total Environ., 624, 1598-1611, 10.1016/j.scitotenv.2017.12.135, 2018.

Srivastava, D., Favez, O., Petit, J. E., Zhang, Y., Sofowote, U. M., Hopke, P. K., Bonnaire, N., Perraudin, E., Gros, V., Villenave, E., and Albinet, A.: Speciation of organic fractions does matter for aerosol source apportionment. Part 3: Combining

615 off-line and on-line measurements, Sci. Total Environ., 690, 944-955, 10.1016/j.scitotenv.2019.06.378, 2019.

Stieger, B., Spindler, G., Fahlbusch, B., Müller, K., Grüner, A., Poulain, L., Thöni, L., Seitler, E., Wallasch, M., and Herrmann, H.: Measurements of PM_{10} ions and trace gases with the online system MARGA at the research station Melpitz in Germany – A five-year study, J. Atmos. Chem., 10.1007/s10874-017-9361-0, 2017.

Stieger, B., Spindler, G., Fahlbusch, B., Muller, K., Gruner, A., Poulain, L., Thoni, L., Seitler, E., Wallasch, M., and Herrmann,

620 H.: Measurements of PM10 ions and trace gases with the online system MARGA at the research station Melpitz in Germany - A five-year study, J. Atmos. Chem., 75, 33-70, doi:10.1007/s10874-017-9361-0, 2018.

Tilgner, A., Schone, L., Brauer, P., van Pinxteren, D., Hoffmann, E., Spindler, G., Styler, S. A., Mertes, S., Birmili, W., Otto, R., Merkel, M., Weinhold, K., Wiedensohler, A., Deneke, H., Schrodner, R., Wolke, R., Schneider, J., Haunold, W., Engel, A., Weber, A., and Herrmann, H.: Comprehensive assessment of meteorological conditions and airflow connectivity during

625 HCCT-2010, Atmos. Chem. Phys., 14, 9105-9128, 10.5194/acp-14-9105-2014, 2014.

Tuch, T. M., Haudek, A., Müller, T., Nowak, A., Wex, H., and Wiedensohler, A.: Design and performance of an automatic regenerating adsorption aerosol dryer for continuous operation at monitoring sites, Atmos. Meas. Tech., 2, 417-422, doi:10.5194/amt-2-417-2009, 2009.

Twigg, M. M., Di Marco, C. F., Leeson, S., van Dijk, N., Jones, M. R., Leith, I. D., Morrison, E., Coyle, M., Proost, R., Peeters,

630 A. N. M., Lemon, E., Frelink, T., Braban, C. F., Nemitz, E., and Cape, J. N.: Water soluble aerosols and gases at a UK background site - Part 1: Controls of PM2.5 and PM10 aerosol composition, Atmos. Chem. Phys., 15, 8131-8145, 2015.

Ulbrich, I. M., Canagaratna, M. R., Zhang, Q., Worsnop, D. R., and Jimenez, J. L.: Interpretation of organic components from Positive Matrix Factorization of aerosol mass spectrometric data, Atmos. Chem. Phys., 9, 2891-2918, doi:10.5194/acp-9-2891-2009, 2009.

635 van Pinxteren, D., Brüggemann, E., Gnauk, T., Müller, K., Thiel, C., and Herrmann, H.: A GIS based approach to back trajectory analysis for the source apportionment of aerosol constituents and its first application, J. Atmos. Chem., 67, 1-28, doi:10.1007/s10874-011-9199-9, 2010.

van Pinxteren, D., Fomba, K. W., Spindler, G., Muller, K., Poulain, L., Iinuma, Y., Loschau, G., Hausmann, A., and Herrmann, H.: Regional air quality in Leipzig, Germany: detailed source apportionment of size-resolved aerosol particles and comparison

640 with the year 2000, Faraday Discuss., 189, 291-315, doi: 10.1039/c5fd00228a, 2016.

van Pinxteren, D., Mothes, F., Spindler, G., Fomba, K. W., and Herrmann, H.: Trans-boundary PM10: Quantifying impact and sources during winter 2016/17 in eastern Germany, Atmos. Environ., 200, 119-130, doi:10.1016/j.atmosenv.2018.11.061, 2019.

Waked, A., Bourin, A., Michoud, V., Perdrix, E., Alleman, L. Y., Sauvage, S., Delaunay, T., Vermeesch, S., Petit, J. E., and

645   Riffault, V.: Investigation of the geographical origins of PM10 based on long, medium and short-range air mass back-trajectories impacting Northern France during the period 2009-2013, Atmos. Environ., 193, 143-152, doi:10.1016/j.atmosenv.2018.08.015, 2018.

Wu, Z. J., Poulain, L., Birmili, W., Gross, J., Niedermeier, N., Wang, Z. B., Herrmann, H., and Wiedensohler, A.: Some insights into the condensing vapors driving new particle growth to CCN sizes on the basis of hygroscopicity measurements,

650   Atmos. Chem. Phys., 15, 13071-13083, 2015.

Zhang, Q., Jimenez, J. L., Worsnop, D. R., and Canagaratna, M. R.: A case study of urban particle acidity and its influence on secondary organic aerosol, Environ. Sci. Technol., 41, 3213-3219, doi:10.1021/es061812j, 2007.

Zhang, Q., Jimenez, J. L., Canagaratna, M. R., Ulbrich, I. M., Ng, N. L., Worsnop, D. R., and Sun, Y. L.: Understanding atmospheric organic aerosols via factor analysis of aerosol mass spectrometry: a review, Anal. Bioanal. Chem., 401, 3045-

655   3067, 2011.

Zhu, Q., Huang, X. F., Cao, L. M., Wei, L. T., Zhang, B., He, L. Y., Elser, M., Canonaco, F., Slowik, J. G., Bozzetti, C., El-Haddad, I., and Prevot, A. S. H.: Improved source apportionment of organic aerosols in complex urban air pollution using the multilinear engine (ME-2), Atmos. Meas. Tech., 11, 1049-1060, 10.5194/amt-11-1049-2018, 2018.

660

Table 1: Properties of the different air mass clusters

	Cluster 1	Cluster 2	Cluster 3	Cluster 4	Cluster 5	Cluster 6
Air mass origin	West	Northwest	Southwest	South	Northeast	East
Frequency (%)	31	17	18	8	9	17
Average Residence Time Index (RTI)						
Water	0.34	0.47	0.12	0.6	0.18	0.4
Agriculture area	0.40	0.31	0.41	0.41	0.46	0.59
Natural vegetation	0.24	0.19	0.44	0.51	0.33	0.35
Urban area	0.2	0.2	0.1	0.1	0.2	0.2
Other global properties						
Average length (km)	3111	3438	2141	1716	2514	2561
Average solar radiation ($W\ m^{-2}$)	133	103	138	155	96	137
Average condition at the sampling site						
Temperature (°C)	7.7	5.6	11.3	22.8	6.2	7.4
RH (%)	91.6	92.7	89.6	90.5	88.2	72.0
Precipitation (mm)	0.30	0.16	0.18	0.08	0.08	0.17
Wind speed ($m\ s^{-1}$)	4.21	3.95	3.84	3.67	3.41	3.58
Particle mass concentration ($\mu g\ m^{-3}$)	7.54	6.38	11.50	11.38	7.97	12.64

Figure 1: Time series of the ambient temperature (a), estimated boundary layer height (BLH) obtained from HYSPLIT GDAS input (b), the particulate near-PM1 chemical composition as measured by the AMS and completed by MAAP for equivalent black carbon (c), the corresponding mass fraction (d), and particle number size distribution (e) during HCCT-2010 at the site of Goldlauter. The colored bars and numbers at the top refer to the six different air mass clusters (see section 3.4), and the grey bars refer to the different cloud and non-cloud events as defined in Table SI-2. Time series of the ambient temperature (a), the particulate near-PM1

23

chemical composition as measured by the AMS and completed by MAAP for equivalent black carbon (b), the corresponding mass fraction (c), and particle number size distribution (d) during HCCT-2010 at the site of Goldlauter. The colored bars and numbers at the top refer to the six different air mass clusters (see section 3.4), and the grey bars refer to the different cloud and non-cloud events as defined in Table SI-2.

675

Chemical species:
- OC (green)
- Nitrate (blue)
- Ammonium (orange)
- Sodium (light blue)
- Potassium (light gray)
- EC (dark gray)
- Sulfate (red)
- Chloride (pink)
- Magnesium (purple)
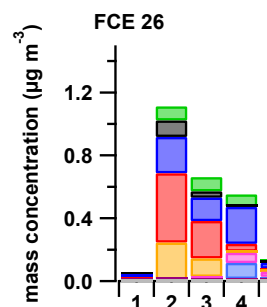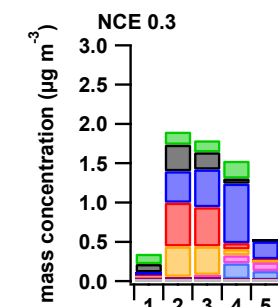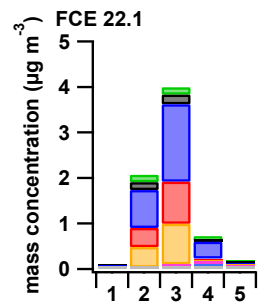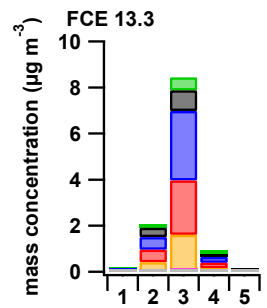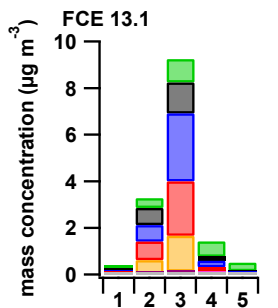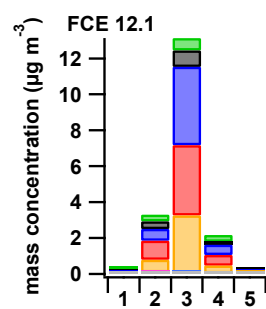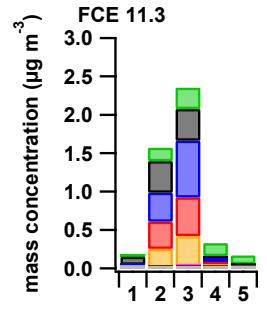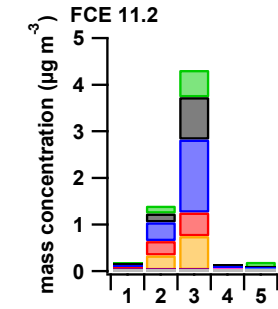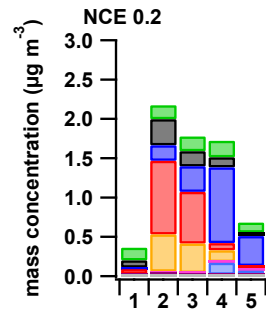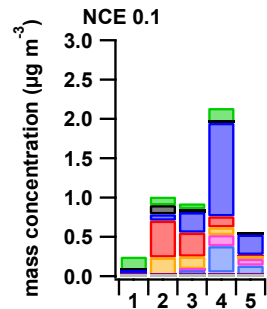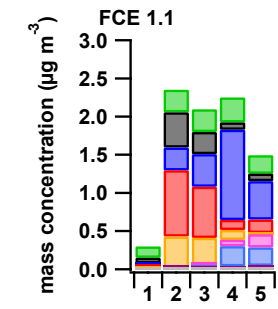
Size cutting:
stage 1 : 0.04 - 0.14 μm
stage 2 : 0.14 - 0.42 μm
stage 3 : 0.42 - 1.2 μm
stage 4 : 1.2 - 3.5 μm
stage 5 : 3.5 - 10 μm
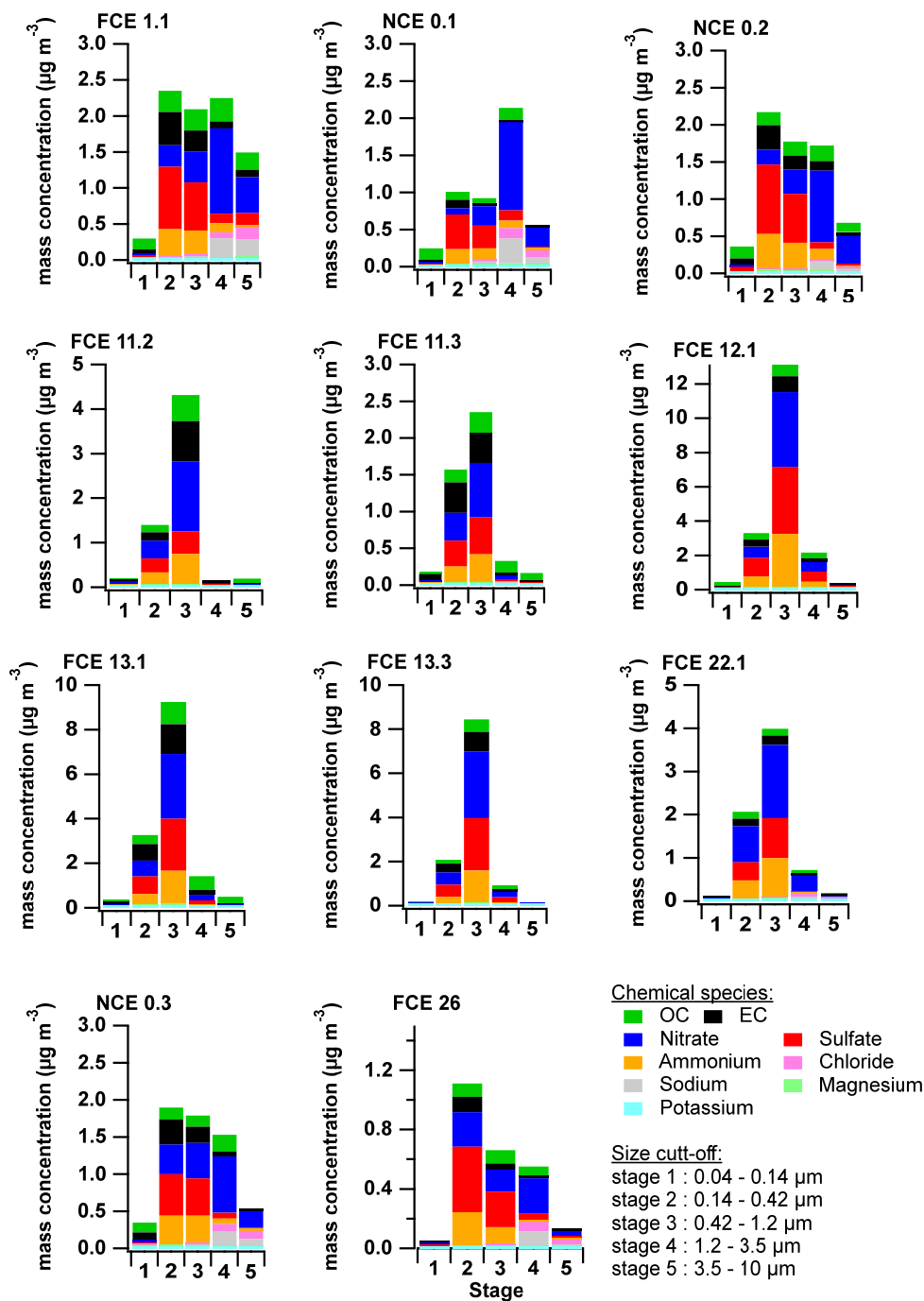
Figure 2: Size distribution of OC, EC, and major water-soluble ions from Berner-impactor measurements for the different full cloud events (FCE) and non cloud events (NCE).

685
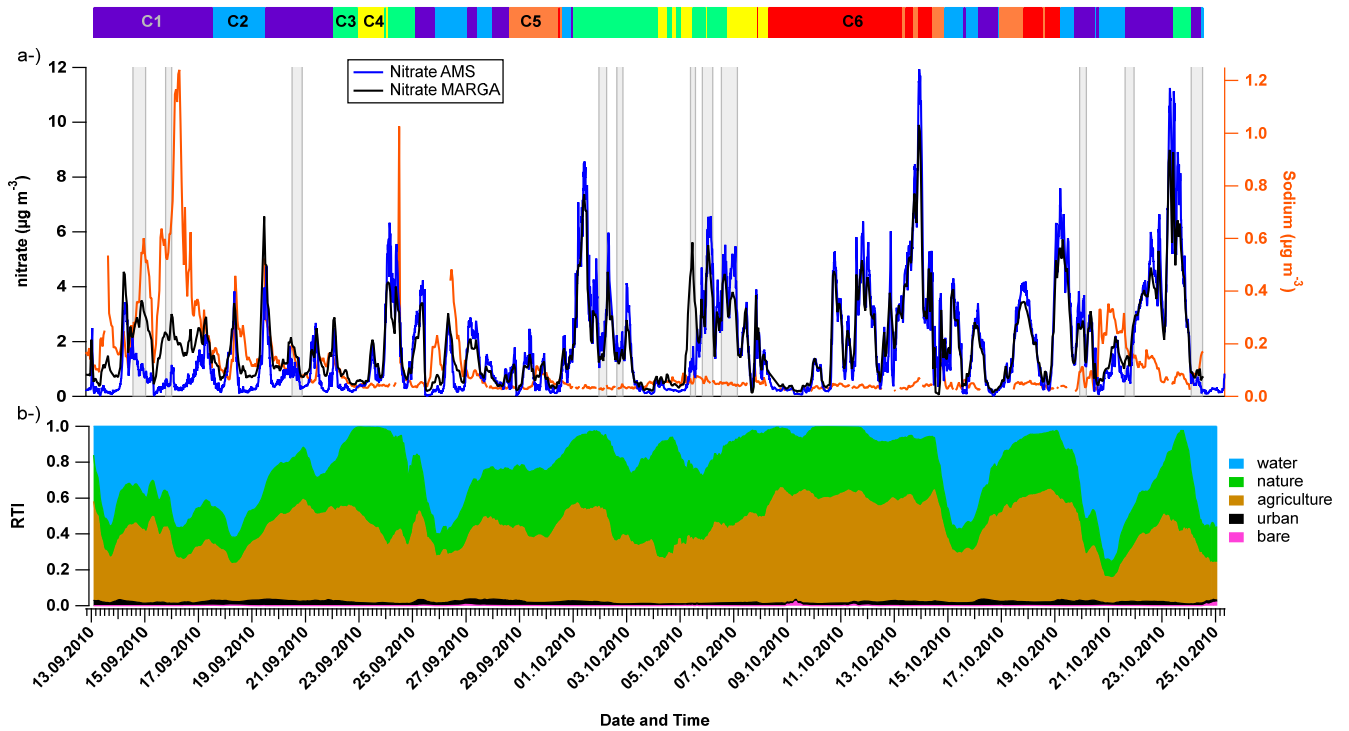
Figure 3: Influence of marine air masses on nitrate size distribution: (a) nitrate mass concentrations measured by AMS and MARGA as well as sodium mass concentrations by MARGA, (b) the residence time index (RTI) of the 96 h backward trajectories above different land cover as developed by van Pinxteren et al. (2010). The colored bars and numbers at the top refer to the 6 different air mass clusters (see section 3.4), and the grey bars refer to the different cloud and non-cloud events as defined in Table SI-2.

690

27
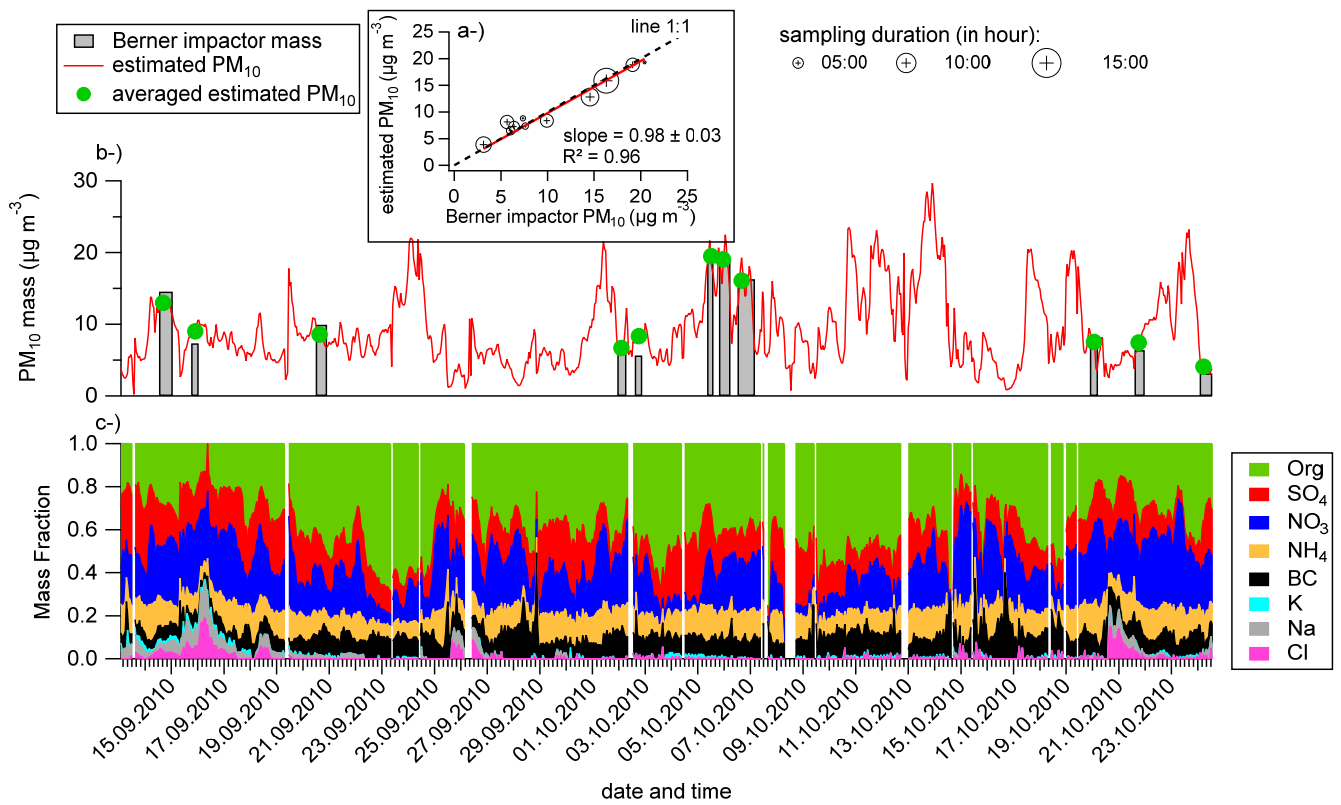
Figure 4: Estimation of the PM₁₀ mass concentration by combining AMS, MAAP, and MARGA: (a) Comparison with total PM₁₀ mass concentration measured by Berner-impactors during intensive sampling periods, (b) mass concentration time series, (c) mass fraction of the main components. The size of the point on the scatter plot (a) refers to the sampling duration of the Berner-impactor. The red line in the insert panel represents regression fit by least orthogonal distance fit forced to zero.

695
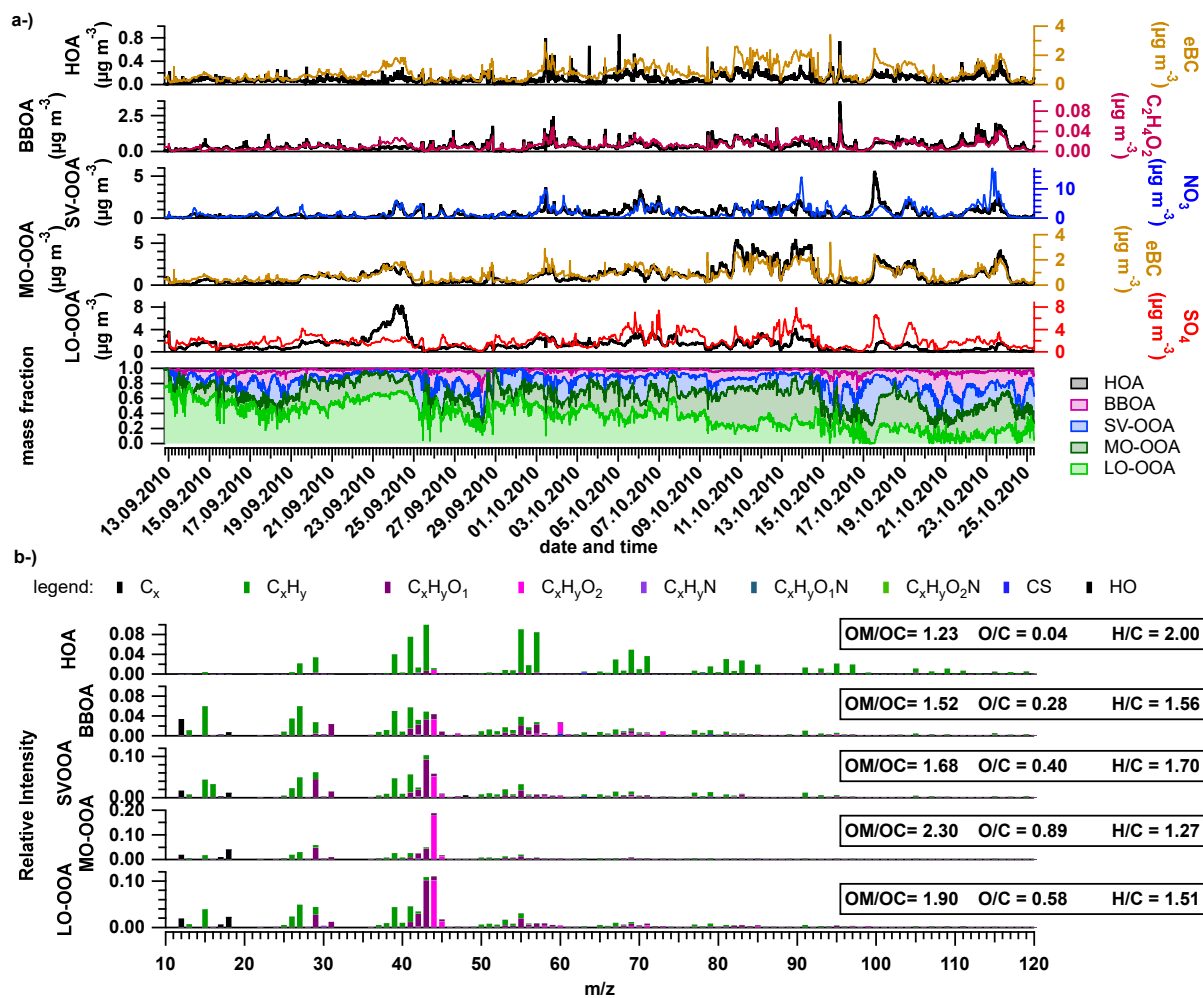
Figure 5: Overview of the ME-2 results. a) Time series of the 5-factors solution mass concentration and their corresponding tracers as well as mass fraction of each factor throughout the experiment. b) High-resolution mass spectra colored by the different groups of fragments and the elemental ratios of the identified factors.

700
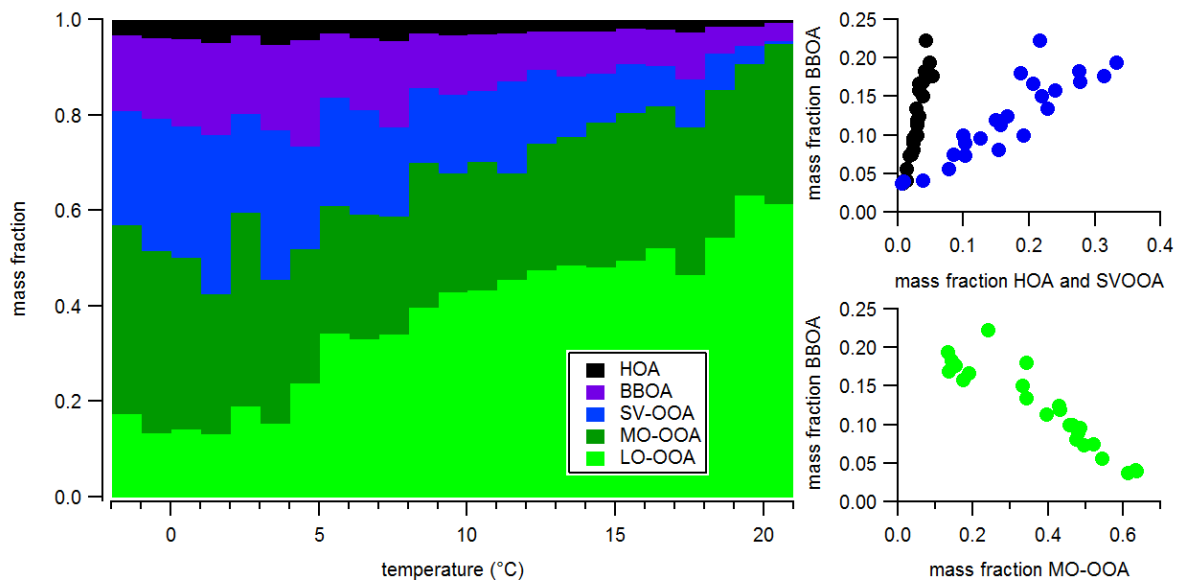
Figure 6: Temperature dependency of the identified factors' contribution to OA (left) and their individual correlations (right). The OA mass concentrations were averaging to a one-degree Celsius resolution.
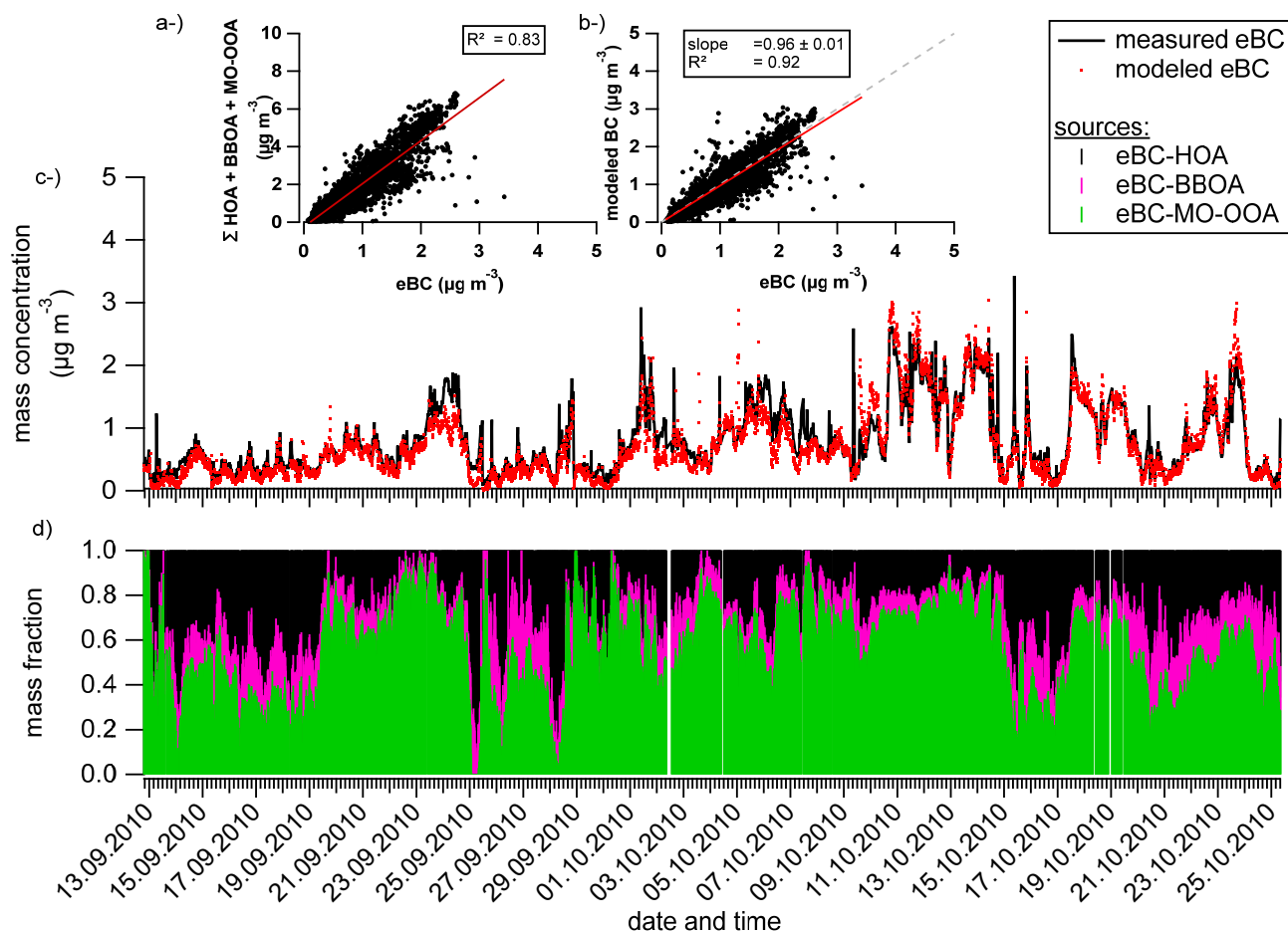
Figure 7: Contribution of the different organic factors to the eBC mass concentration. The scatter plots present the correlation between the sum of the OA factors and the measured eBC (a), and the estimated eBC concentration compared to the measured one (b). Time series show comparisons between measured and modeled eBC (c) and contributions of each source to the modeled eBC concentration (d). The correlation curves (red lines) were calculated using the least orthogonal distance fit method.
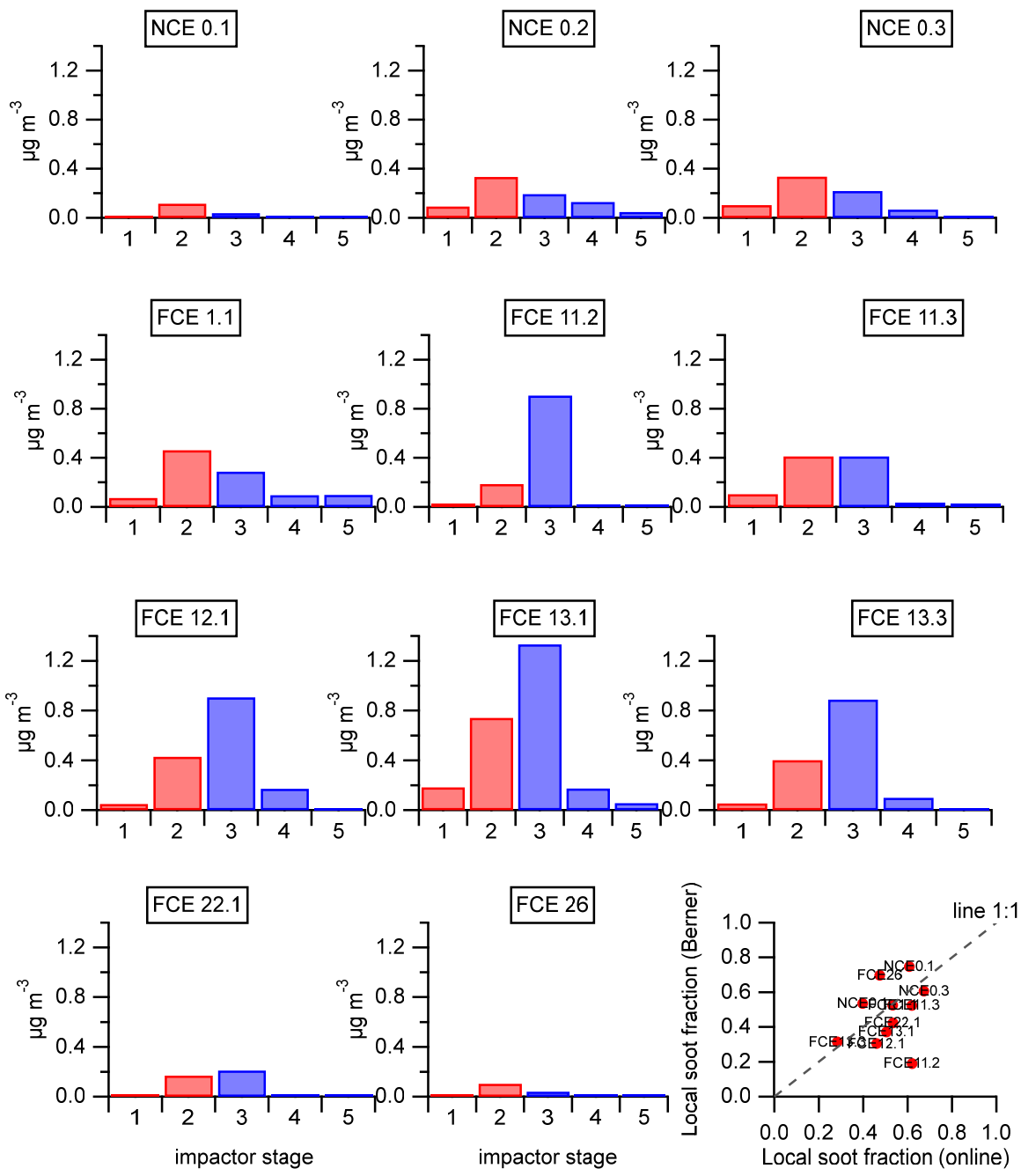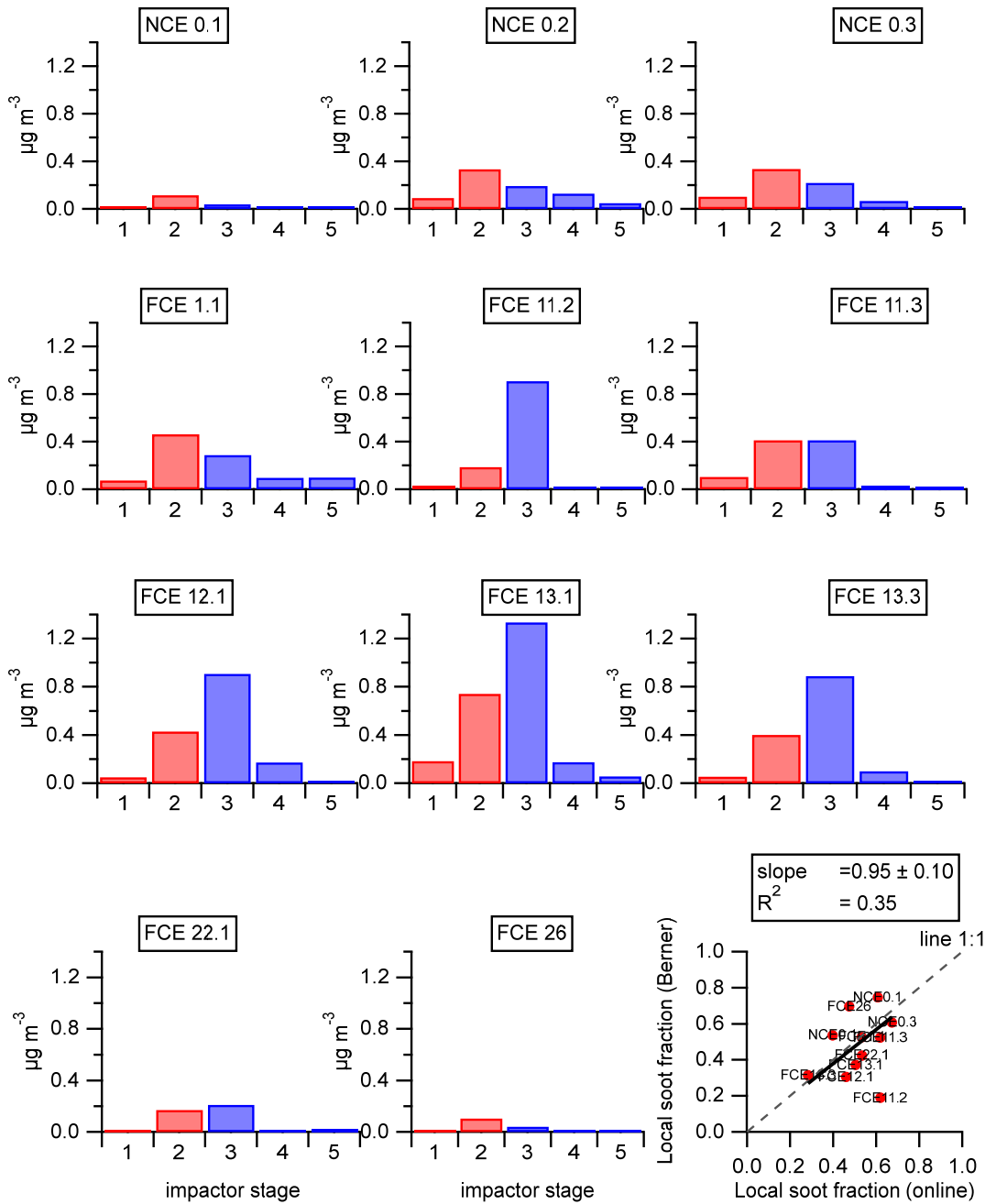
Figure 8: Overview of the EC size distribution measured by the 5-stages ~~Berner~~ Berner-impactor. Color corresponds to the following EC classification: red = local and blue = regional/transport. The scatter plot on the bottom right shows the comparison between the local soot fractions estimated using the two different approaches: ~~Berner~~ Berner-impactor (y-axis) and on-line multilinear regression (x-axis). Regression (black line) was made using the least orthogonal distance fit method.

33
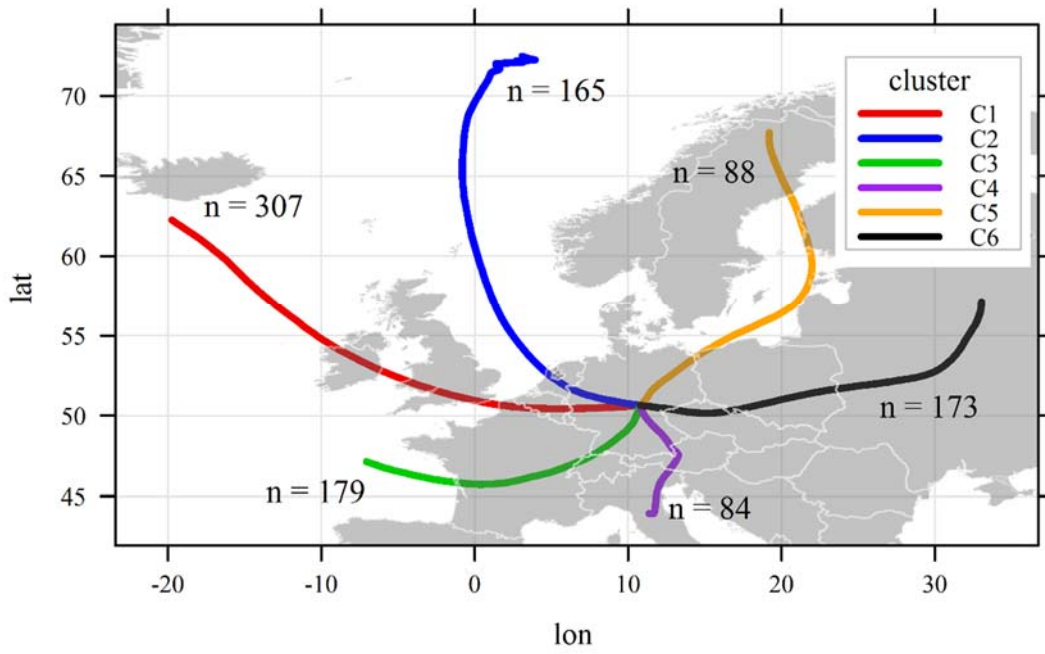
Figure 9: Cluster results of the 96 h backward air mass trajectories calculated for the entire sampling period. The "n" indicates the sum of air mass trajectories associated with each cluster.
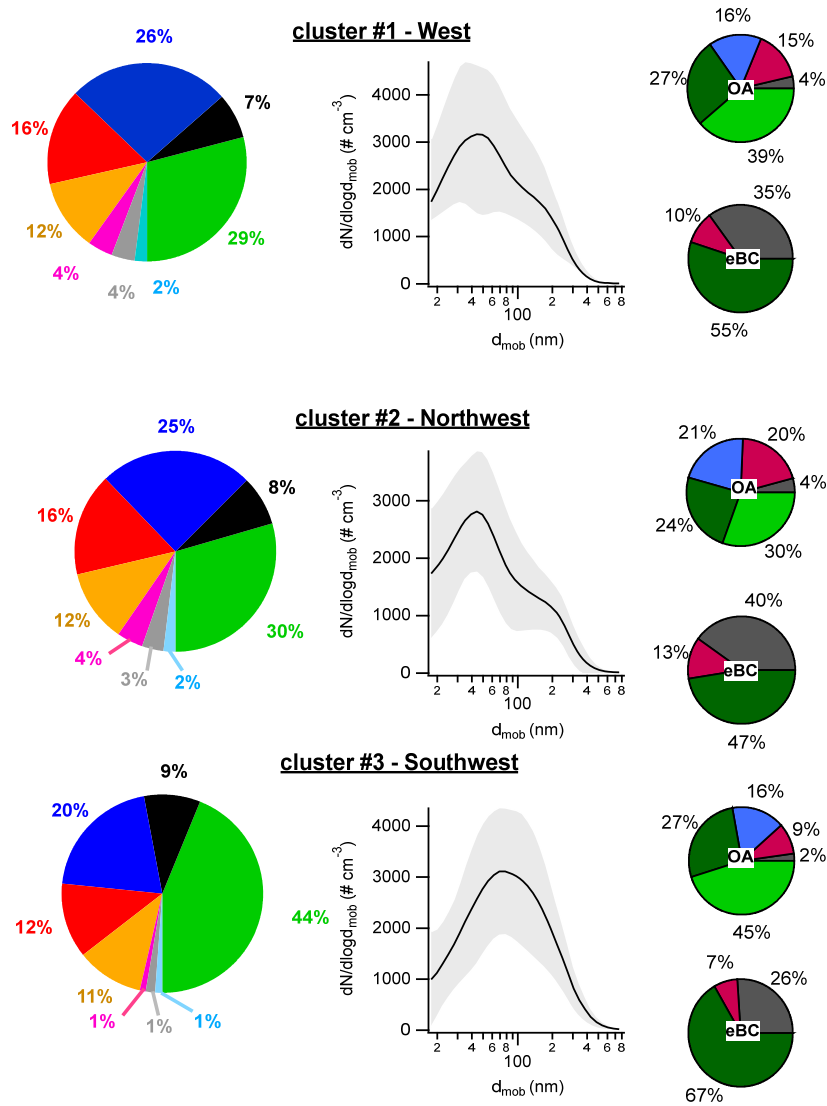
Figure 10: Overview of the chemical composition and the PNSD for each cluster: on the left, the mean estimated PM$_{10}$ aerosol particle chemical composition; in the middle, the averaged particle number size distribution (± standard deviation in grey); and on the right, the source apportionment results for organic aerosol (top right) and eBC (bottom right).

cluster #4 - South

cluster #5 - Northeast

cluster #6 - East

Figure 10: Continued

36

Source apportionment and impact of long-range transport on carbonaceous aerosol particles in Central Germany during HCCT-2010

5 Laurent Poulain[1], Benjamin Fahlbusch[1, *], Gerald Spindler[1], Konrad Müller[1], Dominik van Pinxteren[1], Zhijun Wu[1,**], Yoshiteru Iinuma[1,***], Wolfram Birmili[1,****], Alfred Wiedensohler[1], Hartmut Herrmann[1]

[1] Leibniz Institut für Troposphärenforschung, (TROPOS), Leipzig, 04318, Germany
[*] Now at Eurofins, Friedrichsdorf, 61381, Germany
[**] Now at College of Environment Sciences and Engineering, Peking University, Beijing, 100871, China
10 [***] Now at: Okinawa Institute of Science and Technology Graduate University (OIST), Okinawa, 904-0495, Japan
[****] Now at: Umweltbundesamt (UBA), Berlin, 14195, Germany

Correspondence to: Hartmut Herrmann (herrmann@tropos.de) and Laurent Poulain (poulain@tropos.de)

15

1

SI-1 Instrumental set-up and analytical methods

Table SI-1: Instrumentation used for trace gas measurements.

parameter	Type	Time resolution	Detection limits	Technique/Method/size ~~cutting~~cutt-off	Measured species
Gas samplers [*]					
Ozone	TE49C-TL (Thermo Fischer Scientific Inc.)	< 2 min	1 ppb	UV-absorption	Ozone
NO_x (NO/NO_2)	TE42S Thermo (Fischer Scientific Inc.)	0.5 min	0.5 ppb	Chemiluminescence	NO and NO_2
SO_2	TE43C-TL (Thermo Fischer Scientific Inc.)	<2 min	0.2 ppb	UV-fluorescence	SO_2
CO	ML 9830 (Monitor Europe)				
Water soluble gases	MARGA	1 hour		Denuder sampling for gases and online IC analysis	NH_3, HCl, HONO, HNO_3, SO_2
VOC		2 h during IOPs		Thermal desorption GC-FID	26 NMHC (C2-C8)

[*] SO_2 and NO_x analyzers were calibrated using test gas cylinders (air liquid, Germany), NO_2 by a gas-phase-titration system
20 (Sycos K/GPT; Ansyco GmbH, Germany), and an O_3 analyzer by the calibrator system TE49PS

2

SI-2 Sample preparation and chemical analysis of the 5-stage Berner-impactor

25

Samples of the 5-stage Berner-impactor were collected on aluminum foils (Table SI-2). Each foil was weighed after a 72 h equilibration under constant temperature (20±1 °C) and humidity (50±5 %) before and after collection using an electronic microbalance (UMT 2, Mettler Toledo, Switzerland) with a reading precision of 0.1 µg and a reproducibility of 1 µg. A part of the impactor foils was extracted with 1.5 ml MilliQ-water (> 18.2 MΩ cm; 15 min shaker, 15 min ultrasonic bath, 15 min

30 shaker). Sample extracts were then filtered through a 0.45 µm disposable syringe filter to remove insoluble materials prior to ion analysis by ion chromatography (ICS300, Dionex, USA) for cations (Column CS16, eluent methane sulfonic acid) and anions (Column AS18, eluent KOH). Calibrations were carried out daily using a four point's standard diluted from a stock solution (Fluka, Switzerland). The detection limits for all ions measured by conductivity detection were within 0.1 mg l^{-1}, except for sulfate and nitrate (0.2 mg l^{-1}). Nitrite was detected using UV/VIS detection (VWD-1, Dionex) with a detection

35 limit of 0.1 mg l^{-1}, which leads to a general detection limit ranging between 0.005 and 0.05 µg m^{-3} depending on the sampling volume and species. Blank corrections were made according to the analyzed field blank impactor foils. The organic carbon (OC) and elemental carbon (EC), in sum total carbon (TC), analyses were made using a carbon analyzer type C-mat 5500 with a non-disperse infrared detector (NDIR) (Ströhlein, Germany) based on a modification of the German VDI guideline 2465 (Gnauk et al., 2008). Finally, sugars and anhydrosaccharides (e.g. levoglucosan, galactosan and mannosan) were analyzed

40 from the water extract prepared for ion chromatography using an ICS3000 system (Dionex, U.S.A.) equipped with a pulsed amperometric detector (Engling et al., 2006;Iinuma et al., 2009).

Table SI-2: Berner-impactor measurements periods associated to full cloud events (FCE) and non-cloud events (NCE) taken during the sampling periods. More details on the FCEs and NCEs can be found in Tilgner et al. (2014).

	FCE 1.1	NCE 0.1	NCE 0.2	FCE 11.2	FCE 11.3	FCE 12.1	FCE 13.1	FCE 13.3	FCE 22.1	NCE 0.3	FCE 26
Starting time	14.09.2010 11:00	15.09.2010 18:00	20.09.2010 11:25	01.10.2010 22:30	02.10.2010 14:30	05.10.2010 08:30	05.10.2010 19:15	06.10.2010 12:15	19.10.2010 21:30	21.10.2010 14:15	24.10.2010 01:30
Stopping time	15.09.2010 02:00	15.09.2010 23:30	20.09.2010 20:30	02.10.2010 05:30	02.10.2010 19:30	05.10.2010 13:00	06.10.2010 04:30	07.10.2010 03:15	20.10.2010 03:30	21.10.2010 22:15	24.10.2010 11:45
Back-trajectory Cluster	C1	C1	C1	C3	C3	C4 to C3	C3	C3 to C4	C1	C1	C3 to C2 via C1

45

3

SI-3 AMS data validation

Prior to mass closure analysis, conversion of the particle number concentration of the T-MPSS to the volume concentration was made assuming spherical particles, and to the mass concentration using a time dependent density estimated using the equation of Salcedo et al. (2006) and based on the measured PM_1 chemical composition as previously described in Poulain et al. (2014). A good correlation was obtained (slope of 0.93, $R^2 = 0.94$, Fig. SI-1), indicating that non-detected compounds (i.e. AMS refractory compounds except eBC) do not significantly contribute to the PM_1 mass concentration.
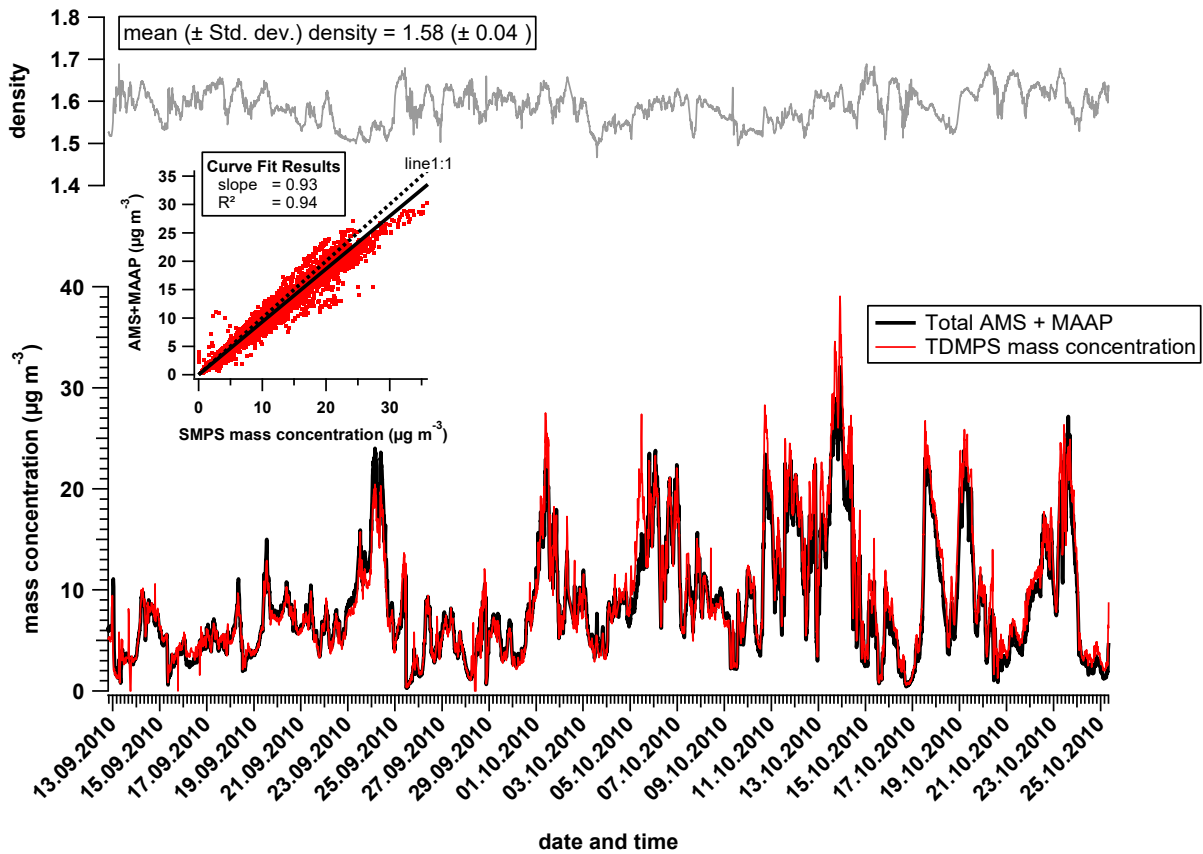
Figure SI-1: Mass closure between online aerosol chemical composition (AMS and MAAP) and TDMPS estimated mass concentration (bottom and insert). Time and chemical dependent density (top) was used to convert the volume concentration of the TDMPS into mass concentration. The correlation curve (black line) was calculated using the least orthogonal distance fit method

The MARGA (PM_{10}, Fig. SI-2 & SI-3) and ~~Berner~~ Berner-impactor $PM_{1.2}$ (sum of the three first stages, Fig. SI-4) mass concentration of ammonium, nitrate, and sulfate also present an excellent correlation with the AMS measurements regarding individual instrumental limitations. This includes the limited number of samples and the reduced sampling time of the ~~Berner~~ Berner-impactor, as well as the specific upper size ~~cutting~~ cut-off (near-PM_1 for the AMS, $PM_{1.2}$ for the ~~Berner~~ Berner-

4

impactor, and PM$_{10}$ for MARGA). <u>The size distribution measured by the Berner-impactor and the AMS was compared to each other for organic (Organic mass for the AMS, OC for the Berner-impactor), nitrate, sulfate, and ammonium (Fig. SI-5). Similar size distributions were obtained for the inorganic species, except for FCE 12.1 which shows higher nitrate and ammonium mass concentrations on stage 3 compared to the AMS size distribution. A comparison between the two organics measurement methods is more difficult since the AMS directly measures the organic mass concentration, while the OC from the Berner-impactor was obtained according to the two-step thermographic method (VDI standard).</u> Moreover, the presence of different nitrate salts can also explain the discrepancy between AMS and MARGA (see discussion on main text).

70

Figure SI-2: Sulfate (top) and ammonium (bottom) time series measured by AMS (colored line) and MARGA (black line).
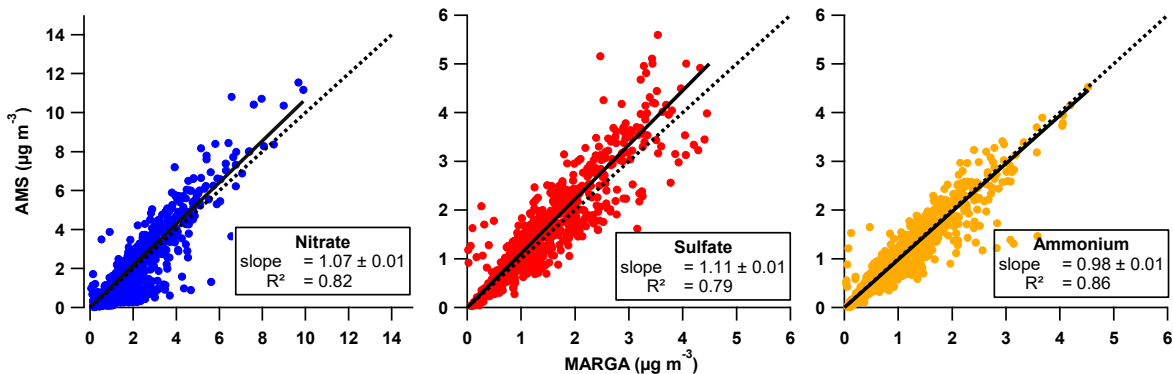

Figure SI-3: Scatter plots of the nitrate, sulfate, and ammonium mass concentrations measured by AMS and MARGA. The correlation curves (red lines) were calculated using the least orthogonal distance fit method.
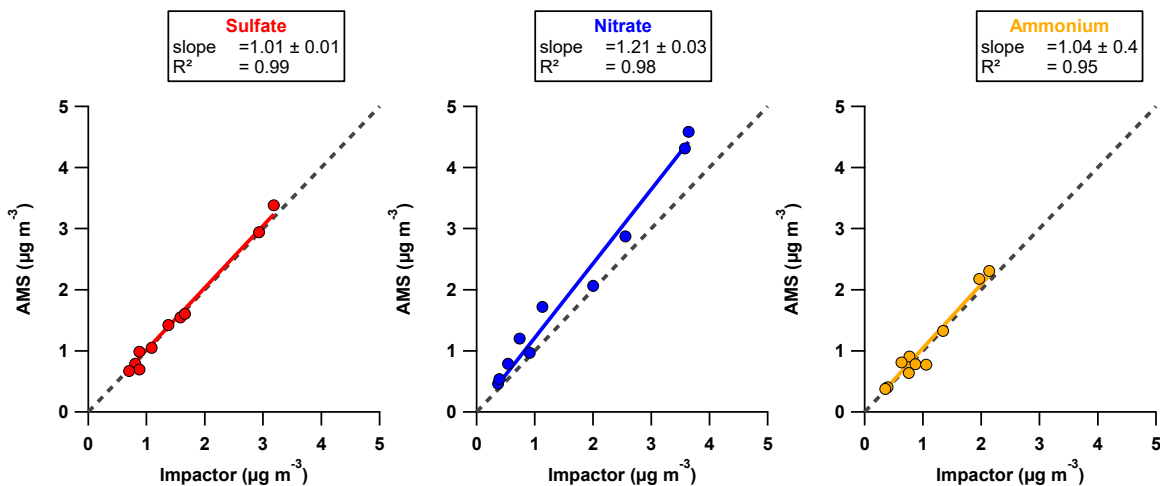
Figure SI-4: Comparison of AMS and impactor measurements (stages 1-3, i.e. PM1.2) during the different cloud and non-cloud events (see text for details on sampling periods). The correlation curves (red lines) were calculated using the least orthogonal distance fit method
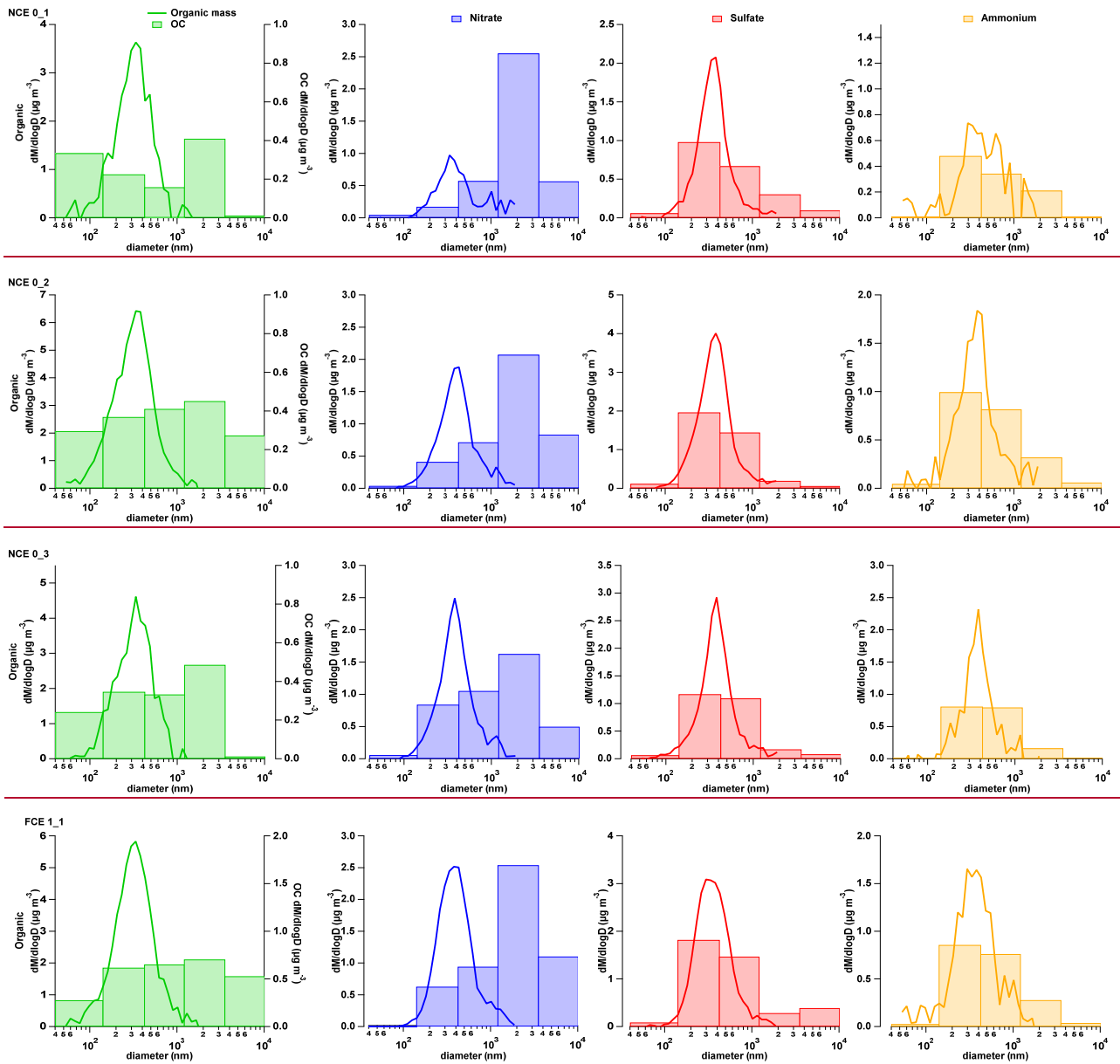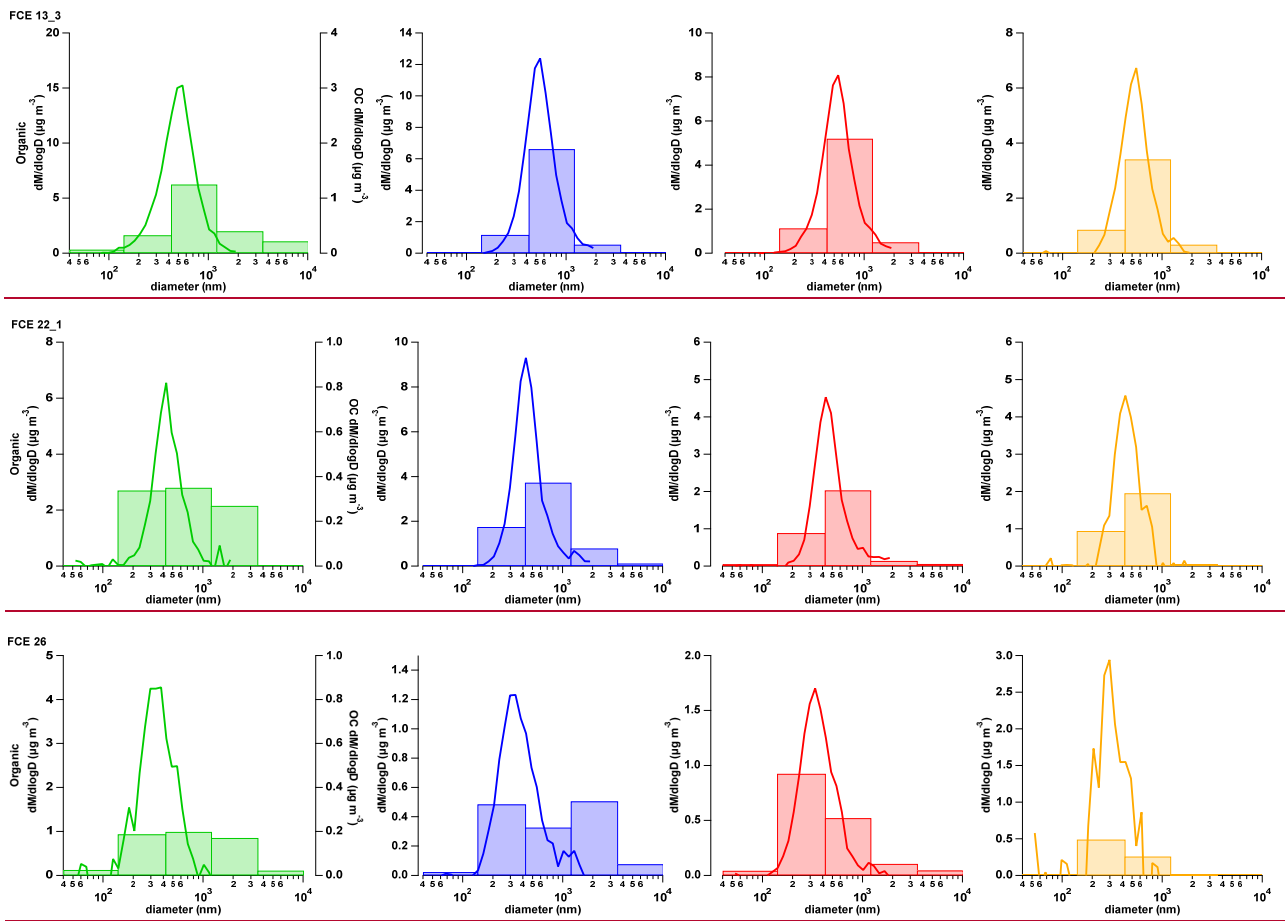
Figure SI-5: Comparison between the AMS and Berner-impactor size distribution for organic (organic mass for the AMS and OC for the Berner-impactor), nitrate, sulfate, and ammonium for the different FCE and NCE events.
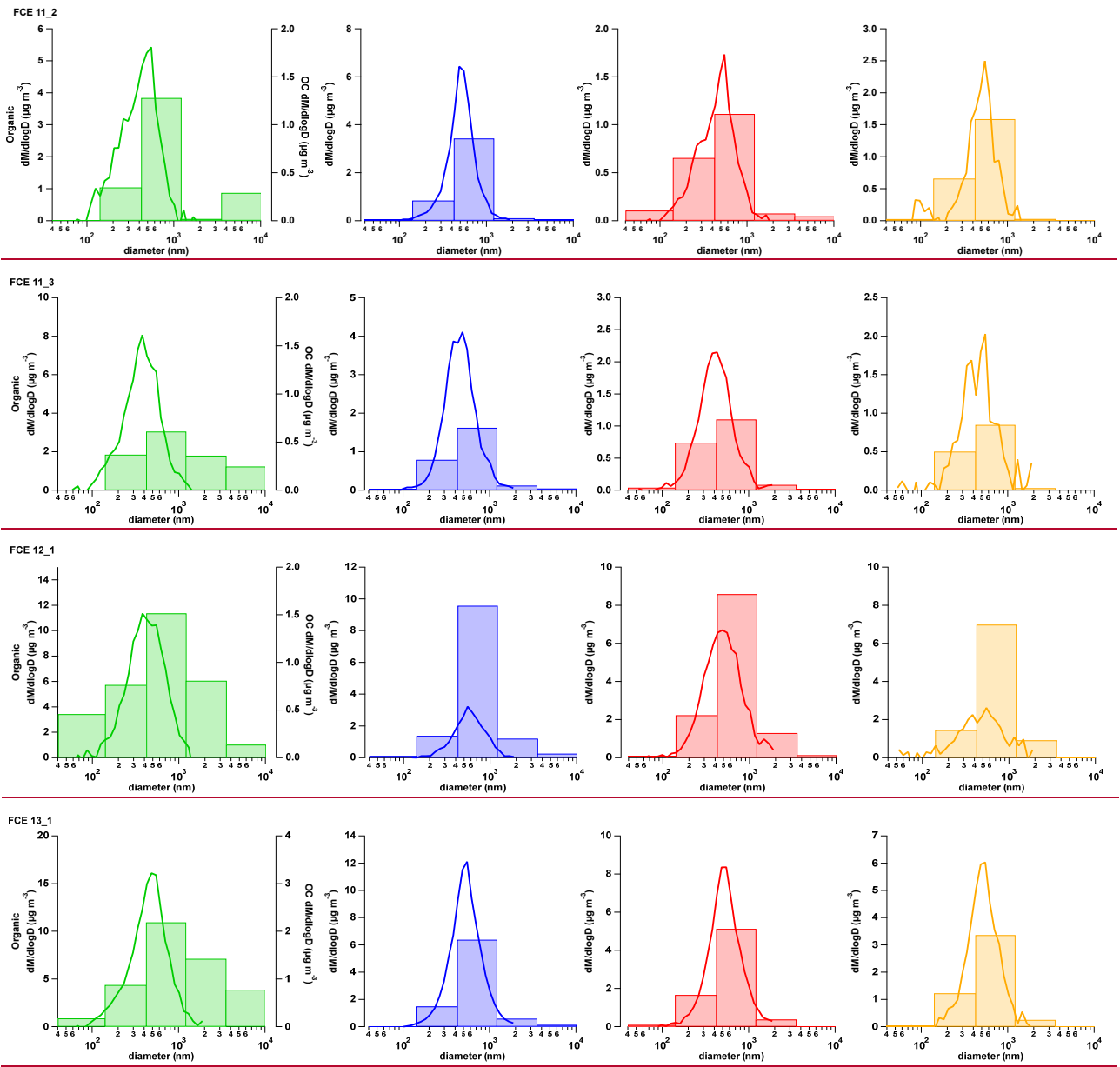
Figure SI-5: Continued

Figure SI-5: Continued
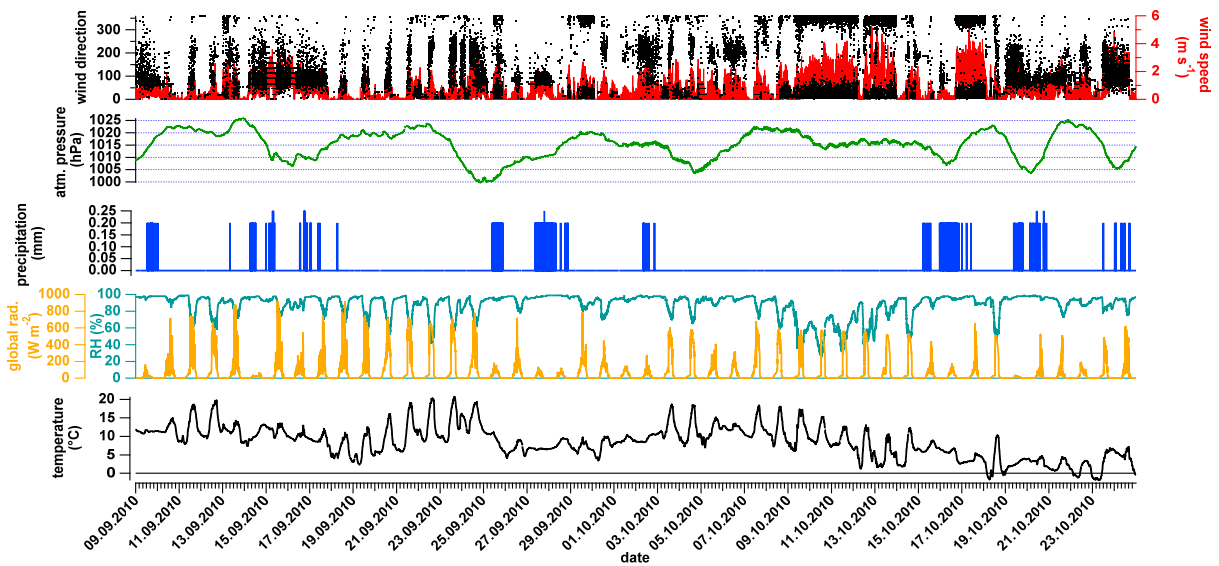
100

9

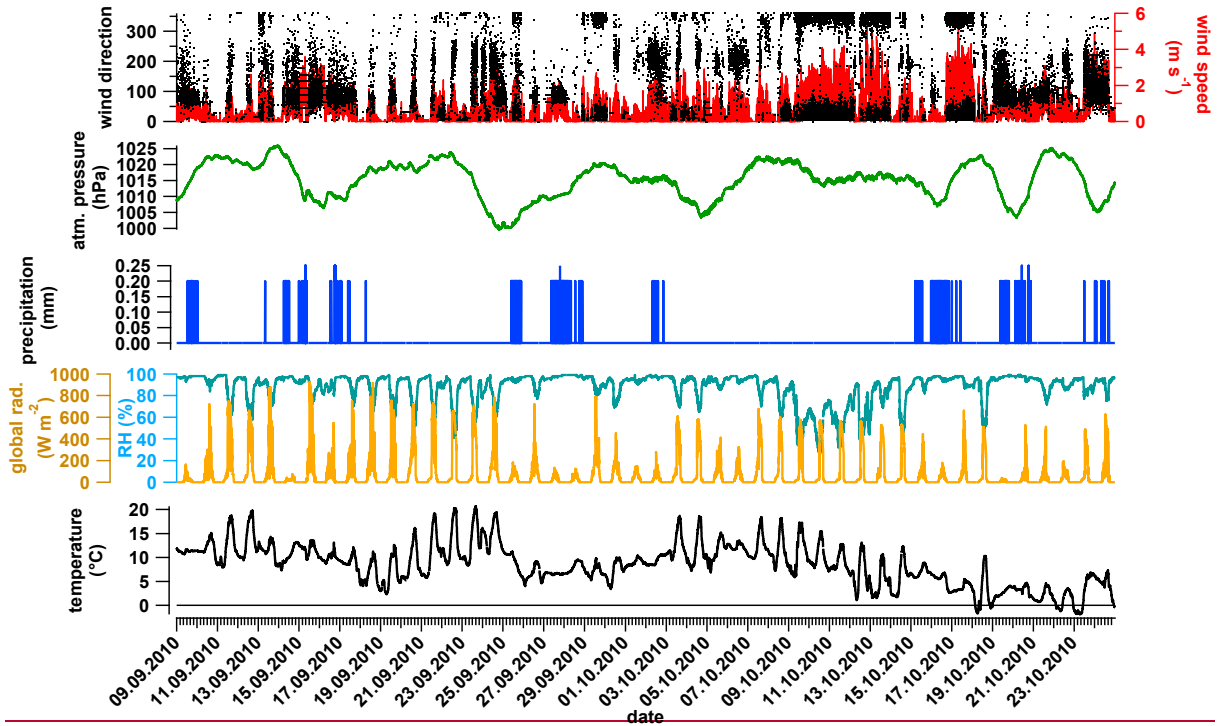## SI-4 Overview of the meteorological conditions

Figure SI-65: Overview of the meteorological conditions during the sampling period.

SI-5 Organic aerosol source apportionment

Source apportionment was performed on the high-resolution organic mass spectra dataset using the Multi-linear Engine (ME-2) model developed by Paatero (1999) and using the Source Finder tool Sofi4.9 (Canonaco et al., 2013) developed at the Paul Scherrer Institute (Switzerland). The source apportionment was made following the recommendation of Crippa et al. (2014): for the first time a non-constrained model approach was investigated and since primary factors were not properly resolved in this first model, a partially constrained approach was investigated during a second time.

SI-5-1 Non-constrained model (PMF)

In the non-constrained ME-2 model, solutions were investigated in a range from 2 to 10 factors, each within 20 seeds (Fig. SI-67). The best solution was obtained for the 4-factors solution and the different factors were identified as primary OA (POA; 20 % of the total OA), semi-volatile OA (SV-OOA; 17 %), and 2 OOAs (named LV-OOA1 and LV-OOA2; 28 % and 34 %, respectively) (Fig. SI-78). The POA factor was identified based on its low oxidation (O:C = 0.27) and presence of typical tracers from two primary OAs (Hydrocarbon-like OA (HOA) with the m/z 55 and 57 and Biomass Burning OA (BBOA) with m/z 60 and 73). Moreover, similarity between its diurnal profile and the ones of the different anthropogenic emission tracers (eBC, CO, and NO_2, Fig. SI-89) confirm its primary origin. The presence of the BBOA tracers (m/z 60 and m/z 73) on the POA mass spectra indicates a dominant biomass burning influence on the primary OA sources. Increasing the number of factors to 5 leads to an additional split of the POA factor without providing clear HOA and BBOA factors. However, it is interesting to note the relative stability of the two OOA mass spectra in the range from 3- to 5-factors (Fig. SI-910). Changes on their individual concentrations highlight the influence of the additional splitting when increasing the number of factor solutions. This stability indicates that these two factors can easily be extracted from the OA matrix by the model and therefore, their identification can be considered as quite robust in the range of 3- to 5-factors solutions. By increasing the factor's number above 5, additional splits of the two OOAs were observed without providing either with more details on their sources or a better identification of the POAs.

The LV-OOA1 factor correlates better with eBC than the POA factor (R^2 = 0.80 for LV-OOA1 vs. eBC, while R^2=0.38 for POA vs. eBC). Since the LV-OOA1 is quite oxygenated (O:C = 0.91) and does not show a similar diurnal pattern to eBC (Fig. SI-78 & SI-89), it is quite difficult to link this factor to any local primary emission. Consequently, and due to its stability over the investigated factor solutions, it should be related to process anthropogenic and long-range transport of polluted air masses (see discussion in section 3.2.4 of the manuscript). Therefore, it clearly indicates the presence of two distinct sources of eBC: a local one related to the POA factor and a second one related to regional or transported aged primary emissions associated to LV-OOA1 (details on the eBC source apportionment can be found in the dedicated section of the manuscript).
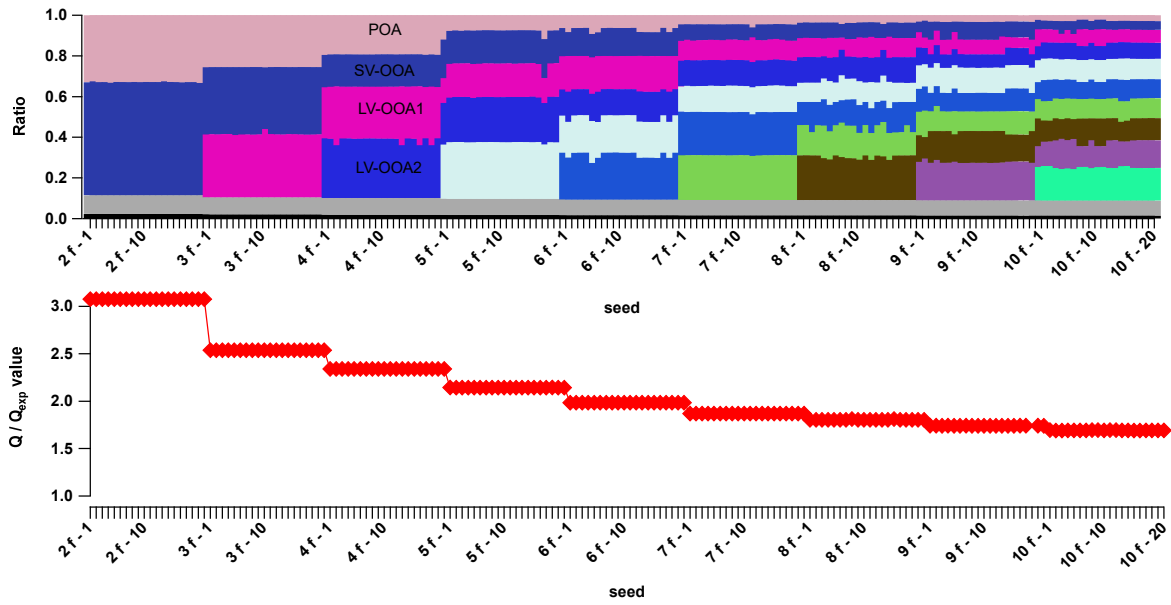
Figure SI-76: Variation of the factor contributions (top) and Q/Q_exp (bottom) over the investigated solution area for the unconstrained model.
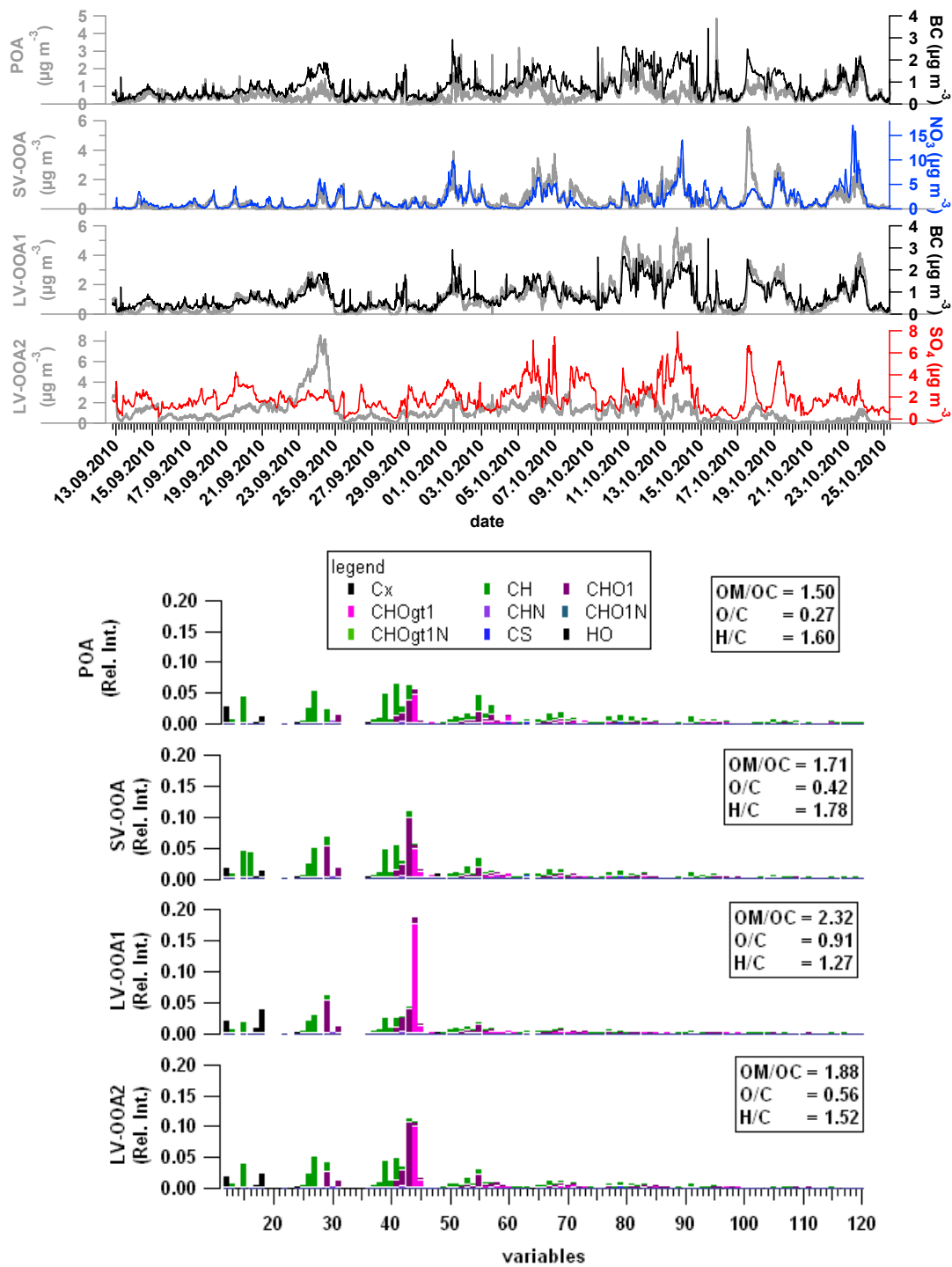
145

Figure SI-~~8~~7: Time series of the PMF 4-factor solutions and comparison with collocated measurements (top). The corresponding high-resolution mass spectra colored by fragment family codes is presented on the bottom.
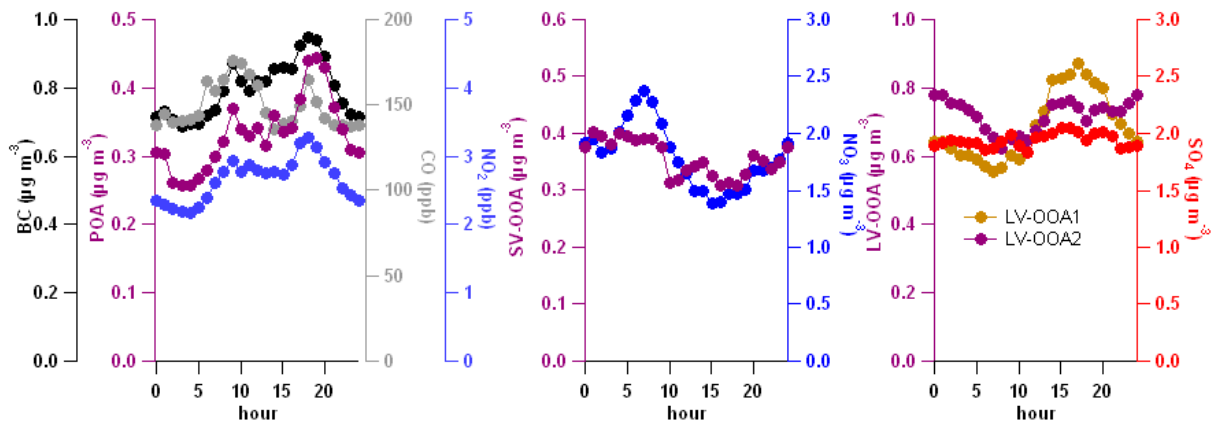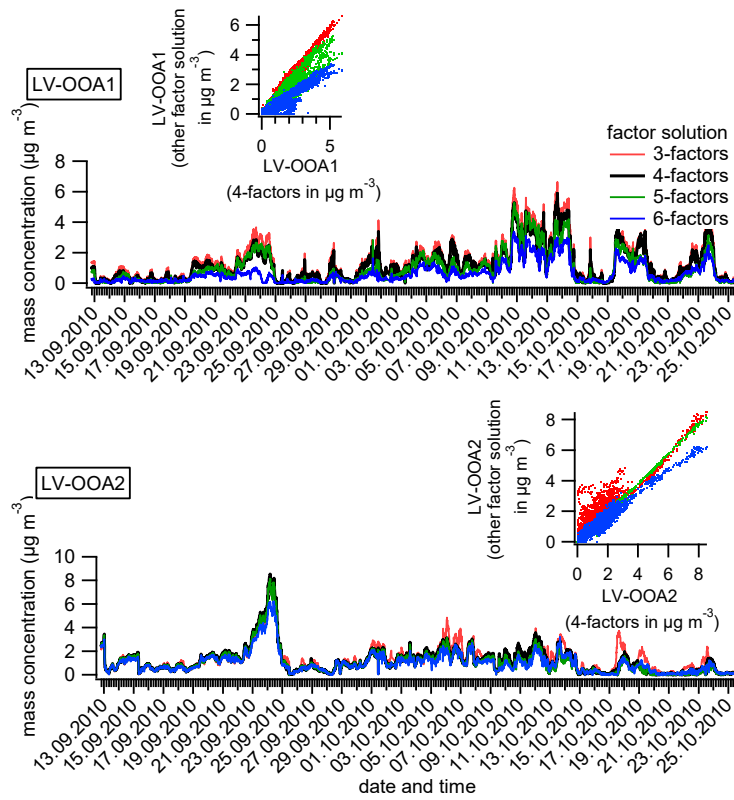
14

Figure SI-98: Diurnal pattern of the identify factors and collocated measurements for the non-constrained model.
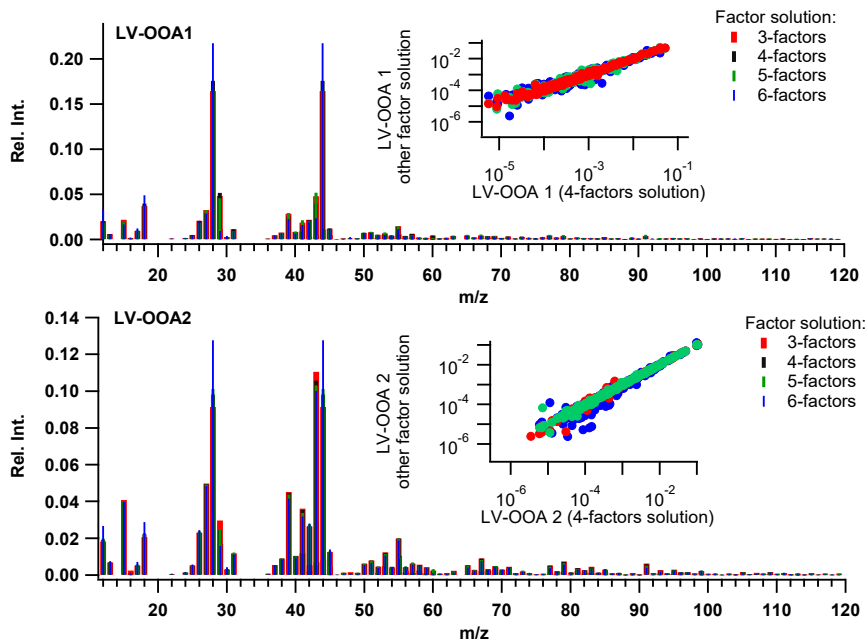
155

Figure SI-~~109~~: Comparison of the time series (top) and mass spectra (bottom in relative intensity) of the two LV-OOA factors ranging from 3- to 6-factor solutions.

SI-5-2 Partly constrained model

SI-5-2-1 Constraining HOA

Two different POA factors were expected based on the local emissions: an HOA factor related to traffic and fossil fuel combustion and biomass burning OA (BBOA). The presence of biomass burning OA is also confirmed when looking at the contribution of the fragment 60 to the total OA (f_{60}), which went above the threshold value of 0.3 % suggested by Cubison et al. (2011) (not shown). In order to better distinguish the different primary sources, the source apportionment model was therefore partly constrained, using as reference the HOA mass spectra from Mohr et al. (2012) obtained at Barcelona (Spain) and available on the reference mass spectra database (http://cires.colorado.edu/jimenez-group/HRAMSsd/, Ulbrich et al., 2009). Results were investigated using a factor number ranging from 2 to 9 with an anchor for the HOA factor ranging from 0.05 to 0.5 (Fig. SI-~~10~~11 & SI-~~11~~12). Contribution of HOA to total OA was relatively stable over the entire investigated factor solution as well as over the different a-values, as can be seen in Figure SI-~~11~~12. Therefore, in the following, a solution with an a-value of 0.1 was considered. This corresponds to a quite constrained mass spectrum. From the 5-factors solution a possible BBOA factor can be suspected based on the high contribution of m/z 60 and 73. However, comparing the mass spectra of the 5-factor solutions BBOA with reference ones (Fig. SI-~~12~~13) shows a very high contribution of CO_2^+ fragments, which might suggest a possible contribution of OOA and is therefore a non-properly resolved factor.

Additionally, the three OOAs (SV-OOA, LV-OOA1, and LV-OOA2) already identified in the non-constrained model were also found. The two LV-OOAs are extremely close to the ones identified in the non-constrained analysis (Fig. SI-~~11~~12; LV-OOA1: R^2= 0.97, slope 1.05; and LV-OOA2 R^2= 0.95, slope 0.98 for their respective time series comparison). A larger discrepancy was observed for SV-OOA when comparing it to the non-constrained model (R^2= 0.73, slope 0.67). This could result from a possible contribution of the BBOA factor to the non-constrained SV-OOA factor, confirming the non-ideal apportionment of the BBOA factor.

Increasing the number of factors leads mainly to an additional split of the OOAs. Interestingly, a well-defined BBOA mass spectrum was found for the 9-factors solution. This BBOA factor is in agreement with the reference mass spectra proposed by Ng et al. (2011), as well as with the averaged BBOA factor obtained during the EUCAARI project in Europe Crippa et al. (2014) (Fig. SI-~~12~~13). Consequently, a third model was built, constraining the HOA mass spectra as previously, as well as a BBOA factor using the identified BBOA mass spectra on the 9-factors solution. Since the BBOA directly results from the present dataset, the BBOA mass spectrum was constrained with a fixed a-value of 0.1.

17
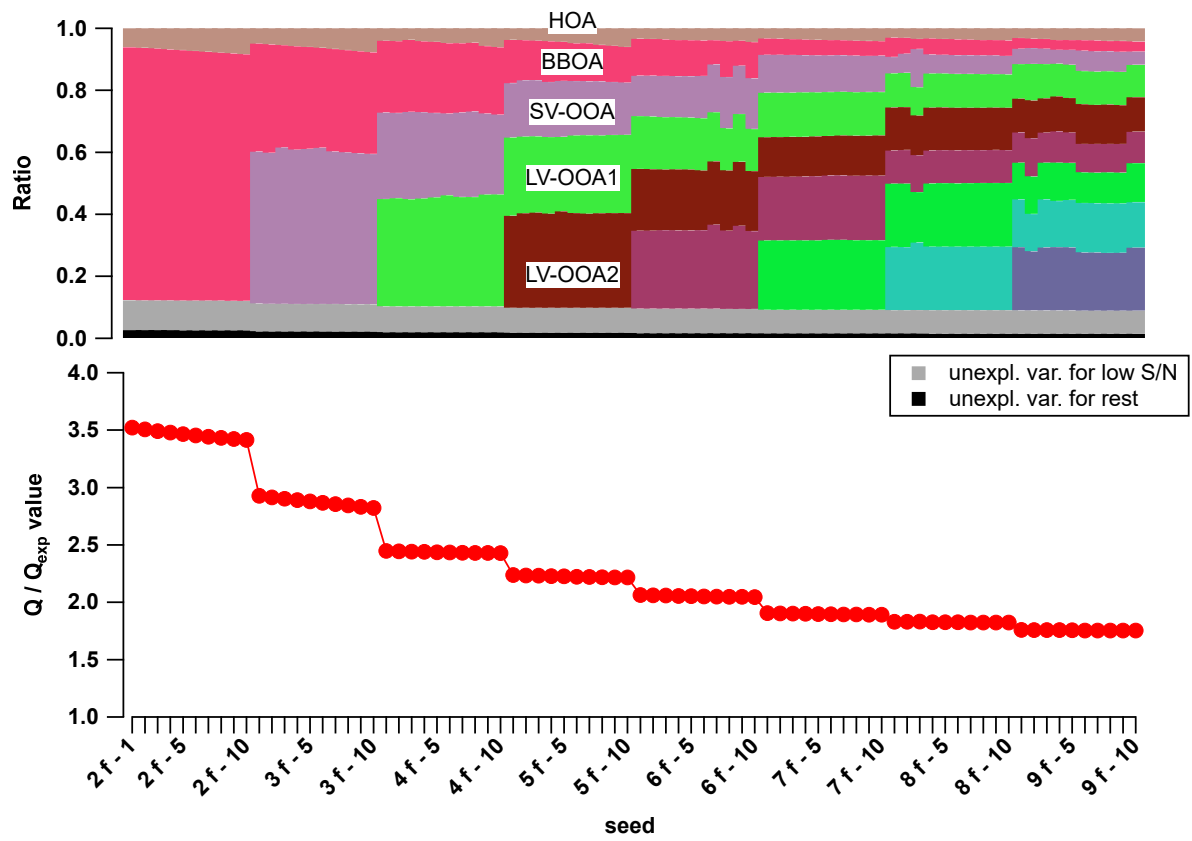
Figure SI-11~~10~~: Variation of the Q/Q_{exp} (top) and factor contributions (bottom) over the investigated solution area with constrained HOA.
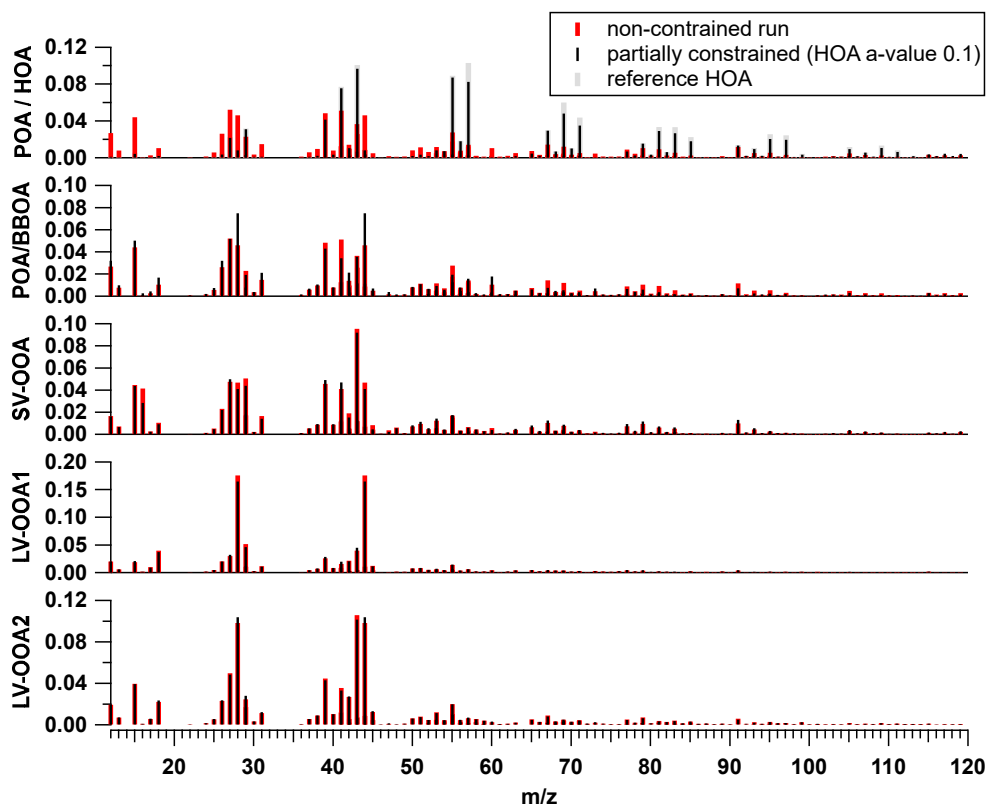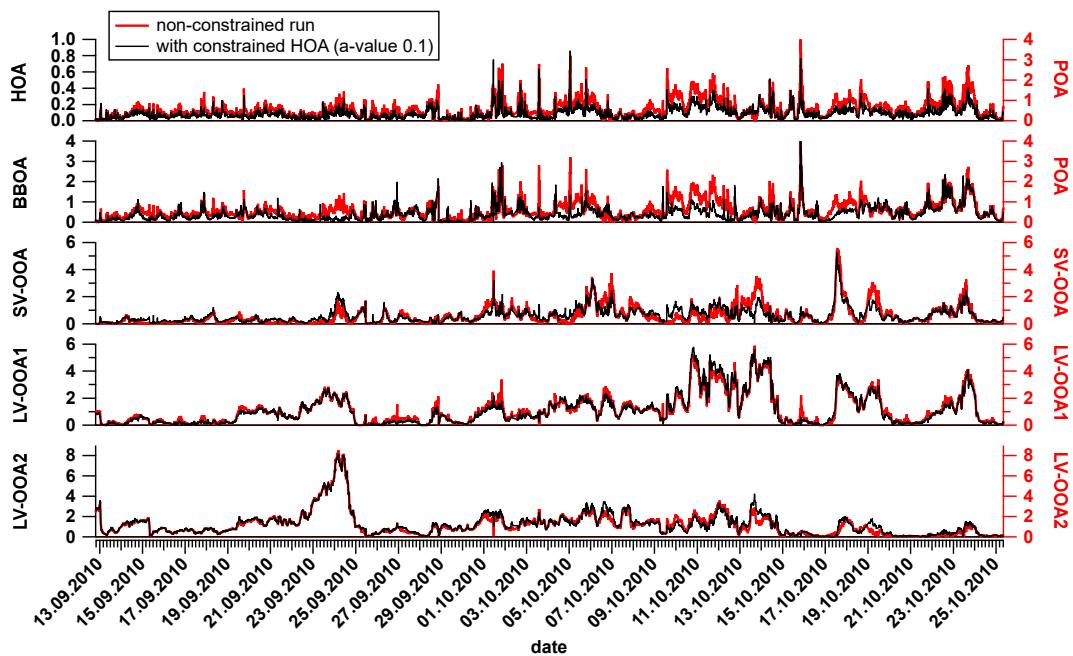
195　**Figure SI-12~~11~~: Comparison of the time series (top, in µg m⁻³) and mass spectra (bottom) of the 5-factors solution partly-constrained approach (fixed HOA with a-value = 0.1) and the non-constrained one (red).**
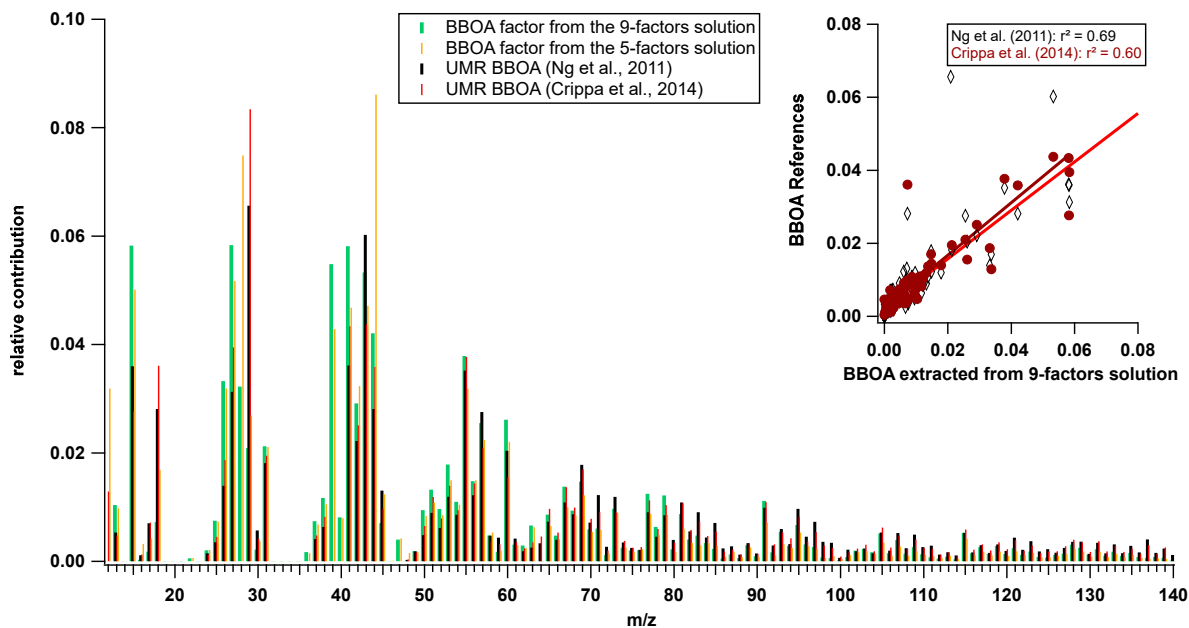
Figure SI-1312: Comparison of the identified BBOA factor for the 9-factors solution with reference mass spectra from Ng et al. (2011) and Crippa et al. (2014). The insert panel represents the scatter plots between the identified BBOA factor (after averaging to unit mass resolution (UMR)) and the 2 references.

SI-5-2-2 Constraining HOA and BBOA

The investigation of the third model run is presented in Figure SI-14Figure SI-13. Here, the 5-factors solution was retained as a final source apportionment result, which corresponds to the identification of the expected two primary OA (HOA and BBOA) and three additional OOA factors (SV-OOA, LO-OOA, and MO-OOA) (Fig. 5 on the manuscript). Both mass spectra and time series of the three OOA factors identified in this third model are similar to the ones obtained in the non-constrained model (Fig. SI-1415 & 1516). This confirmed the robustness of the OOAs identification, as well as the correct speciation of the POA factor identity on the non-constrained model. The larger variation in the elemental composition was found for the SV-OOA factor, which could be related to a small contribution from BBOA on the non-constrained results, as was mentioned before. The identification of the BBOA factor is confirmed by the comparison of the factor mass concentrations with the levoglucosan concentrations obtained from the off-line filter measurements made during IOPs (Fig. SI-1617).

20

215 **Figure SI-14~~13~~: Variation of the Q/Q_{exp} (top) and factor contributions (bottom) over the investigated solution area with constrained HOA and BBOA.**
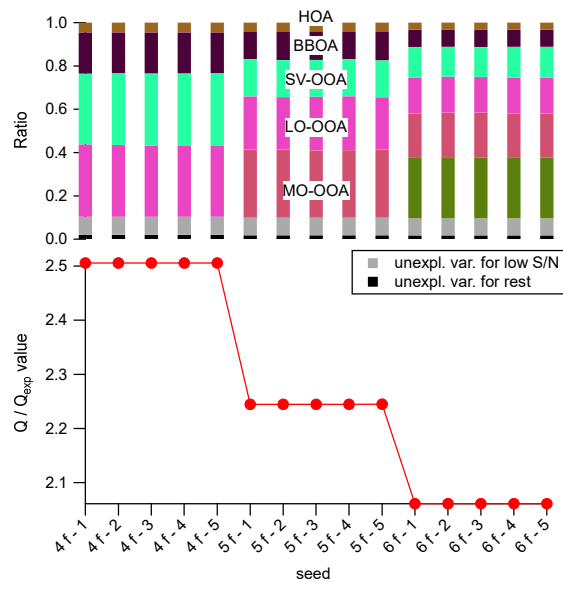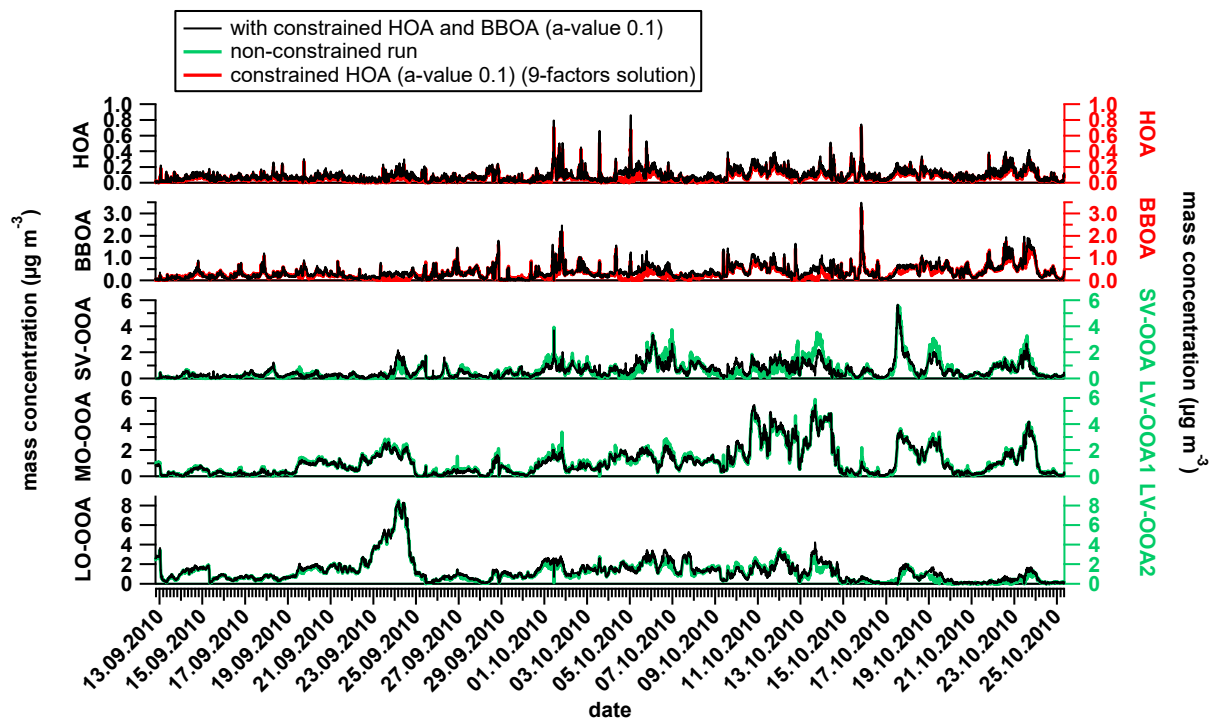
21

220

Figure SI-15~~14~~: Comparison of 5-factors solution time series with constrained HOA and BBOA (left axis) with the previously identified ones (right axis) obtained during the 9-factors solution (with fixed HOA) for HOA and BBOA (red) and the PMF results (non-constrained) for the two OOAs (green).

22
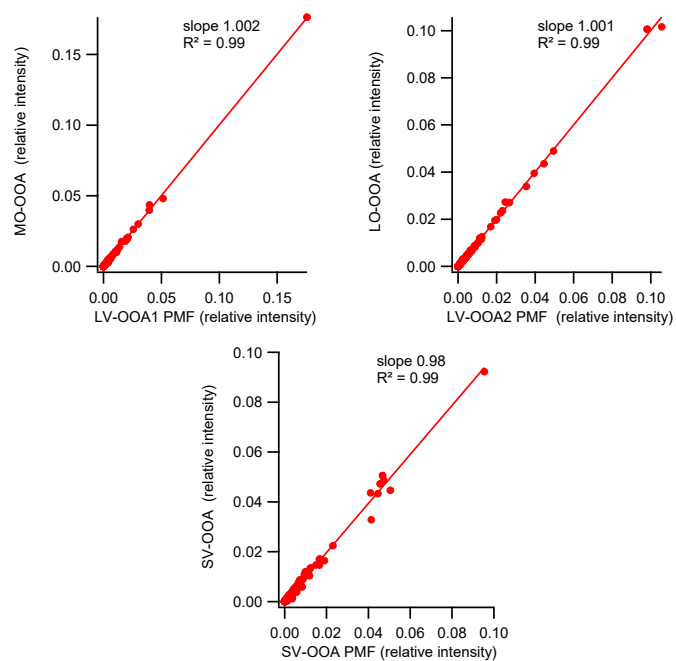
225 **Figure SI-16~~15~~: Comparison of the OOAs mass spectra from the final HOA and BBOA constrained factor solutions with the ones previously obtained on the non-constrained solution.**
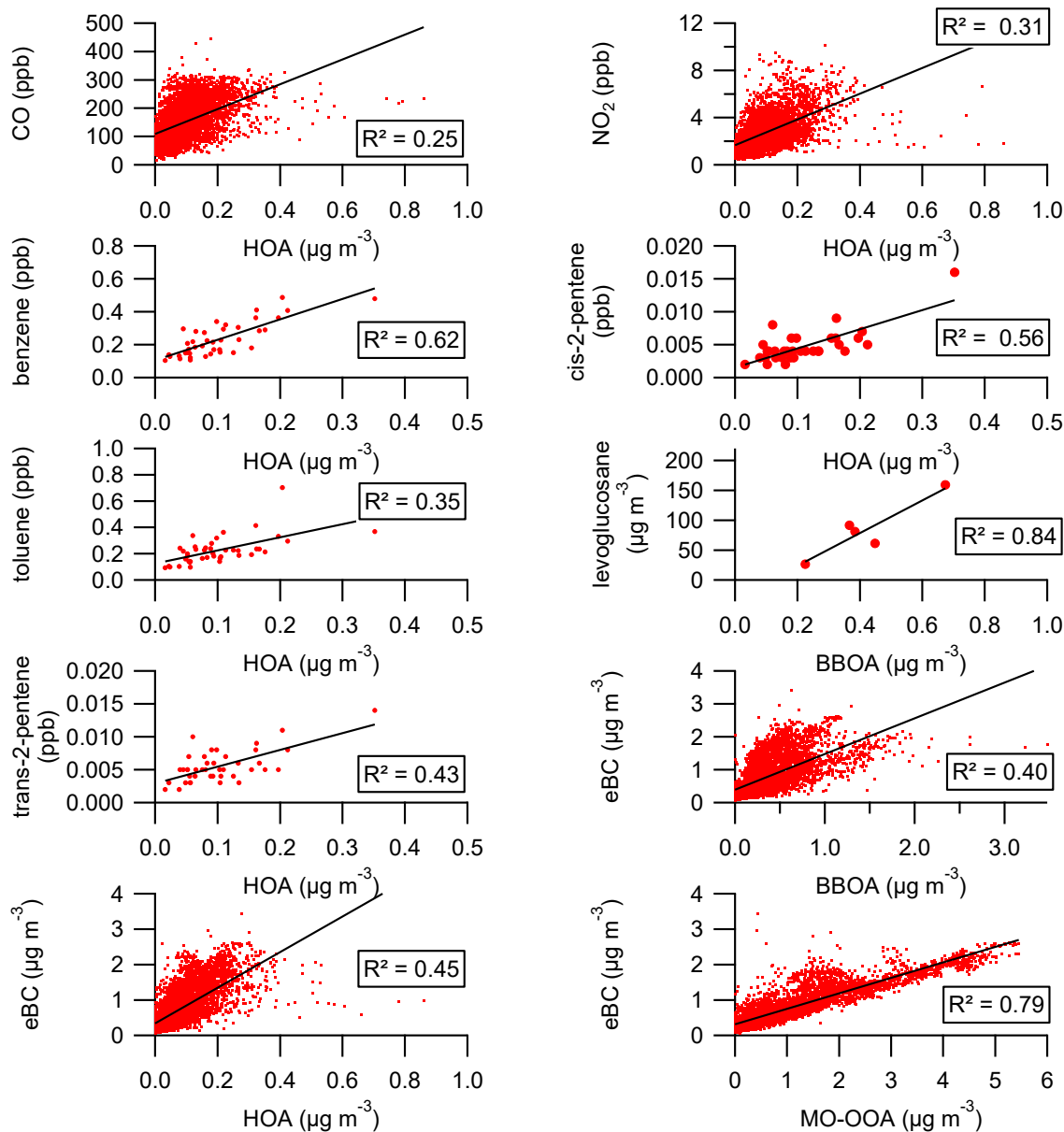
Figure SI-~~17~~16: Scatter plot of the identified factors (HOA, BBOA, and MO-OOA) vs. their corresponding tracers during intensive sampling periods. The correlation curves (red lines) were calculated using the least orthogonal distance fit method.
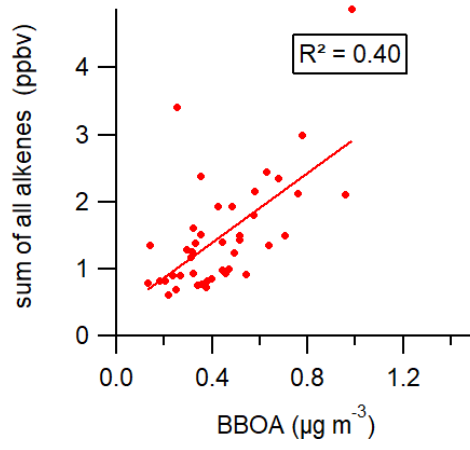
Figure SI- ~~16~~17: Continued

235   **Figure SI-~~18~~17: Diurnal profiles of the 5-factors solutions and their corresponding tracers.**

Figure SI-~~19~~18: Scatter plot of the SV-OOA vs. anthropogenic NMHC gases. The correlation curves (red lines) were calculated using the least orthogonal distance fit method.

240

245

SI-6: Overview of the NMHC measurements

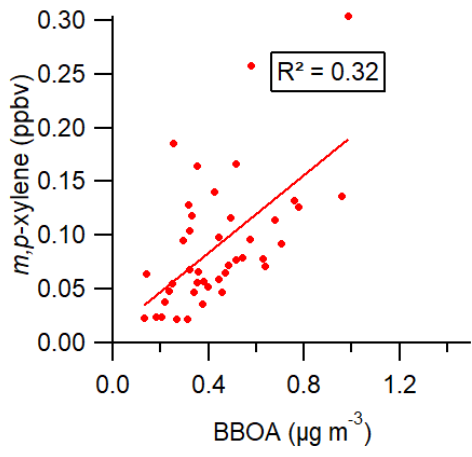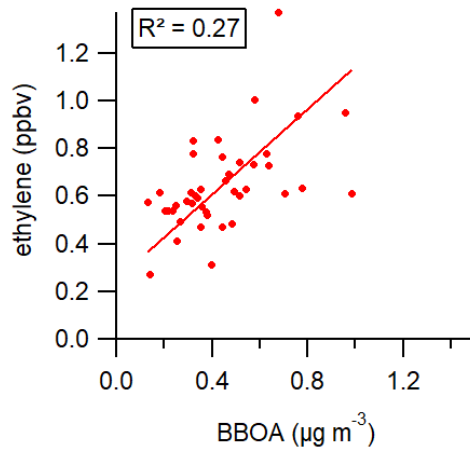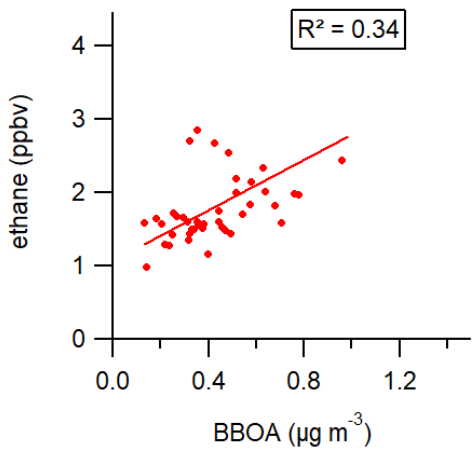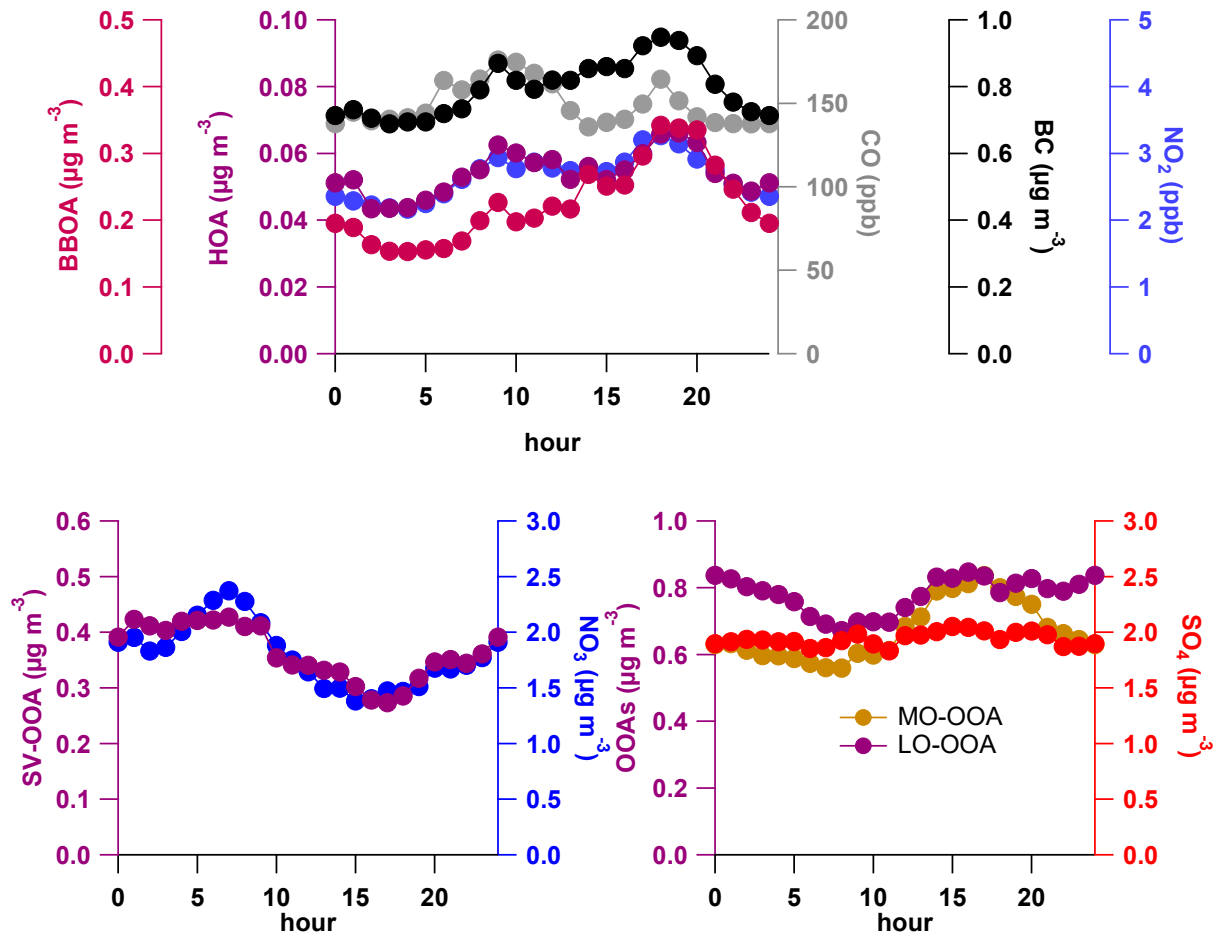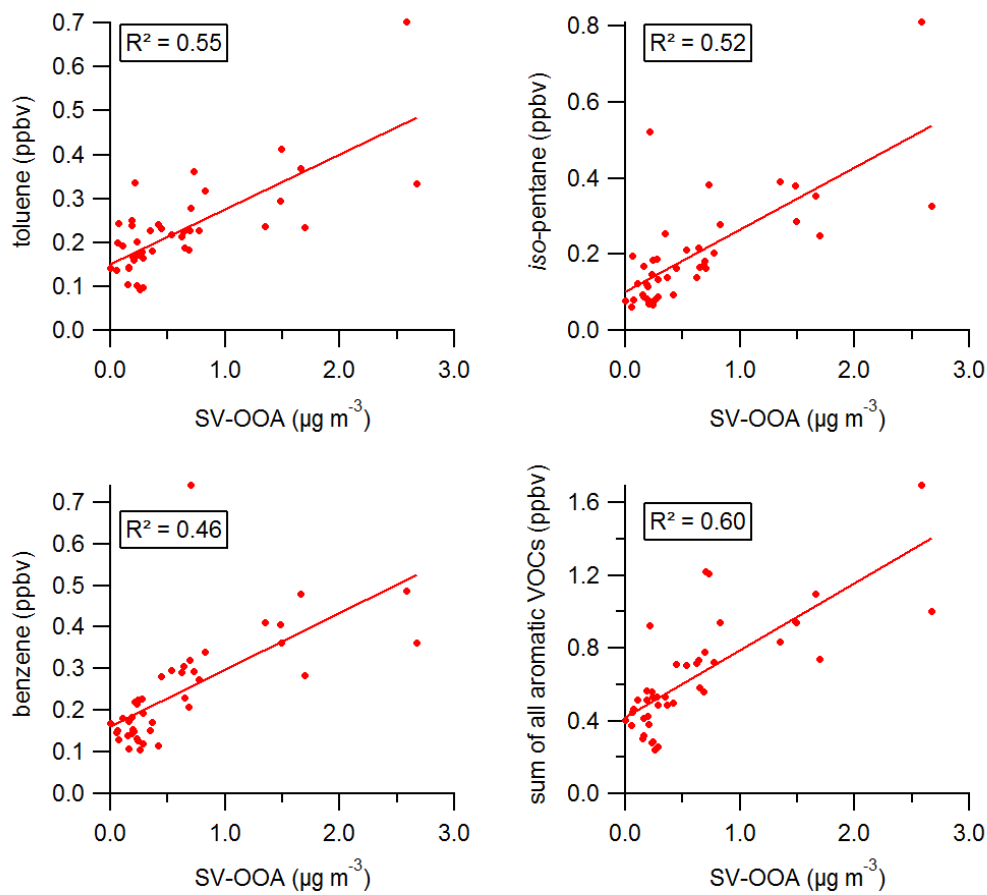**Table SI-3: Overview of the average gas-phase concentrations NMHC (in ppbv ± standard deviation) during full-cloud events (FCE) and non-cloud events (NCE).**

	FCE 1.1	NCE 0.1	NCE 0.2	FCE 11.2	FCE 11.3	FCE 12.1	FCE 13.1	FCE 13.3	FCE 22.1	NCE 0.3	FCE 26
Starting time	14.09. 2010 12:44	15.09. 2010 18:00	20.09. 2010 11:25	01.10.2 010 22:33	02.10. 2010 14:33	05.10. 2010 08:30	05.10. 2010 19:15	06.10. 2010 12:15	19.10. 2010 21:30	21.10. 2010 14:15	24.10. 2010 01:30
Stopping time	15.09. 2010 00:00	15.09. 2010 23:30	20.09. 2010 20:30	02.10. 2010 05:30	02.10. 2010 20:00	05.10. 2010 13:00	06.10. 2010 04:30	07.10. 2010 02:45	20.10. 2010 03:30	21.10. 2010 22:15	24.10. 2010 11:45
Cluster	C1	C1	C1	C3	C3	C4 to C3	C3	C3 to C4	C1	C1	C3 to C2 via C1
NMHC											
Nb of samples	5	3	6	4	3	2	5	0	3	3	6
Acetylene	0.61± 0.16	0.46± 0.13	0.62± 0.09	0.60± 0.03	0.87± 0.44	0.81± 0.04	0.82± 0.15		0.71± 0.23	0.60±0. 13	0.55± 0.06
Alkenes	1.35± 1.15	0.79± 0.16	0.86± 0.11	1.36± 0.12	1.70± 0.58	1.77± 0.23	2.24± 0.54		1.78± 0.37	1.72±0. 57	1.07± 0.44
Aromatics	0.60± 0.18	0.41± 0.08	0.44± 0.08	0.78± 0.11	0.88± 0.29	0.89± 0.08	1.09± 0.39		0.64± 0.12	0.49± 0.07	0.31± 0.09
n-alkanes	3.36± 1.45	2.33± 0.66	2.64± 0.24	3.35± 0.34	2.97± 0.29	6.06± 0.28	5.02± 0.36	No data	3.35± 0.27	4.15± 0.37	2.96± 0.87
i-alkanes	0.66± 0.52	0.43± 0.19	0.36± 0.06	0.67± 0.07	0.49± 0.03	1.31± 0.09	1.09± 0.38		0.61± 0.07	0.67± 0.06	0.37± 0.11
Total NMHC	6.59± 3.17	4.42± 1.03	4.91± 0.50	6.74± 0.59	6.90± 1.58	10.82± 0.72	10.25± 1.21		7.08± 0.92	7.63± 0.81	5.26± 1.43
Benzene-to-toluene ratio	0.83	0.68	0.97	1.25	1.74	1.56	1.03		1.26	1.26	1.20
Xylene-to-toluene ratio	0.58	0.35	0.47	0.74	0.70	0.64	0.58		0.74	0.57	0.42

SI-7 Influence of air mass origin on local aerosol and gas composition

255   **Table SI-4: Gas phase tracer and particle mean composition for the different air mass clusters (all concentrations in μg m^{-3})**

cluster (hours)	C1 (307)	C2 (165)	C3 (179)	C4 (84)	C5 (88)	C6 (173)
region of air mass origin	West	Northwest	Southwest	South	Northeast	East
Gas-phase measurements						
HCl mean (median) in μg m^{-3}	0.15 (0.11)	0.09 (0.09)	0.29 (0.21)	0.36 (0.37)	0.21 (0.21)	0.13 (0.14)
Min. /Max.	0.05 / 0.65	0.06 / 0.15	0.05 / 0.75	0.07 /0.62	0.21 /0.21	0.06 /0.30
HONO mean (median) in μg m^{-3}	0.76 (0.74)	0.72 (0.67)	0.67 (0.62)	0.78 (0.76)	0.38 (0.39)	0.43 (0.32)
Min. /Max.	0.11 / 2.44	0.10 / 2.42	0.17 / 1.81	0.16 /1.39	0.08 / 0.92	0.08 / 1.64
SO$_2$ mean (median) in μg m^{-3}	0.32 (0.24)	0.30 (0.25)	0.40 (0.26)	0.37 (0.25)	0.66 (0.21)	2.48 (1.49)
Min. /Max.	0.10 /1.46	0.10 / 0.68	0.1 / 2.00	0.11 / 1.71	0.10 / 3.50	0.14 / 13.27
HNO$_3$ mean (median) in μg m^{-3}	0.16 (0.13)	0.14 (0.12)	0.32 (0.23)	0.25 (0.18)	0.17 (0.11)	0.34 (0.30)
Min. /Max.	0.05 / 1.04	0.05 / 0.83	0.06 / 5.77	0.05 / 1.21	0.05 / 0.53	0.05 / 1.15
Ozone mean (median) in ppb	42.69 (41.39)	38.40 (40.27)	39.96 (35.37)	38.46 (33.13)	42.77 (40.50)	57.01 (60.01)
Min. /Max.	8.73 / 81.09	7.86 / 71.6	7.77 / 94.78	8.28 / 99.75	14.92 / 81.13	8.01 / 90.73
NO mean (median) in ppb	0.42 (0.15)	0.32 (0.12)	0.52 (0.28)	0.95 (0.19)	0.35 (0.21)	0.71 (0.42)
Min. /Max.	0.01 / 5.88	0.01 / 4.51	0.01 /8.08	0.01 / 7.78	0.01 / 1.47	0.01 / 4.88
NO$_2$ mean (median) in ppb	5.17 (4.57)	4.51 (4.19)	5.87 (5.63)	4.75 (4.64)	4.53 (4.65)	5.60 (5.21)
Min. /Max.	0.96 / 16.04	1.04 / 13.19	1.86 / 13.79	1.76 / 10.17	1.05 / 11.07	1.88 / 15.22

Table SI-4: Continued

cluster (hours)	C1 (307)	C2 (165)	C3 (179)	C4 (84)	C5 (88)	C6 (173)
region of air mass origin	West	Northwest	Southwest	South	Northeast	East
Aerosol measurements in µg m⁻³						
Total mass concentration mean (median)	7.54 (7.61)	6.38 (5.83)	11.50 (9.93)	11.38 (10.78)	7.97 (5.75)	12.65 (11.40)
Min. / Max.	0.23 / 18.70	1.07 / 20.28	4.23 / 23.22	4.08 / 21.33	1.13 / 27.47	0.73 / 29.66
Organic (AMS) mean (median)	2.07 (1.90)	1.86 (1.57)	4.99 (4.44)	5.39 (5.05)	3.18 (2.12)	5.76 (5.66)
Min. /Max.	0.18 / 5.06	0.28 / 6.62	1.52 / 12.0	2.30 / 11.36	0.30 / 9.73	1.19 /10.55
eBC (MAAP) mean (median)	0.52 (0.49)	0.50 (0.41)	1.03 (0.91)	1.01 (0.93)	0.74 (0.41)	1.31 (1.32)
Min /Max.	0.08 / 1.5	0.10 / 1.83	0.31 / 2.22	0.56 / 3.07	0.11 / 2.31	0.16 / 3.2
Chloride (MARGA) mean (median)	0.29 (0.21)	0.27 (0.23)	0.11 (0.10)	0.08 (0.08)	0.14 (0.12)	0.21 (0.22)
Min. /Max.	0.05 / 1.45	0.05 / 0.78	0.05 / 0.25	0.05 / 0.10	0.06 / 0.27	0.05 / 0.33
Nitrate (MARGA) mean (median)	1.87 (1.67)	1.55 (1.20)	2.33 (1.92)	1.64 (1.32)	1.40 (0.88)	2.25 (1.90)
Min. /Max.	0.14 / 8.99	0.29 / 6.56	0.20 / 8.91	0.14 / 4.68	0.11 / 7.40	0.17 / 9.90
Sulfate (MARGA) mean (median)	1.12 (1.11)	1.04 (0.96)	1.39 (1.12)	1.96 (1.75)	1.36 (1.04)	1.83 (1.76)
Min. /Max.	0.09 / 2.49	0.14 / 3.34	0.46 / 4.41	0.29 / 4.29	0.10 / 4.49	0.55 / 4.45
Ammonium (MARGA) mean (median)	0.83 (0.74)	0.74 (0.59)	1.23 (1.10)	1.28 (1.14)	0.94 (0.61)	1.38 (1.12)
Min. /Max.	0.08 / 3.18	0.11 / 2.96	0.29 / 3.58	0.21 / 3.14	0.10 / 4.06	0.25 / 4.53
Potassium (MARGA) mean (median)	0.14 (0.13)	0.12 (0.11)	0.13 (0.12)	0.14 (0.14)	0.12 (0.12)	0.13 (0.12)
Min. /Max.	0.1 / 0.26	0.10 / 0.18	0.10 / 0.20	0.11 / 0.22	0.10 / 0.18	0.10 / 0.20
Sodium (MARGA) mean (median)	0.26 (0.17)	0.22 (0.20)	0.17 (0.10)	0.10 (0.09)	0.11 (0.10)	n.d.
Min. /Max.	0.08 / 1.24	0.08 / 0.52	0.08 / 1.02	0.08 / 0.12	0.08 / 0.16	n.d.

260   n.d. : not detected

Table SI-4: continued

cluster (hours)	C1 (307)	C2 (165)	C3 (179)	C4 (84)	C5 (88)	C6 (173)
region of air mass origin	West	Northwest	Southwest	South	Northeast	East
Organic aerosol factors in µg m⁻³						
HOA mean (median)	0.08 (0.07)	0.07 (0.06)	0.11 (0.10)	0.07 (0.05)	0.08 (0.05)	0.13 (0.13)
Min. /Max.	0.00 / 0.44	0.00 / 0.26	0.01 / 0.39	0.01 /0.53	0.01 /0.29	0.01 /0.32
BBOA mean (median)	0.37 (0.29)	0.30 (0.25)	0.44 (0.34)	0.27 (0.23)	0.26 (0.13)	0.53 (0.53)
Min. /Max.	0.00 / 2.77	0.03 / 1.27	0.06 / 1.88	0.09 /0.90	0.00 /1.43	0.00 /1.27
MO-OOA mean (median)	0.65 (0.50)	0.44 (0.27)	1.32 (1.47)	1.49 (1.47)	1.15 (0.44)	2.52 (2.47)
Min. /Max.	0.00 / 3.55	0.02 /2.87	0.39 / 4.48	0.53 /2.53	0.04 /4.94	0.06 /5.58
LO-OOA mean (median)	0.91 (0.74)	0.55 (0.53)	2.32 (1.76)	2.54 (2.44)	0.87 (0.85)	1.46 (1.41)
Min. /Max.	0.02 / 3.38	0.04 /1.94	0.35 / 8.15	0.82 /5.33	0.00 /3.23	0.26 /3.83
SV-OOA mean (median)	0.36 (0.28)	0.39 (0.25)	0.87 (0.76)	0.60 (0.53)	0.57 (0.39)	1.06 (0.96)
Min. /Max.	0.01 / 1.37	0.02 / 1.94	0.00 / 3.12	0.02 /2.22	0.00 /4.77	0.02 /5.26
eBC aerosol factors in µg m⁻³						
eBC-HOA mean (median)	0.12 (0.11)	0.13 (0.11)	0.18 (0.15)	0.13 (0.10)	0.12 (0.08)	0.22 (0.21)
Min. /Max.	0.01 / 0.48	0.03 / 0.73	0.02 / 0.65	0.02 / 0.89)	0.01 / 0.48	0.02 / 0.53
eBC-BBOA mean (median)	0.03 (0.02)	0.04 (0.03)	0.05 (0.04)	0.03 (0.02)	0.03 (0.01)	0.06 (0.05)
Min. /Max.	0.00 /0.15	0.00 / 0.29	0.00 / 0.19	0.01 / 0.09	0.00 / 0.15	0.00 / 0.14
eBC-MO-OOA mean (median)	0.19 (0.13)	0.15 (0.10)	0.47 (0.45)	0.54 (0.52)	0.38 (0.18)	0.91 (0,89)
Min. /Max.	0.00 / 0.77	0.00 / 1.04	0.00 / 1.48	0.18 / 0.89	0.01 / 1.59	0.11 / 1.92

265   **References**

Canonaco, F., Crippa, M., Slowik, J. G., Prévôt, A. S. H., and Baltensperger, U.: SoFi, an IGOR-based interface for the efficient use of the generalized multilinear engine (ME-2) for the source apportionment: ME-2 application to aerosol mass spectrometer data, Atmos. Meas. Tech., 6, 3649-3661, doi:10.5194/amt-6-3649-2013, 2013.

Crippa, M., Canonaco, F., Lanz, V. A., Äijälä, M., Allan, J. D., Carbone, S., Capes, G., Ceburnis, D., Dall'Osto, M., Day, D.
270   A., DeCarlo, P. F., Ehn, M., Eriksson, A., Freney, E., Hildebrandt Ruiz, L., Hillamo, R., Jimenez, J. L., Junninen, H., Kiendler-

Scharr, A., Kortelainen, A. M., Kulmala, M., Laaksonen, A., Mensah, A. A., Mohr, C., Nemitz, E., O'Dowd, C., Ovadnevaite, J., Pandis, S. N., Petäjä, T., Poulain, L., Saarikoski, S., Sellegri, K., Swietlicki, E., Tiitta, P., Worsnop, D. R., Baltensperger, U., and Prévôt, A. S. H.: Organic aerosol components derived from 25 AMS data sets across Europe using a consistent ME-2 based source apportionment approach, Atmos. Chem. Phys., 14, 6159-6176, doi:10.5194/acp-14-6159-2014, 2014.

275 Cubison, M. J., Ortega, A. M., Hayes, P. L., Farmer, D. K., Day, D., Lechner, M. J., Brune, W. H., Apel, E., Diskin, G. S., Fisher, J. A., Fuelberg, H. E., Hecobian, A., Knapp, D. J., Mikoviny, T., Riemer, D., Sachse, G. W., Sessions, W., Weber, R. J., Weinheimer, A. J., Wisthaler, A., and Jimenez, J. L.: Effects of aging on organic aerosol from open biomass burning smoke in aircraft and laboratory studies, Atmos. Chem. Phys., 11, 12049-12064, 10.5194/acp-11-12049-2011, 2011.

Engling, G., Carrico, C. M., Kreldenweis, S. M., Collett, J. L., Day, D. E., Malm, W. C., Lincoln, E., Hao, W. M., Iinuma, Y.,
280 and Herrmann, H.: Determination of levoglucosan in biomass combustion aerosol by high-performance anion-exchange chromatography with pulsed amperometric detection, Atmos. Environ., 40, S299-S311, doi:10.1016/j.atmosenv.2005.12.069, 2006.

Gnauk, T., Muller, K., van Pinxteren, D., He, L. Y., Niu, Y. W., Hu, M., and Herrmann, H.: Size-segregated particulate chemical composition in Xinken, Pearl River Delta, China: OC/EC and organic compounds, Atmos. Environ., 42, 6296-6309,
285 doi:10.1016/j.atmosenv.2008.05.001, 2008.

Iinuma, Y., Engling, G., Puxbaum, H., and Herrmann, H.: A highly resolved anion-exchange chromatographic method for determination of saccharidic tracers for biomass combustion and primary bio-particles in atmospheric aerosol, Atmos. Environ., 43, 1367-1371, doi:10.1016/j.atmosenv.2008.11.020, 2009.

Mohr, C., DeCarlo, P. F., Heringa, M. F., Chirico, R., Slowik, J. G., Richter, R., Reche, C., Alastuey, A., Querol, X., Seco, R.,
290 Penuelas, J., Jimenez, J. L., Crippa, M., Zimmermann, R., Baltensperger, U., and Prevot, A. S. H.: Identification and quantification of organic aerosol from cooking and other sources in Barcelona using aerosol mass spectrometer data, Atmos. Chem. Phys., 12, 1649-1665, 2012.

Ng, N. L., Canagaratna, M. R., Jimenez, J. L., Zhang, Q., Ulbrich, I. M., and Worsnop, D. R.: Real-Time Methods for Estimating Organic Component Mass Concentrations from Aerosol Mass Spectrometer Data, Environ. Sci. Technol., 45, 910-
295 916, 2011.

Paatero, P.: The multilinear engine - A table-driven, least squares program for solving multilinear problems, including the n-way parallel factor analysis model, J. Comput. Graph. Stat., 8, 854-888, doi:10.2307/1390831, 1999.

Poulain, L., Birmili, W., Canonaco, F., Crippa, e. a., Wu, Z. J., Nordmann, S., Spindler, G., Prévôt, A. S. H., Wiedensohler, A., and Herrmann, H.: Chemical mass balance of refractory particles (T=300°C) at the tropospheric research site Melpitz,
300 Germany, Atmos. Chem. Phys., 14, 10145-10162, doi:10.5194/acp-14-10145-2014, 2014.

Salcedo, D., Onasch, T. B., Dzepina, K., Canagaratna, M. R., Zhang, Q., Huffman, J. A., DeCarlo, P. F., Jayne, J. T., Mortimer, P., Worsnop, D. R., Kolb, C. E., Johnson, K. S., Zuberi, B., Marr, L. C., Volkamer, R., Molina, L. T., Molina, M. J., Cardenas, B., Bernabe, R. M., Marquez, C., Gaffney, J. S., Marley, N. A., Laskin, A., Shutthanandan, V., Xie, Y., Brune, W., Lesher, R., Shirley, T., and Jimenez, J. L.: Characterization of ambient aerosols in Mexico City during the MCMA-2003 campaign with
305 Aerosol Mass Spectrometry: results from the CENICA Supersite, Atmos. Chem. Phys., 6, 925 - 946, doi:10.5194/acp-6-925-2006, 2006.

Tilgner, A., Schone, L., Brauer, P., van Pinxteren, D., Hoffmann, E., Spindler, G., Styler, S. A., Mertes, S., Birmili, W., Otto, R., Merkel, M., Weinhold, K., Wiedensohler, A., Deneke, H., Schrodner, R., Wolke, R., Schneider, J., Haunold, W., Engel, A., Weber, A., and Herrmann, H.: Comprehensive assessment of meteorological conditions and airflow connectivity during
310 HCCT-2010, Atmos. Chem. Phys., 14, 9105-9128, 10.5194/acp-14-9105-2014, 2014.

Ulbrich, I. M., Canagaratna, M. R., Zhang, Q., Worsnop, D. R., and Jimenez, J. L.: Interpretation of organic components from Positive Matrix Factorization of aerosol mass spectrometric data, Atmos. Chem. Phys., 9, 2891-2918, doi:10.5194/acp-9-2891-2009, 2009.